NASA Contractor Report 198548
ASC–95–1002

/115-4
013158
p 102

Multi-Disciplinary Development of a Smart CMC Combustor for an Intelligent Engine System

Frank Abdi, Roy Lorenz, and Jeff Hadian
Alpha STAR Research Corporation
Los Angeles, California

Harvey Niska
Allied Signal Propulsion Engines
Phoenix, Arizona

November 1996

Prepared for
Lewis Research Center
Under Contract NAS3–27443

National Aeronautics and
Space Administration

ASC-95-1002

Alpha STAR

Advanced Technology Project (ATP) Phase I Final Report

Multi-Disciplinary Development Of A Smart CMC Combustor For An Intelligent Engine System

Prepared for:

NASA Lewis Research Center
Advanced Technology Project (ATP) Phase I Final Report
Contract No.: NAS3-27443

Prepared by:

Dr. Frank Abdi, Roy Lorenz, Dr. Jeff Hadian
Alpha STAR Research Corporation
Los Angeles, California

And

Harvey Niska
Allied Signal Propulsion Engines
Phoenix, Arizona

Contents

Section		Page
1.0	INTRODUCTION	1-1
2.0	OBJECTIVES	2-1
3.0	APPROACH	3-1
4.0	SENSOR REVIEW	4-1
4.1	Sensor Summary	4-1
4.1.1	Optical Fiber Sensors	4-1
4.1.2	Clearance Sensors	4-2
4.1.3	Thermocouple Sensors	4-2
4.1.4	Resistive Temperature Device (RTD) Sensors	4-3
4.1.5	Single Spot Optical (Infrared) Pyrometer	4-3
4.1.6	2D Optical Pyrometer Imaging Systems	4-4
4.1.7	Laser Activated Temperature (LAT) Sensors	4-4
4.1.8	Survey of AE Sensor Technology (Allied Signal Engines)	4-4
4.1.9	AE Thin Films	4-7
4.1.10	Pd/CR Thin Film Strain Sensors	4-9
4.1.11	Radiation Pyrometry	4-12
4.1.12	Laser Induced Fluorescence (LIF)	4-13
4.1.13	Thermography	4-13
4.1.14	Acoustic Emission	4-13
4.1.15	Ultrasound	4-15
5.0	MATERIAL SELECTION	5-1
5.1	CMC Material Characterization	5-10
5.1.1	Nicalon™ SiC	5-10
5.1.2	HI Nicalon™ SiC Fiber/Enhanced SiC CMC	5-11
5.2	SiC/SiC CMC Combustor Tests	5-18
5.2.1	Subelement Tests	5-18
5.2.2	Full Scale Tests	5-18

Contents

Section **Page**

6.0 MULTIDISCIPLINARY COMPUTER CODE DEVELOPMENT FOR STOCHASTIC ANALYSIS OF CMC COMPOSITE SMART STRUCTURE 6-1

6.1 An Integrated Multi-Disciplinary Constituent Material Strength and Risk Assessment Analysis 6-1

6.1.1 Modularization of HITCAN: A Source For Baseline Analytical Capabilities 6-3

6.1.2 CEMCAN Integration For GENOA 6-5

6.1.3 PROMISS Integrated With CEMCAN 6-6

6.1.4 Probabilistic Analysis in GENOA 6-9

6.1.5 Micromechanical Risk Assessment 6-10

6.1.6 Integration of Environment and Test Data With A Stochastic Simulation 6-11

6.1.7 NESSUS: 3-D Inelastic Finite Element Analysis 6-11

6.2 Temperature and Strain Distribution in a CMC Combustor 6-13

6.3 Computational Simulation of CMC CREEP Behavior 6-13

7.0 SIMULATION AND MODEL VERIFICATION 7-1

7.1 Prediction Structural Response Under Combined Loading 7-1

7.2 Verify Numerical Probabilistic Simulation Model With Coupon Test Data 7-2

7.2.1 Verification of Composite Mechanics Analysis Based on the Coupon Test Results 7-2

7.2.2 Finite Element Analysis 7-6

7.2.3 Identification of Important Parameters by Mans of Sensitivity Analysis 7-7

7.2.4 Effect of Incorporating Sensors on Ply Reliability 7-9

7.3 Structural Reliability of CMC Combustor 7-13

7.3.1 CMC Combustor Without Sensors 7-13

7.3.2 CMC Combustor With Sensors 7-15

8.0 HEALTH MONITORING 8-1

9.0 REFERENCES 9-1

Illustrations

Figure **Page**

1-1. Graphic Comparison of Kyocera Ceramic Material Properties Presented in Table 1-1 1-3

1-2. Description of Hexoloy Silicon Carbide Ceramics Available Commercially 1-4

1-3. Graphical Comparison of Properties of Hexoloy Ceramic Materials Showing Silicon Carbide Ceramics to be Superior in all Properties Shown Excepting the Fracture Toughness of Tungsten Carbide 1-5

1-4. Comparison of Properties of Several Commercially Available Hexoloy Silicon Silicon Carbide Ceramics 1-6

1-5. Typical Combustor Configuration 1-6

1-6. Cross-section of the AE TFE731 as Turbine Engine Identifies Candidate CMC Components; (1) Combustor; (2) HP Turbine Shroud; (2) Inter-turbine Transition Liner (Outer), and (3) Inter-turbine Transition Liner (Inner), and (4,5) LP Turbine Shroud 1-7

4-1. Fiber and Sensor Technologies EPI Optical Fiber Strain Gauge 4-2

4-2. Displacement Transducer Based on Quantum Mechanical Tunneling Between Electrodes (NASA JPL) 4-2

4-3. Thin Film Sensors Applied to the Inside Surface of Turbine Engine Combustor Offer Negligible Impedance to Flow Compared to Wire Thermocouple Sensors 4-3

4-4 Resistance of Laser Activated SiC as a Function of Temperature, to 500°C, in Air 4-5

4-5. Example of AE Sensors Currently Used on SiC Material 4-5

4-6. A Reliable Means of Thermocouple Attachment to SiC Using a Silicate Cement With an Aluminum Oxide Substrate and Overlayer 4-5

4-7. Plot Showing Direct Relationship Between AE Thin Film and Reference Thermocouple 4-8

4-8. Allied Signal's Class 100 Cleanroom With Target Library and Complete Photo Fabrication Capability 4-8

4-9. Example of Thin Film Sensor Application at AE 4-9

4-10. Apparent Microstrain Versus Temperature of a NASA Lewis Dynamic Pd/Cr Thin Film Strain Gage and Associated Drift in Microstrain as Function of Time 4-10

4-11 Pd/Cr Thin Film Strain Gages From NASA Lewis Research Center, Cleveland, Measures Static and Dynamic Strain to 1,040°C 4-10

4-12. A NASA Lewis Pd/Cr Thin Film Gage Made Portable by Application to a Metal Shim for Attachment by Welding 4-11

4-13. Static Pd/Cr Strain Gage Characteristics 4-12

4-14. Linear Mechanical Strain Response in Tension and Compression 4-12

4-15. Lifetime of Various Phosphors as Functions of Temperature 4-14

4-16. Laser Induced Fluorescence Probe 4-16

4-17. Laser Induced Fluorescence Sensor Schematic 4-17

Illustrations

Figure **Page**

5-1. Room Temperature Stress Strain Curve for Enhanced SiC/SiC CMC 5-9

5-2. Stress Strain Cr Enhanced SiC/SiC CMC at 815°C (1500°F) in Air 5-9

5-3. Stress Strain Curve for Enhanced SiC/SiC CMC at 1090°C (2000°F) in Air 5-9

5-4. Stress Strain Cr Enhanced SiC/SiC CMC at 1370°C (2500°F), in Air 5-10

5-5. Mechanical Tensile Test Results at Room and Elevated Temperatures on 2-D Triaxial Braided SiC/SiC CMC With 40% Nicalon™ SiC Fiber 5-11

5-6. Through-Thickness Thermal Conductivity and Expansion for the Standard Nicalon/SiC Material 5-12

5-7. Enhanced Hi Nicalon/SiC Tensile Stress-Strain Behavior 5-14

5-8. Enhanced Hi Nicalon/SiC: Low Cycle Fatigue 5-14

5-9. Enhanced SiC/SiC: Low Cycle Fatigue 5-15

5-10. Stress-Staircase Evaluation 5-15

5-11. Linear Elastic Limits of Enhanced Hi Nicalon/SiC From Tensile Test 5-16

5-12 Combustor Subelement Testing 5-18

5-13. The Cold- and Hot-Side Surface Temperature of Model Were Mapped From the Uncooled Subelement Thermal Paint Data 5-19

5-14. A Full Scale Experimental SiC/SiC CMC Small Gas Turbine Engine Combustor Tested by AE 5-20

5-15. Thermal Paint Temperature Profile Map of a Unit Section of Tested SiC/SiC CMC, Combustor of Figure 5-14

5-16. Thermography Data Obtained in Real-time by AE During Full Scale SiC/SiC CMC Combustor Testing 5-21

6-1. Architecture of GENOA Parallel Software System 6-2

6-2. Illustration of GENOA Integrated Stochastic Analysis Package 6-3

6-3. Illustration of the Computational Iterative Procedure Utilized by HITCAN to Perform Composite Micromechanics Within a Finite Element-Based Analysis 6-5

6-4. Ceramic Constituent Stress Plot - YY Slice 6-6

6-5. Ceramic Constituent Stress Plot - XX Slice 6-6

6-6. Procedure for Assessment of Material Reliability 6-8

6-7. Illustration of the Overlapping Probability Densities Functions Representative of the Probable Event of Failure 6-11

6-8. Iterative Method Utilized by HITCAN to Perform Nonlinear Structural Analysis 6-12

6-9. Parametric Mapping Technique Couples with Bi-linear Shape Function Interpolation Provides and Efficient and Robust Means of Data Communication 6-13

Illustrations

Figure **Page**

6-10. CEMCAN was Calibrated With Stress Rupture Test Results 6-14

7-1. Cold-side Thermal Stress 7-2

7-2. Uncooled Subelement Posttest Condition 7-2

7-3. Influence of Porosity and Temperature on Composite Elastic Modulus E_{11} 7-4

7-4. Influence of Porosity and Temperature on Composite Elastic Modulus E_{22} 7-5

7-5. Influence of Porosity and Temperature on Composite Elastic Modulus E_{33} 7-5

7-6. Cumulative Distribution Function for SiC/SiC (0/+60) 24 Laminate Ply Thickness 0.08-in. Under Thermal Load of 2500°F 7-6

7-7. Composite Tensile Coupon Model Used to Demonstrate the Preliminary Probabilistic Analysis Capability of PROMISS Integrated With HITCAN 7-7

7-8. Axial Stress Contour Plot for Coupon Test Model 7-7

7-9. Transverse Stress Contour Plot for Coupon Test Model 7-7

7-10. Reliability Contour Plot for Top Layer of the Coupon Test Model 7-7

7-11. Cumulative Distribution Function (CDF) for the Strength Ply With the Highest Temperature 7-8

7-12. Strength Variation for 0.99 Reliability 7-8

7-13. Strength Sensitivity at 0.99 Reliability for Coupon Test Model 7-9

7-14. The Effect of Temperature on Cumulative Distribution Function Due to (a) Longitudinal Stress (11), and (b) Transverse Stress (22) 7-10

7-15. The Sensitivity of Strength With Respect to Temperature at 0.99 Reliability Due to (a) Longitudinal Stress (11), and (b) Transverse Stress (22) 7-11

7-16. The Strength Sensitivity of First Ply With Respect to Various Parameters of SiC/SiC at 0.99 Reliability Due to Longitudinal (11) and Transverse (22) Stress 7-11

7-17. Allied Signal Technique of Sensor Insertion in CMC Combustor 7-12

7-18 The Effect of Sensor on Cumulative Distribution Functions - NS = Without Sensor; S = With Sensor 7-12

7-19 The Effect of the Sensor on Cumulative Distribution Function - NS = Without Sensor; S = With Sensor 7-13

7-20. A Generic Finite Element Model of CMC Combustor (1188 Quad Elements, 1334 Nodes, 8004 DOF) 7-13

7-21. Stress Contour Plots for Combustor Without Sensors 7-14

7-22. Reliability Contour Plot (at 0.99 Reliability) for Combustor Without Insertion of Sensors 7-14

7-23. Stress Contour Plots for Combustor With Imbedded Sensors 7-15

Illustrations

Figure **Page**

7-24 Reliability Contour Plot (at 0.99 Reliability for Top Layer of the Combustor With Inserted Sensors 7-16

8-1. CMC Combustor Health Monitoring Control Flow Diagram 8-2

Tables

Table		Page
1-1.	Properties of Kyocera* Ceramic Materials Available Commercially	1-2
4-1	Allied Signal's Flame Spray Techniques for Attaching Wire Thermocouple Elements and Strain Gages to SiC/SiC CMC	4-6
5-1	Properties of Ceramic Materials With Potential For Combustor Applications - Parts A-F	5-2
5-2	High Temperature Properties of SiC/SiC Composite Made for AE by DuPont Lanxide	5-10
5-3.	Comparison of SiC/SiC CMC Materials Available From DuPont Lanxide	5-13
5-4.	Mechanical Properties of Enhanced SiC/SiC	5-17
5-5.	Enhanced SiC/SiC Stress-Rupture Results (Uncoated Samples, Tested in Air)	5-17
5-6.	Results From Subelement Testing	5-18
6-1	Input/Output Parameter Panel for High Temperature Composite Analyzer (HITCAN)	6-4
6-2	Procedure of Interactive Material Risk Assessment	6-9
6-3	Uncertainties in the Constituent Properties	6-9

1.0 Introduction

Turbine engine operating temperatures above 2000°F offer significantly increased propulsion capability in the form of thrust, and specific fuel consumption (SFC) that can translate into lower fuel costs, improved performance, and increased payloads for aircraft. Metal alloys are limited for use as a combustor material above 1700°F in that parasitic cooling with air is required to keep the metal alloys below their temperature limits. Refractory metals (Tantalum, Molybdenum, Niobium and Tungsten) have adequate strengths well above 2000°F but have poor oxidation resistance that, despite many attempts, cannot be adequately improved for use in critical structure by application of oxidation resistant coatings.

Monolithic ceramic materials such as SiC have significant strengths and excellent oxidation resistance's at temperatures up to 2000°F and above but their poor fracture toughness precludes their use in critical structure (Table 1-1 and Figures 1-1 through 1-4). However, reinforcing monolithic ceramic materials with high strength ceramic fibers results in ceramic matrix composites (CMCs) with significantly increased fracture toughness compared to that of monolithic ceramics. Thus, the use of CMCs offers potential for achieving increased propulsion capability via higher turbine engine operating temperatures without penalty of parasitic air cooling. Additionally, the dimensional stability of CMC materials can reduce blade clearance, minimize shroud distortion, and lead to improved durability and performance.

Hot static structures from the combustor through the low turbine are candidates for the application of CMCs (Figures 1-5 and 1-6). At Allied Signal (AE) numerous product lines such as the TFE731, CFE738, and TFE1042 (FI24) turbofan engines and the CTS800 engine would immediately benefit from the development and application of CMC technology. However, before the high temperature capabilities of CMCs can be utilized, means must be developed to keep stress and temperature gradients within bounds that are less tolerant than those of metal alloys.

Reinforcement of SiC matrix with SiC fiber results in CMC material (SiC/SiC) that has significantly improved fracture toughness compared to that of monolithic SiC DuPont Lanxide Composites Inc. has fabricated SiC/SiC combustors for an Allied Signal IHPTET combustor liner application by embedding braided preforms of Nicalon SiC fiber yarns in a SiC matrix by a chemical vapor infiltration (CVI) process. Short term (10 hour) tests at Allied Signal of these SiC/SiC combustors have been made. Some crack development in the SiC matrix was found to occur due primarily to thermal gradient strains with some associated combustor design deficiencies. However, the SiC matrix cracks did not result in catastrophic failure because the SiC fibers, which have significantly higher strains to failure than the CVI SiC matrix, remained intact and held the combustor liner material together. Thus, crack development in SiC/SiC material leads to "graceful" rather than catastrophic failure.

Vendors are currently working to improve the SiC/SiC material. An enhanced SiC/SiC CMC is under development whereby an additive to the matrix acts to seal matrix cracks and thereby prevent oxidation of otherwise exposed fibers. Another possible CMC improvement is that of reducing matrix permeability thereby reducing oxygen permeation to fibers and increasing the CMC modulus.

A promising approach for achieving improved control of temperature and temperature gradients is that of utilizing smart composite structure that is under real time computerized control responding to feedback from sensors monitoring the health of the structure. Such a control system could automatically adjust engine parameters (e.g. fuel injection rates, air to fuel ratio or cooling air flow) to maintain temperature and temperature gradients within the capabilities of the CMC material to avoid crack development.

Table 1-1. Properties of Kyocera Ceramic Materials Available Commercially*

Materials			Silicon Nitride			Silicon Carbide		Zirconia			Alumina
Kyocera No.			SN-220	SN-220M	SN-733	SC-211	SC-221	Z-201N	Z-701N	Z-703	A-479
Color			Black	Gray	Gray	Black	Black	Ivory	Yellow Ocher	Light Gray	White
Bulk Density		–	3.2	3.2	3.2	3.2	3.0	6.0	6.05	5.5	3.8
Water Absorption		%	0	0	0	0	0	0	0	0	0
Vickers Hardness	Load 500g	GPa	HRA 91	HRA 92	HRA 92	HRA 94	HRA 94	12.3	12.7	13.2	16.2
Flexural Strength (4-Point Bending / *3-Point Bending)	R.T.	Kpsi MPa	86 590	98 676	142 980	78 539	71 490	* 142 980	* 199 1370	* 284 1960	* 44 304
	800°C	Kpsi MPa	87 600	98 676	107 735	–	–	* 60 412	* 100 686	* 128 882	* 40 274
	1000°C	Kpsi MPa	74 510	87 600	100 686	68 470	–	* 40 274	* 60 412	* 60 412	* 26 176
	1200°C	Kpsi MPa	47 323	57 392	–	57 392	–	* 24 167	* 30 206	–	–
	1300°C	Kpsi MPa	17 117	–	–	–	–	–	–	–	–
	1400°C	Kpsi MPa	–	–	–	51 353	71 490	–	–	–	–
Fracture Toughness (K_{1C})M.I.		MPa$\sqrt{m}$	5.7	5.9	7.0	5.6	3.4	6.7	5.9	6.9	–
Young's Modulus	R.T.	$\times 10^6$ psi GPa	43 294	43 294	44 304	63 431	54 372	30 206	31 216	37 255	50 343
Poisson's Ratio	R.T.	–	0.28	0.28	0.27	0.16	0.16	0.31	0.31	0.3	0.25
Coefficient of Linear Thermal Expansion	40 to 400°C	$\times 10^{-6}$/°C	2.6	–	2.5	4.0	3.9	10.5	11.5	9.6	7.1
	40 to 800°C		3.2	3.1	3.0	4.4	4.4	11.0	11.8	10.3	7.9
Thermal Conductivity	R.T.	cal/cm·sec·°C	0.05	0.06	0.07	0.15	0.17	0.009	0.009	0.014	0.06
		W/m·K	21	25	29	63	71	4	4	6	25
Specific Heat	R.T.	cal/g·°C	0.16	0.16	–	0.15	0.16	0.12	0.12	0.12	0.19
Heat Shock Resistance	ΔT	°C	550	670	–	400	350	300	350	300	200
Volume Resistivity	R.T.	Ω·cm	$>10^{14}$	$>10^{14}$	–	8×10^4	10^3	2×10^{12}	–	3×10^{12}	$>10^{14}$

ASC-1050

*Kyocera Corp, Kyoto 607, Japan

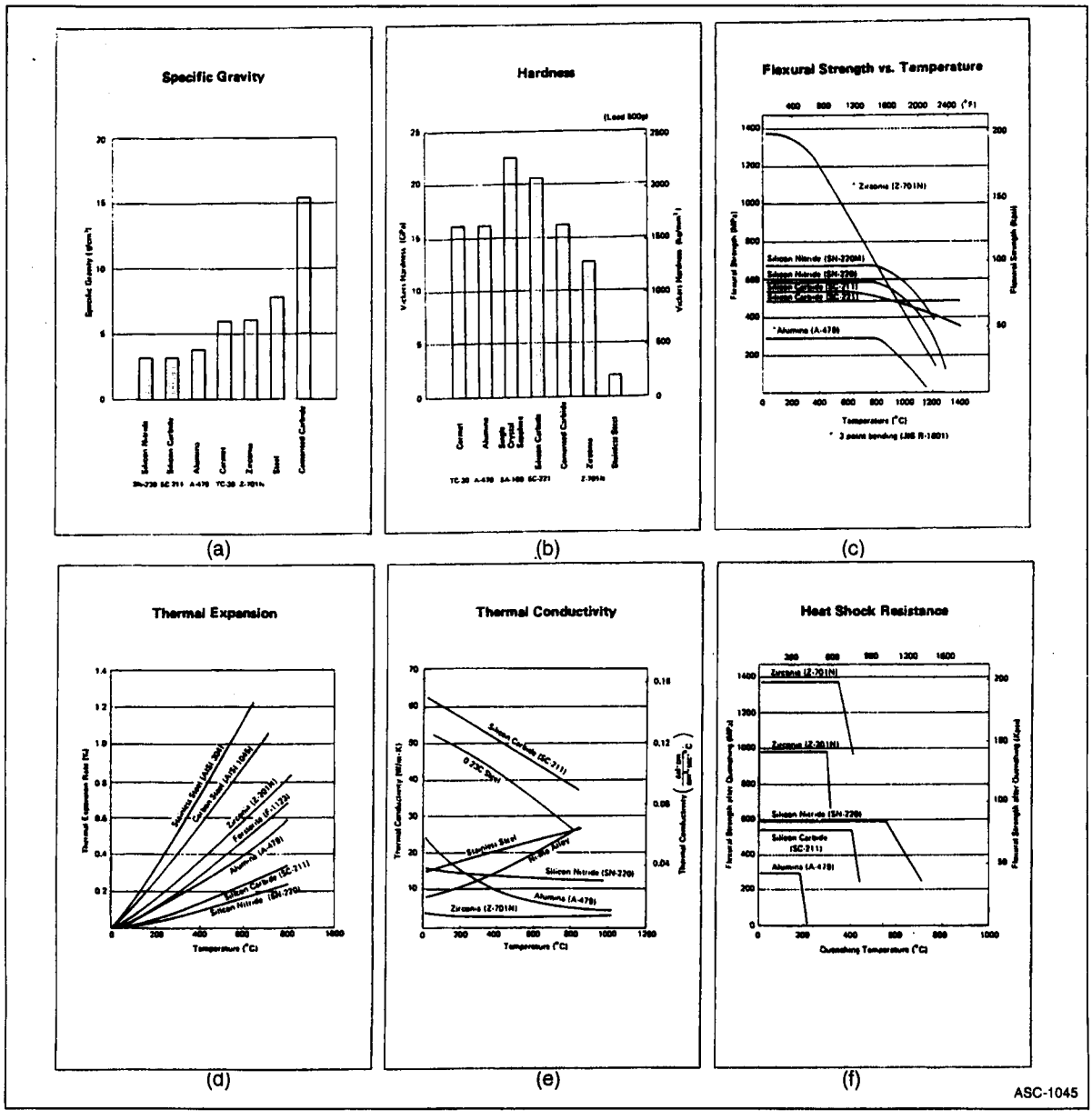

Figure 1-1. Graphic Comparison of Kyocera Ceramic Material Properties Presented in Table 1-1

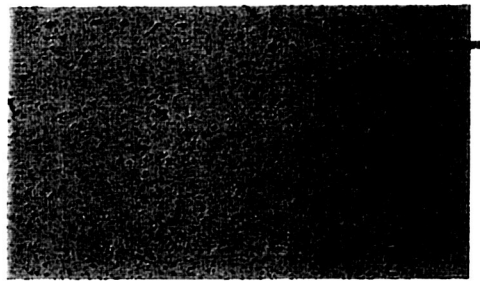

Hexoloy SA Silicon Carbide

Hexoloy SA SiC is a pressureless, sintered form of alpha silicon carbide, with a density greater than 98 percent theoretical. It has a very fine grain structure (8 microns) for excellent wear resistance and contains no free silicon, which makes it highly chemically resistant in both oxidizing and reducing environments.

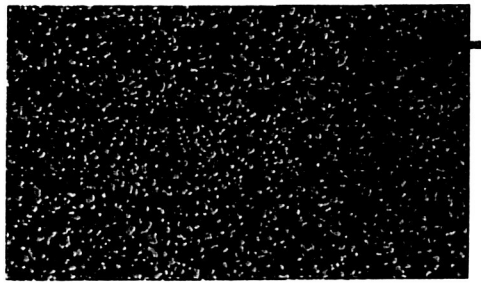

Hexoloy ST Silicon Carbide

Hexoloy ST SiC is a particulate-reinforced, two-phase ceramic composite material with a microstructure consisting of titanium diboride (TiB_2) particles from 1 to 5 microns in diameter in a fine-grain silicon carbide matrix. The TiB_2 particles improve the fracture toughness and strength, while the composite maintains the other desirable properties inherent in the silicon carbide matrix.

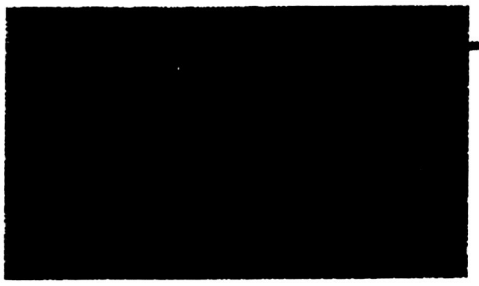

Hexoloy SG Silicon Carbide

Hexoloy SG SiC is a unique, patented analogue of Hexoloy SA SiC. It is a sintered silicon carbide and has no free silicon metal. It is electrically conductive, permitting DC-magnetron sputtering rates approximately half that of aluminum. It also has excellent thermal conductivity.

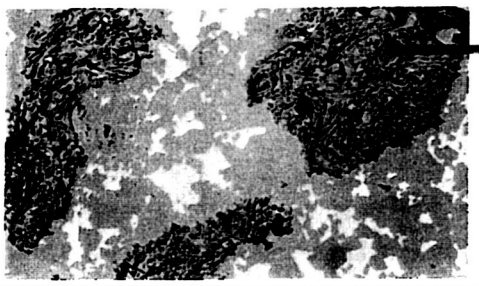

Hexoloy KG Silicon Carbide

Hexoloy KG SiC is a reaction-bonded silicon carbide with free silicon and graphite. Compared with Hexoloy SA SiC, it sacrifices thermal oxidation resistance for improved thermal shock resistance. At very high thermal shock loads, the graphite absorbs uneven expansion, preventing high stress concentrations and failure.

ASC-1046

Figure 1-2. Description of Hexoloy* Silicon Carbide Ceramics Available Commercially

*Trademark of the Carbonundium Company

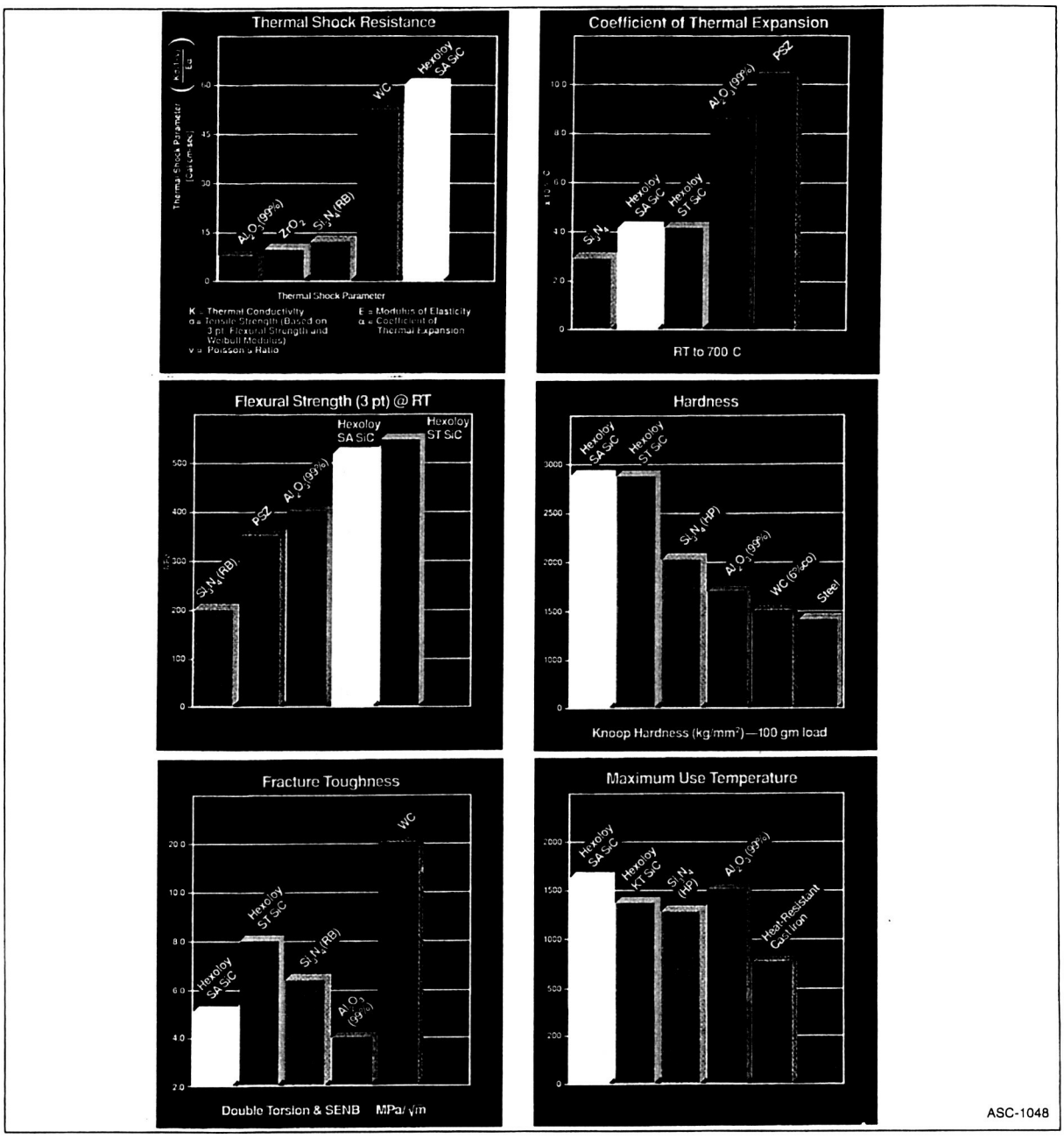

Figure 1-3. Graphical Comparison of Properties of Hexoloy Ceramic Materials Showing Silicon Carbide Ceramics to be Superior in all Properties Shown Excepting the Fracture Toughness of Tungsten Carbide.

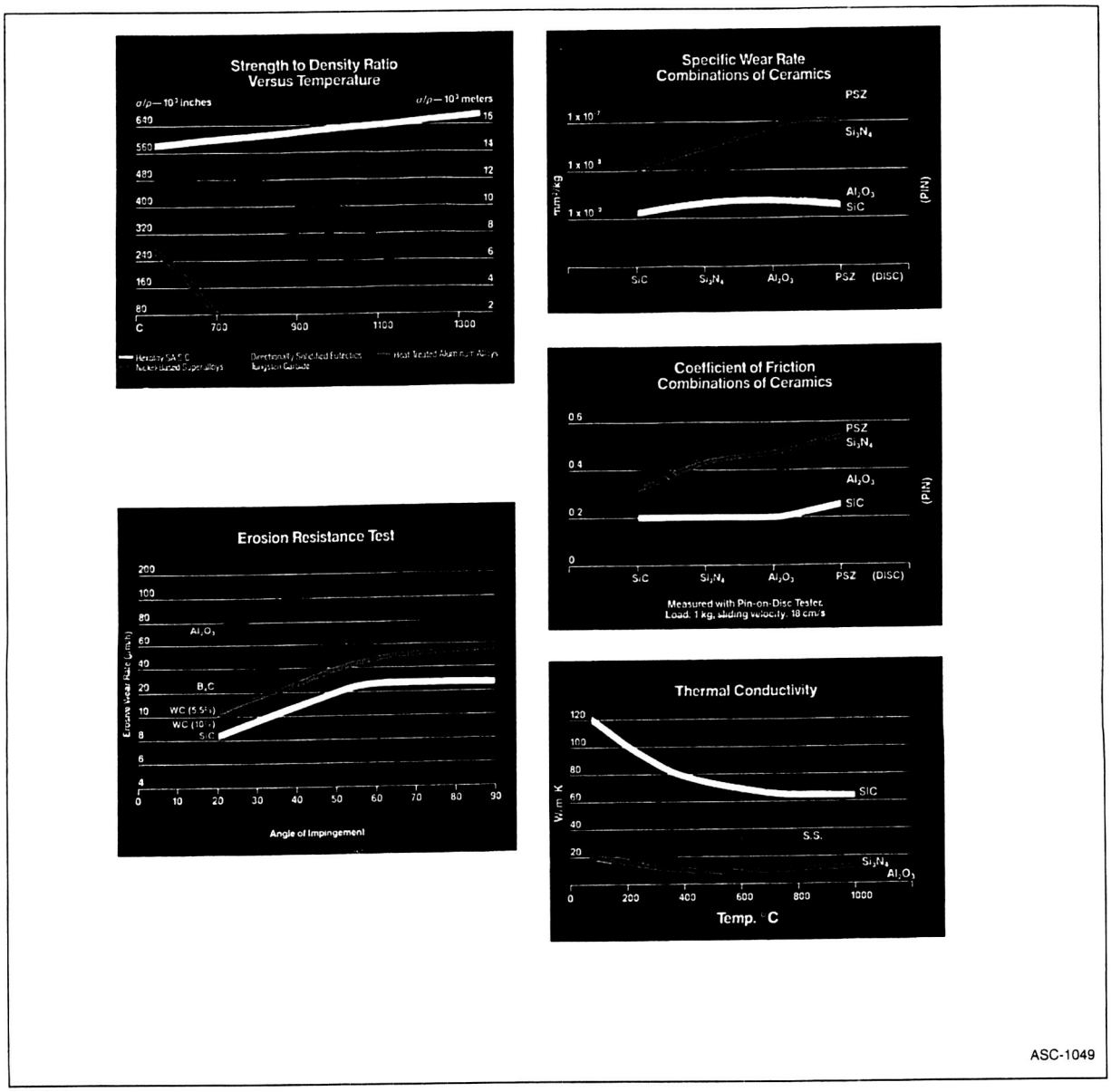

Figure 1-4. Comparison of Properties of Several Commercially Available Hexoloy Silicon Carbide Ceramics

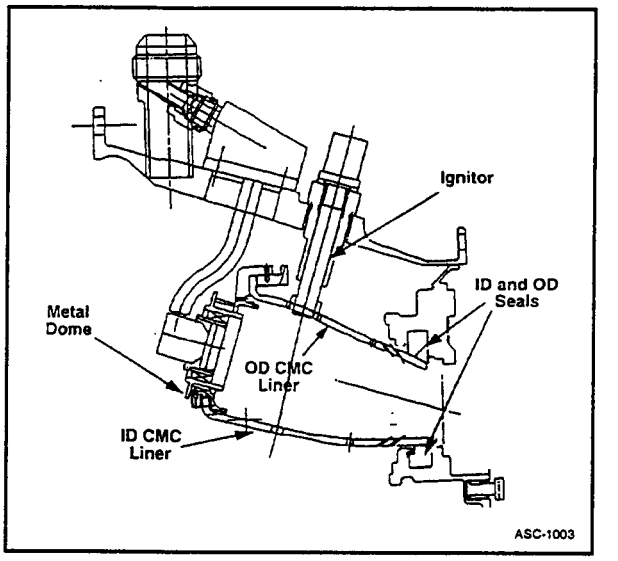

Figure 1-5. Typical Combustor Configuration

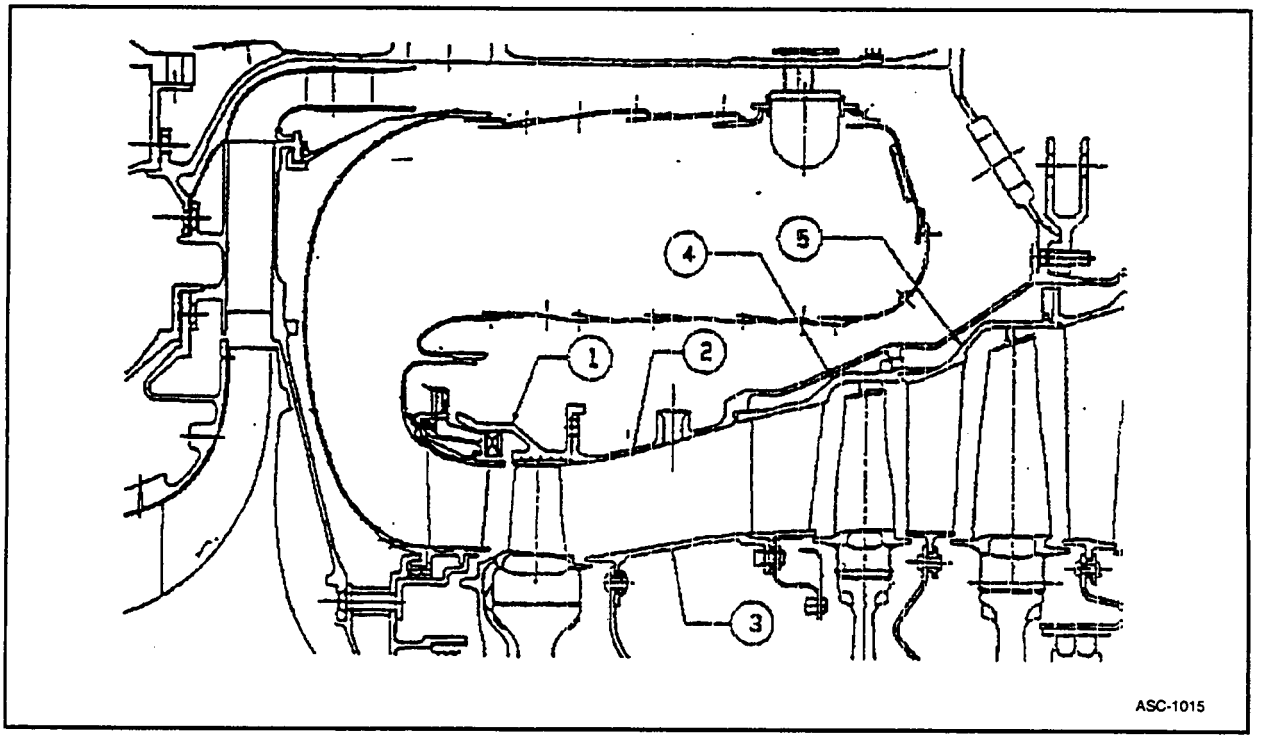

Figure 1-6. Cross-Section of the AE TFE731 as Turbine Engine Identifies Candidate CMC Components; (1) Combustor; (2) HP Turbine Shroud, (2) Inter-turbine Transition Liner (Outer), and (3) Inter-turbine Transition Liner (inner), and (4,5) LP Turbine Shrouds

Smart CMC structure for use in a turbine engine combustor is anticipated to consist of an integrated system whereby sensor information is input to a computer programmed to process this information on the basis of a combustor model and experimentally established limits of critical combustor operating parameters. Establishment of a smart composite system to monitor and act to sustain the health of a CMC combustor requires effort in five areas:

1. Development of sensor application technology to monitor the health of CMC structure,
2. CMC combustor modeling,
3. Establishing parameter sensitivities and limits of CMC combustor operation
4. Simulating combustor response to stresses induced by temperature gradients,
5. Programming a computer to provide real time control of engine operations affecting the combustor health.
6. Modifying digital engine controls to accommodate automated computer control.

The effort of this report was directed towards investigating the feasibility of Items 2, 3, and 4.

2.0 Objectives

The effort of this report is to determine the feasibility of utilizing temperature and/or strain and stress sensor data in a computer program to monitor the health, in real time, of a ceramic gas turbine combustor operating at elevated temperatures (>2000°F) with the ultimate purpose of providing feedback to initiate corrective action should a threat to combustor health occur. This effort entails evaluation of the feasibility of the following objectives:

1. Selection of sensor technology and CMC material for potential use in developing a smart CMC combustor.

2. Development of a finite element simulation model of a sensor equipped, smart, CMC combustor based on and verified with test data.

3. Use of a simulation model and GENOA, NESSUS, and CEMCAN computer codes, to calibrate, and perform: (1) finite element analysis to predict CMC combustor structural response under load, (2) probabilistic analysis of the CMC combustor operating with benefit of sensor input, and (3) probabilistic determination of sensor influence coefficients needed to enhance existing CEMCAN code capability for prediction of the structural response of a CMC combustor with embedded sensors.

4. Modification of existing CMC data bank using CEMCAN to account for material property changes due to embedded sensors.

5. Use of GENOA to assist in design of a ceramic combustor for a gas turbine engine.

3.0 Approach

Sensor methods and technologies, as well as ceramic combustor material selections were based on information from vendors, literature, and Allied Signal, a turbine engine manufacturer with elevated temperature combustor and sensor experience. Allied Signal also supplied the ceramic combustor geometry thus assuring that the model used for finite element simulations was realistic and manufacturable. Extensive finite element simulations to predict structural response and perform probabilistic analyses of the SiC-fiber/SiC-Matrix CMC combustor model, with and without embedded sensors, were performed by using existing GENOA, NESSUS, and CEMCAN computer codes modified as necessary to accommodate demands occasioned by the selection of fiber reinforced combustor material. Simulation results were verified by comparison with test data supplied by Allied Signal. CEMCAN was used for simulations to determine properties of CMC materials with proposed embedded sensors for inclusion in the existing CMC data bank.

The following considerations guided the approach taken to ready the GENOA software:

1. Thermal stresses are major causes of crack formation in a CMC combustor.

2. Combustor health monitoring requires real-time simulation of an operational combustor to detect incipient crack formation resulting from creep and flaw initiated fatigue mechanisms driven largely by temperature gradients.

3. The wide scatter in available CMC test data and CMC processing variations requires calibration of CEMCAN code by probabilistic methods.

4. Uncertainties in temperature distribution can be accounted for within the reliability analysis utilizing experimental data.

5. The involvement of the above considerations can be handled by the GENOA code.

6. The effect of CMC performance caused by application of sensors can be simulated by the probabilistic failure analysis capability of GENOA.

4.0 Sensor Review

4.1 SENSOR SUMMARY

Very few options exist that will provide the desired robust and durable feedback sensor system for strain or elevated temperature measurements on a CMC combustor in an operational turbine engine. Each sensor or system brings with it a combination of hardware, application, or system limitations. For example, all sensor applications except optical pyrometry, fiber optical wave guides, and laser induced fluorescence (LIF) require that leads be attached at some point to the CMC combustor to bring the sensor signal out for data reduction and analysis. Routing of a sizable number of leads and establishing reliable techniques for long term lead attachment to ceramic materials are prime concerns. Although optical pyrometry and laser induced fluorescence avoid the lead routing and attachment problems they require a means of viewing the hot combustor within a confined space and without suffering heat damage or optics degradation due to build up of dirt on the optics. The use of high temperature fiber optic wave guides made of materials such as garnet or sapphire brings with it routing, CMC design, CMC fabrication, and demodulation problems although avoiding the need to attach leads to sensors on the combustor.

All contacting sensors are subject to interdiffusion with substrate material (and any other dissimilar material interfaces) over extended periods at elevated temperatures. Thus stability of sensor readings over time at elevated temperature is critical and must be evaluated. Evaluation of thin film temperature and strain gage sensors at AE has shown these to be stable in bench testing to 1000°C for up to 50 hours. Oxidation, drift, TCE mismatch, and erosion are issues of merit when thin film sensors are evaluated. In the case of optical pyrometry, surface and bulk diffusion as well as surface contamination cause emmissivity changes over time. Promising methods have been developed to take into account these emissivity changes. LIF sensors and Applicote's laser activated SiC temperature sensor (LAT) are also affected by contaminants and elevated temperature diffusion, and as a consequence may also change their characteristics at elevated temperatures and must also be evaluated for long term service. Presently, the Applicote SiC sensor is stable to only 800°F in air making it unsuited for application to a high temperature gas turbine combustor at this time.

Contacting sensors, such as thermocouples, (thin films or wire) or LAT must deal with leadout and attachment issues. All sensor applications, and in particular non contacting methods such as LIF and optical pyrometry, have hardware constraints and access problems to contend with. Current off the shelf contact sensor instrumentation methods are limited by availability of cements for attachment and sensor temperature capabilities. No one technique now provides an overall solution. Presently the most promising approaches appear to be: 1) using optical fiber wave guides to conduct infrared radiation to a remotely located sensor, and 2) using thin film temperature and/or Pd/Cr thin film strain gages.

4.1.1 Optical Fiber Sensors

Optical fiber wave guides can be embedded in fiber reinforced composites to act as sensors that can be used to monitor quasi-static strain, temperature, acoustic emission, and impact location [1]. Optical fiber sensors are rugged, immune to electromagnetic radiation, and have the potential for high level sensitivity, having been used to detect strain on the order of 10^{-8}. Optical fibers would be used primarily for strain and temperature measurements. Fiber optic sensors operate by demodulating a light signal launched into the fiber and relating either demodulated back reflections or through transmission signals to the feature being monitored. As shown in Figure 4-1 light transmitted through a sapphire fiber is reflected off both the near and far sides of a break, (R1 and R2). The times of flight of reflected light can be used to determine the gap distance which is equal to the gage length change.

This can be a complex undertaking because the desired response must be sorted out from multiple reflections of light due to impurities, fiber bending, and changes in parameters such as refractive index. Further, optical time domain reflectometry (OTDR), the only means of locally interrogating perturbations of an optical fiber, usually requires signal averaging to increase the signal to noise ratio. This would preclude use of OTDR for a real time sensing system. Another key requirement of an OTDR is the need for secure bonding between fiber and matrix since slip between fiber and matrix is not detectable. This situation would under-report matrix strain and might even fail to detect a crack in the matrix. Real time reflected light monitoring of a CMC combustor with optical fiber sensors would require embedding a significant number of temperature capable optical fibers such as the sapphire fiber now being explored for this purpose in an on-going Air Force program.

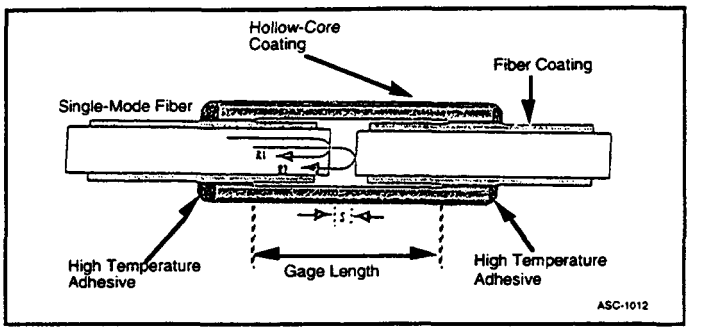

Figure 4-1. Fiber and Sensor Technologies EFPI Optical Fiber Strain Gauge

4.1.2 Clearance Sensors

Capacitive sensors operate by measuring the separation dependent capacitance between two conductive plate electrodes. Ultra high frequency (915 MHz) capacitive position sensors have been demonstrated to have a sensitivity of 10^{-14} m/ $Hz^{1/2}$ [3]. Submillimeter versions can be fabricated using conventional silicon micro-fabrication techniques. However, changes in the separation distance of the electrodes would be a measure of combined thermal and load strains in the region of the composite containing the capacitive sensor. Also, serious problems would arise because leads would have to be attached to the plates and routed to associated electronics. Thus, it appears unlikely that capacitive sensors are suited for application to measure temperature (or strain) in CMC combustors.

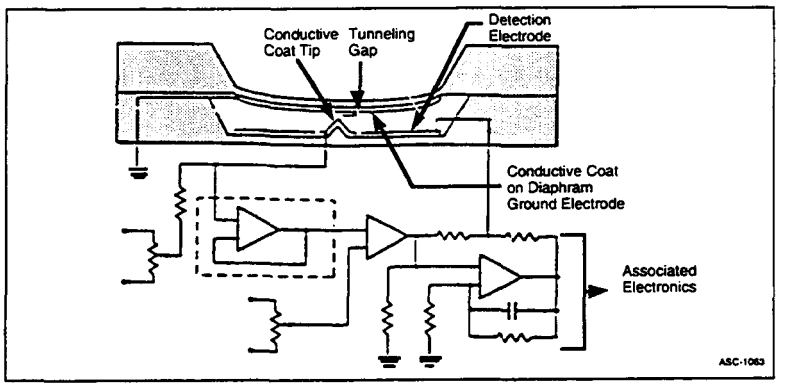

Figure 4-2. Displacement Transducer Based on Quantum Mechanical Tunneling Between Electrodes (NASA JPL)

Semi-conductor sensors utilizing a field emission current that is a function of a gap distance are under development [2] for use as accelerometers, displacement transducers, and infrared sensors (Figure 4-2). However, semi-conductors are currently limited to use at less than 1000°F which precludes their use as sensors in an elevated temperature combustor application.

4.1.3 Thermocouple Sensors

Thermocouple sensors operate on the basis of the electric potential generated at a contacting junction of dissimilar metals or metal alloys. Thermocouples usually consist of two wires joined at one end to form a junction to sense temperature. Associated electronic circuitry measures the electric potential across the dissimilar metal junction relative to a standard reference junction and the result is converted to the corresponding temperature via a calibration curve. Thermocouple technology is well established, low

cost and widely used to measure temperature. Problems arise in using thermocouples to measure temperatures in an operating turbine combustor because of attachment problems, the need to route leads to associated electronics, and (for hot side applications) excessive intrusion into the flow path (Figure 4-3). In particular for ceramics, reliable attachment of thermocouples for long term high temperature applications is difficult to achieve. Recent effort at AE may have solved this problem by using proprietary cements to attach wire thermocouples to a SiC ceramic turbine combustor.

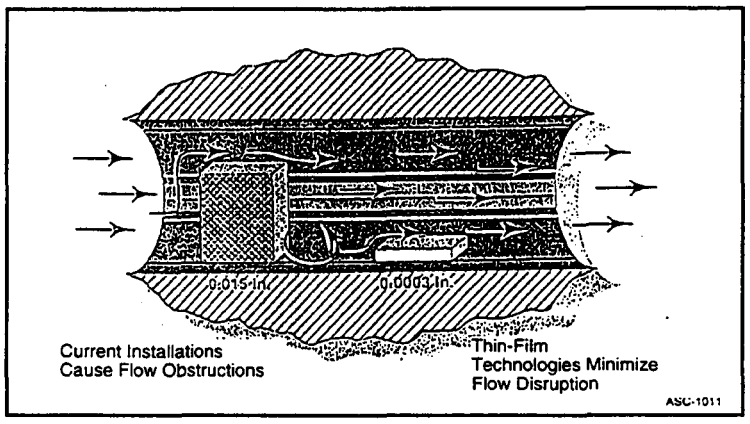

Figure 4-3. Thin Film Sensors Applied to the Inside Surface of Turbine Engine Combustor Offer Negligible Impedance to Flow Compared to Wire Thermocouple Sensors.

4.1.4 Resistive Temperature Device (RTD) Sensors

Resistive sensor technology is well established and widely used. Temperature is determined by measuring the resistance change of a sensing element which has been calibrated as a function of temperature. Platinum is a common metal used as a resistive temperature sensor because of its stability at elevated temperatures. As with thermocouples, lead attachment, and lead routing are difficult to achieve reliably for high temperature applications.

4.1.5 Single Spot Optical (Infrared) Pyrometer

Infrared pyrometry involves single or dual wavelength measurements to accomplish non-contact, remote, line-of-sight measurement of temperatures < 5000°F with response times of 0.5 - 1.5 seconds and accuracies of ~ +/- 1 - 4 percent [3]. Attenuation and bandpass filters can be used to alter the spectral response for specific applications such as measurements through flames. A major factor to be taken into account is the variability of the emissivity of the measurement target. Temperature, surface texture, surface treatment, and observation angle all affect the emissivity. Also, care must be taken to ensure that the radiation being measured is from the target and not background radiation. Some advanced systems can correct the effects of background reflections.

Although pyrometry probes as small as 0.625 inch in diameter by 2.25 inch in length and weighing only 3/4 ounce are available these would not be suitable for use in the hot annular space between the turbine engine combustor and shroud. Rather, it would be expedient to place the probe in a more remote, environment friendly location to avoid heat damage. However, this would require undesirable multiple openings in the combustor shroud. It would appear feasible to avoid openings in the shroud by routing optical fiber wave guides to sense the infrared radiation from a hot surface location. The optical fibers would not have to be in contact with the ceramic turbine combustor but would, however, have to be positioned in close proximity to specified locations.

Optical pyrometers have been employed for temperature measurement in turbine engine development testing where there is adequate access to hardware and the emissivity of the material under test has been adequately characterized. Indeed, optical pyrometers have become the primary tool in the development of advance high temperature turbines for use in modern military and commercial gas turbine engines. They are widely used to provide hot blade detection, full surface mapping, tip rub indication, engine control, abort capability, and general health monitoring during the development

phase and for pre-flight evaluation of advance engine systems[4]. Their use for long term health monitoring of a CMC combustor in an operational turbine engine encounters hardware constraints (especially for smaller reverse flow engines), calibration difficulties and the need to avoid build-up of contaminants on the sensor optics. Nevertheless, the non-contact measuring aspect of optical pyrometer use for temperature measurement is very attractive. Development effort, possibly incorporating optical fibers to conduct infrared radiation from the optical pyrometer sensor, may be required to realize the benefits of this very promising mode of temperature measurement for combustor health monitoring purposes.

4.1.6 2D Optical Pyrometer Imaging Systems

Imaging systems involve scanning a target surface with an optical pyrometer to measure and map the temperature distribution over a specified area. Both mechanical and electronic scanning systems are available. Electronic imaging systems employ detector arrays containing as many as 78080 individual detectors in a space of 0.33 inch by 0.24 inch. Temperature differences of 0.11F can be detected. The use of an electronic scanning imaging system is very attractive from the standpoint of obtaining the temperature distribution over an area. However, hardware constraints (especially for smaller engines), calibration difficulties and the need to avoid build-up of contaminants on the sensor optics would remain as problems to overcome.

4.1.7 Laser Activated Temperature (LAT) Sensors

Applicote associates in Boulder, Co have developed a proprietary process to locally synthesize conductiors and semiconductors as a second phase in insulating alpha SiC and semiconductive beta-SiC. The process employs Nd:YAG and KrF excimer lasers to locally convert the surface of a SiC substate by the addition of oxygen. This laser technique has been used to convert dielectric silicon carbide and aluminum nitride to electro conductors [5, 6, 7, and 8] with near linear resistivity versus temperature relationships up to ~750F (Figure 4-4). Resistivities on the order of 6×10^{-4} ohm are obtained on conversion of an alpha SiC substrate having a resistivity of 10^{11} ohm cm.

The conversion of SiC into an LAT sensor involves formation of amorphous $SiC_{0.73}O_{0.78}$ that can be calibrated in air up to the 800°F. The localized laser activation of SiC can also provide conductive paths on the surface of a SiC substrate. Thus the proprietary laser activation process could potentially be used to provide a SiC/SiC CMC combustor with temperature sensors, and leads, although external leads would still have to be connected to the laser activated surface conductor at some point. Unfortunately, above 800F the $SiC_{0.73}O_{0.78}$ of the LAT sensor becomes sensitive to the presence of oxygen thus precluding use in its present state of development on an elevated temperature SiC/SiC CMC combustor.

4.1.8 Survey of AE Sensor Technology (Allied Signal Engines)

At AE, sensors (Figure 4-5) have been integrated into computational cycles to verify design boundaries under laboratory conditions. Laboratory measurements of temperature and strain are thus available for material characterization. Although very accurate methods are available for measuring temperature and strain (e.g. extensometry for strain and pyrometery for temperature) under laboratory conditions the majority of laboratory instrumentation methods have met with limited success when used on SiC/SiC CMC silicon carbides in test cell and field applications. The rigors of the engine environment; (high temperatures, foreign object damage, accessibility, attachment, and leadouts) severely restrict implementation.

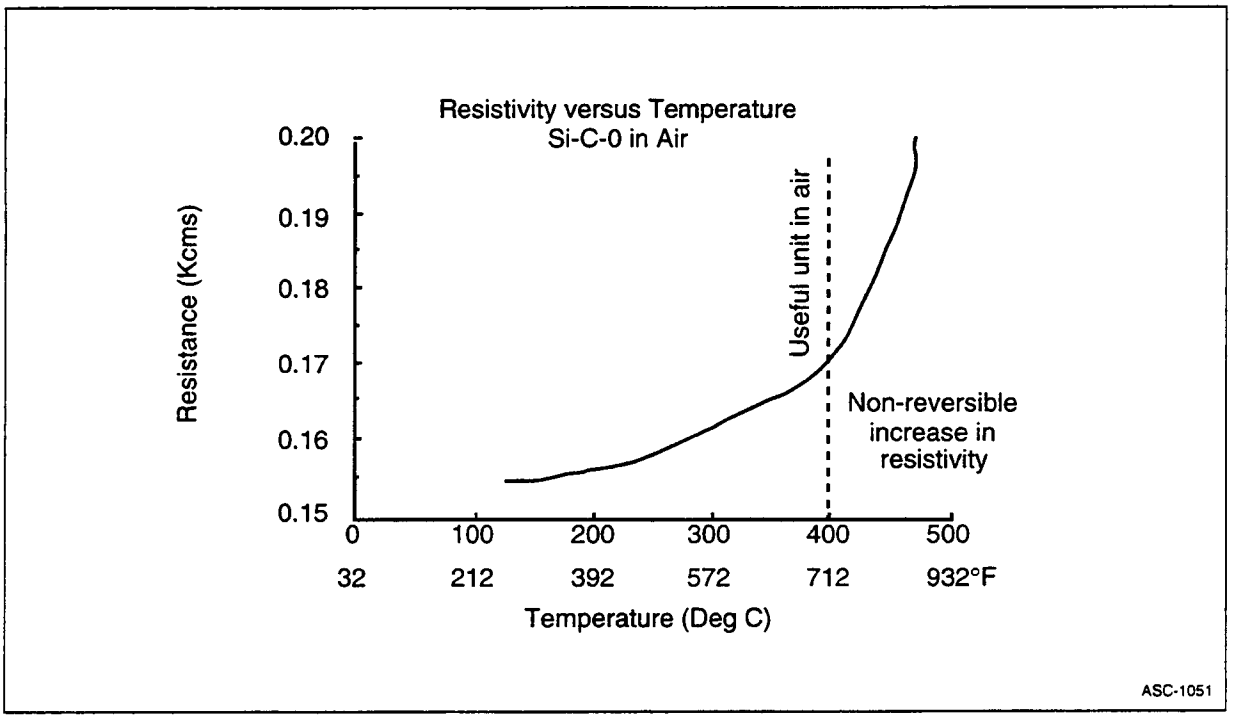

Figure 4-4. Resistance of Laser Activated SiC as a Function of Temperature, to 500°C, in Air

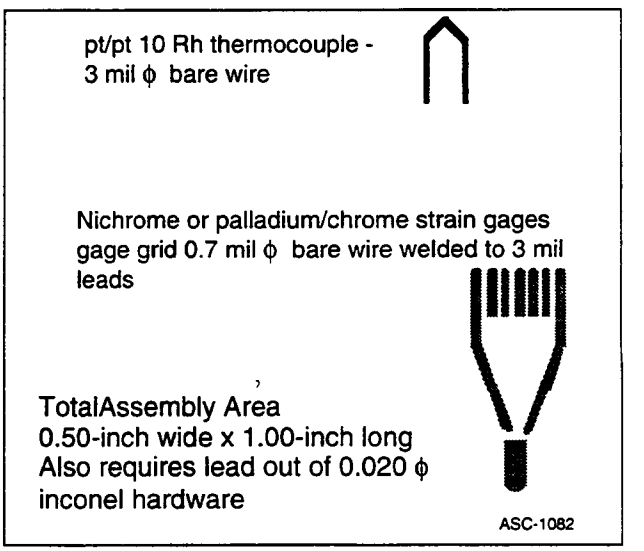

Figure 4-5. Example of AE Sensors Currently Used on SiC Material

AE currently uses conventional wire (swaged) Type K thermocouples to measures temperature when testing silicon carbide CMC in a combustor configuration. Although thermocouple technology is well established and reliable, elevated temperature use must take into consideration possible effects on the electric potential of a thermocouple junction resulting from oxidation, preferential diffusion and/or preferential vaporization of alloying elements in the junction. Mechanical concerns are also present, as the thermocouples must be held securely in place and in contact with the CMC surface and lead-outs must be provided. Attachment reliability and the necessity for leadout wires pose problems at elevated temperatures. Recent work at AE holds promise of providing a reliable means of thermocouple attachment to SiC using a silicate cement with an aluminum oxide substrate and overlayer [9] (Figure 4-6 and Table 4-1). An unfavorable aspect of using wire thermocouples for temperature measurements on the inside surface of a combustor is that thermocouple wire junctions present flow obstructions by protruding on the order of 0.015 inch into the flow path. Thin films protrude as little as 0.0003 inch into the flow path (Figure 4-3) and have exceptional fatigue strength and durability.

Allied Signal is currently working on minimally obstructive thin film sensors to minimize penetration into the flow path. Current technology is applicable to metal and silicon nitride materials. Further thin film development is required to meet applications to SiC/SiC CMC materials.

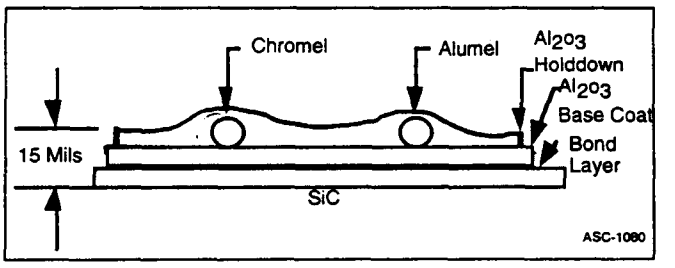

Figure 4-6. A Reliable Means of Thermocouple Attachment to SIC Using a Silicate Cement With an Aluminum Oxide Substrate and Overlayer

Strain in propulsion development rig tests below 800°F is measured with epoxy gages at AE. Difficulties with using these contacting sensors arise because of unfavorable component surface conditions, mismatches between the thermal coefficients of expansion (TCE) of the component material and the sensor wire, and the damaging effects of the rigorous test environment. The use of epoxy strain gages is obviously not suitable for measuring strains in combustors operating at over 2000°F. Free filament wire wound strain gages, are used for tests above 800°F in engine hot sections, are not considered as durable or as unobstrusive as the Pd/Cr thin film strain gage.

AE is actively pursuing the development and application of new sensor and measurement technology for the acquisition of strain and temperature data under engine operating conditions. Currently available, off the shelf technology is inadequate. Effort is required to develop sensors that will provide feedback of temperature and strain during engine operation. This feedback is needed to realize the potential for enhancement of computational structural analysis, calibration of software models, and determination in real time of a component's serviceability condition. A calibration of software models will improve the simulation accuracy and thereby reduce the end design cost. Integration of sensors into a system for real time determination of component serviceability condition will provide the basis for optimizing in-service engine performance and reliability.

Table 4-1. Allied Signal's Flame Spray Techniques for Attaching Wire Thermocouple Elements and Strain Gages to SiC/SiC CMC

The application of a Type K thermocouple on SiC/SiC material is accomplished by the following steps
1. Clean area for t/c installation with Isopropyl alcohol
2. Mix the basecoat thermabond (mixture of sodium silicate, silicon carbide and silicon nitride) and paint a thin layer on the surface identified for t/c installation
3. Flamespray a basecoat of aluminum oxide onto the thermabond basecoat
4. Tape down the 0.003-inch bare wire thermocouple and flame spray it in place using aluminum oxide
5. Remove the tape and respray the area with another layer of aluminum oxide.
6. Before testing in the engine or rig the thermabond basecoat must be cured using a prescribed curing cycle
7. The 0.003-inch wire can now be transitioned to 0.032-inch type K MgO on an adjacent steel ring that is used for mounting the SiC/SiC combustor (if used in the JTAGG combustor).

AE has focused on the following sensor development:

- Thin film contacting sensors, such as strain gages and thermocouples for ceramics and other nonmetallic for use up to 2000°F. AE is actively pursuing development of thin film sensors and has established facilities for this purpose.

- Non-contacting optical pyrometer probes using two-color technology and high speed digital data acquisition and processing.

- Optical non contacting stress measurement technology, involving tip deflection of airfoils to determine mode, frequency, and strain levels via high speed digital processing. This is targeted for fan and compressor blade strain measurements.

- Review of Laser Induced Fluorescence, (LIF) effort at DOE and other government sponsored effort at other engine manufacturers on). This holds promise for temperature measurements via optical techniques similar to pyrometry.

- Cooperative work with Applicote (a small disadvantaged business) to evaluate and demonstrate their new temperature sensor which is embedded into silicon carbides via a laser activation method that changes the surface resistivity.

4.1.9 AE Thin Films

The intent of developing thin film sensors is to improve the reliability and accuracy of engine sensors to measure strain and temperature with minimal intrusion on engine performance. Figure 4-3 shows that a thin film temperature/strain sensor has minimal impact (0.0003 inch) on engine performance in a combustor application as compared to current wire thermocouples (0.015 inch). AE has actively supported and emphasized the need to develop and apply thin film sensors for engine testing and component development. A 360 SF prototype cleanroom constructed in 1988 for use in the development of thin film technology has been followed by construction of a 1200 SF class 100 fully equipped clean room in 1993. AE also maintains an active IR&D program to support the ongoing development and evaluation of thin film processing at the university of Rhode Island, Iowa State University, and divisions within AE.

Thin films offer the following advantages over conventional sensors.

- Minimize airflow perturbation due to the sensor presence
- Minimize component modification and change due to installation
- Have exceptional fatigue life and durability
- Allow highly accurate sensor placement
- Cause negligible aeromechanical distortion
- Exhibit a low profile and low mass below the flow boundary layer.
- Are amenable for application to both metallics and nonmetallic.

Thin film sensors were demonstrated in development engine testing at AE with strain gage programs such as the TFE731 compressor, TFE1042 flight release qualification, TPE331-500 turbine, and the ETEC engine shroud thermal design verification. Thin film thermocouples on SiC have exhibited a linear relationship to 2200°F with temperature measured by a standard reference thermocouple (Figure 4-7) with an agreement of +/-2 percent. Additionally, researchers at AE, GE, JPL, and P&W have successfully used thin film technology on test articles and thin film sensors have been successfully

demonstrated to 2000°F in tests on silicon nitrides. As a result of these successes, AE built and implemented a new 1200 SF state of the art certified class 100 clean room in 1993 to expand the development and application of thin film sensors (Figure 4-8). This facility provides AE with improved control and will accommodate future requirements for thin film sensor technology.

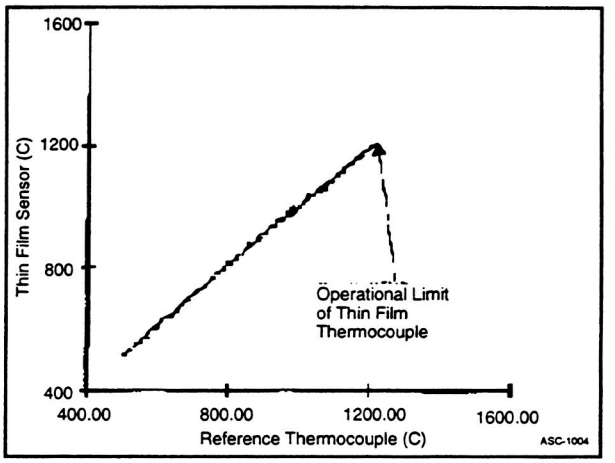

Figure 4-7. Plot Showing Direct Relationship Between AE Thin Film and Reference Thermocouple

Current AE capabilities are tailored to provide thin film resistive temperature devices (RTDs), alloy thermocouples (Type K and Type S), and dynamic strain gages on metallic and nonmetallic components for use in engine testing up to 2000°F. Thin film sensors have been applied to applications are to metallic nickel super alloys, and various non-metallic materials, including silicon nitrides. Figure 4-9 shows examples of current AE thin film sensor applications.

Problem areas still exist in the application of thin film sensors, such as routing of leadouts, techniques for leadout attachment, and surface to sensor passivation coating. Application of thin films has been found to be very dependent on the substrate. Silicon carbides, for example, have surfaces that require significant modification in order to be made amenable to thin film deposition and fabrication processes. Also, since modifications for applying thin films can possibly constitute a defect, their impact on component performance must be evaluated. Although significant, these problem areas appear soluble with further development.

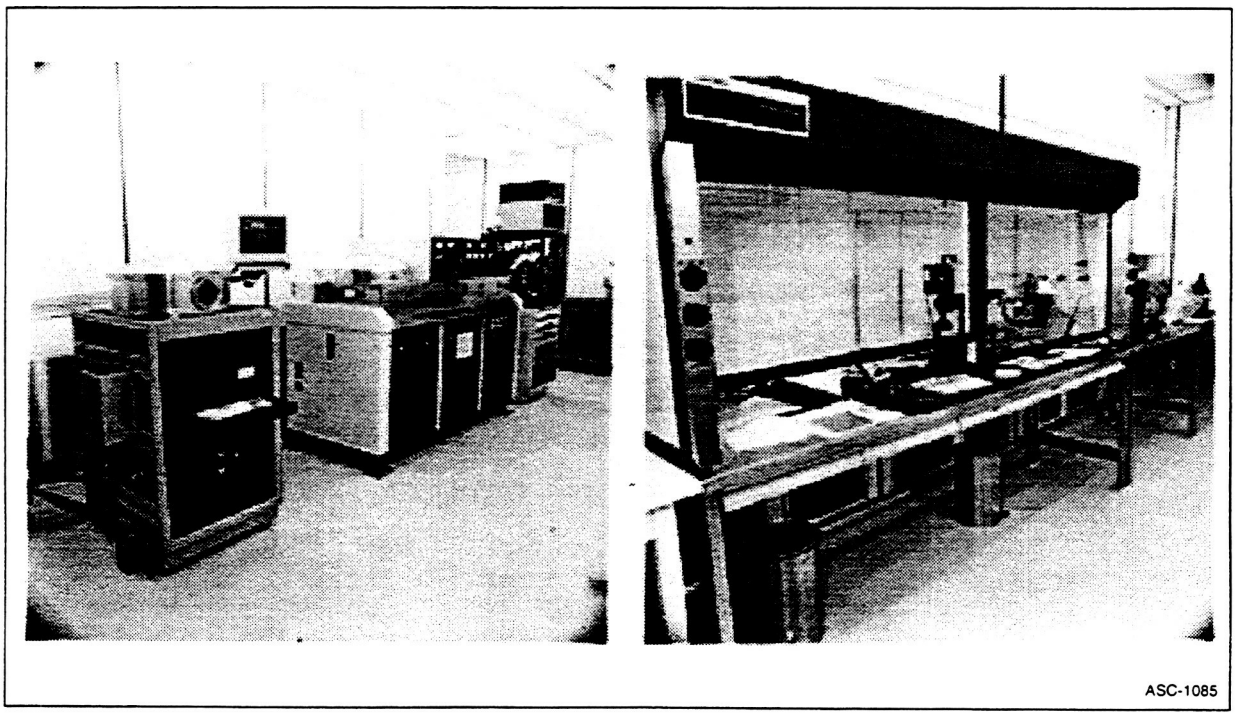

Figure 4-8. Allied Signal's Class 100 Cleanroom With Target Library and Complete Photo Fabrication Capability

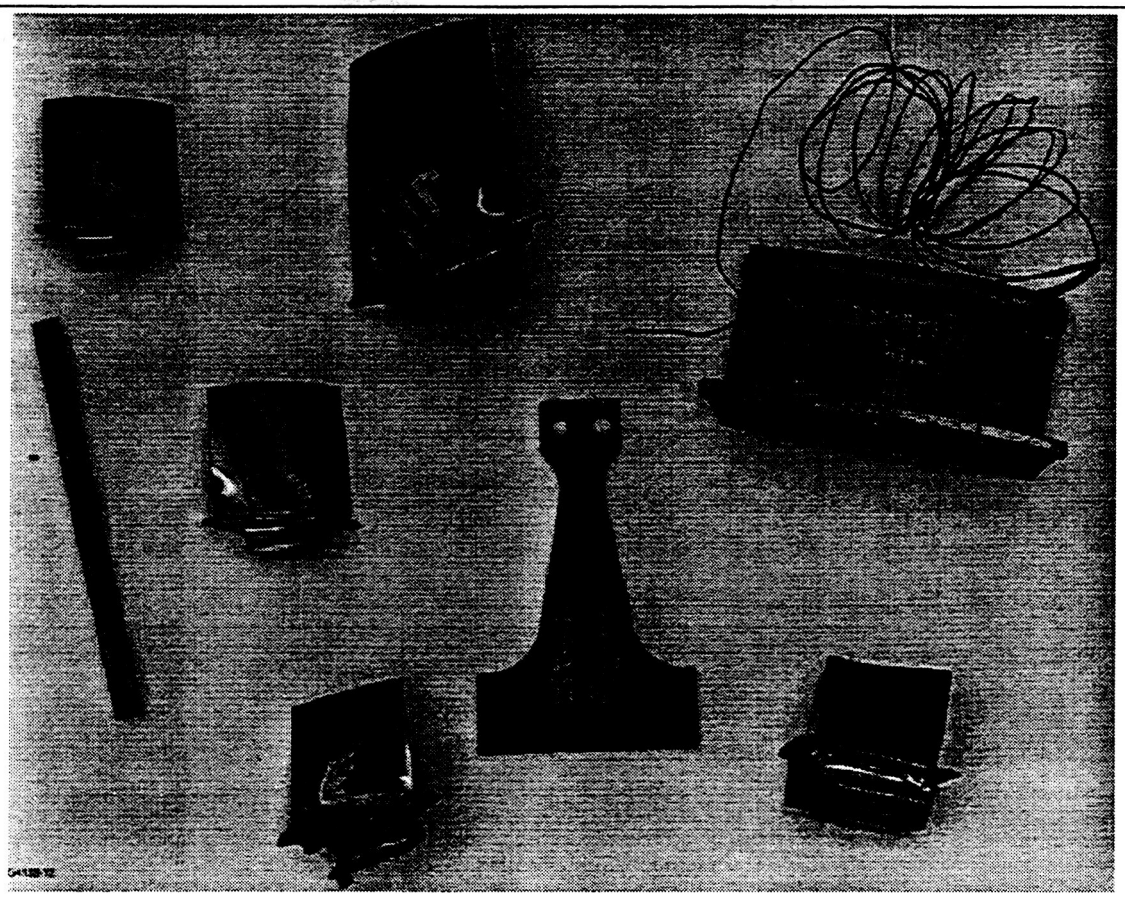

ASC-1078

Figure 4-9. Example of Thin Film Sensor Application at AE

Allied Signal is developing the technology to apply PdCr alloy as a thin film dynamic strain sensor. This effort is currently focused (through IR&D funding) on silicon nitride and metal hot section components. The University of Rhode Island is funded to characterize this alloy as a dynamic strain gage on ASA800 silicon nitride and determine stability, drift, and output as a function of operating temperature. Transitioning NASA thin film technology has assisted this effort.

4.1.10 Pd/Cr Thin Film Strain Sensors

PdCr strain gages are described in papers by Jih-Fen Lei of NYMA, Inc. working at the NASA Lewis Research Center in Cleveland, Ohio [10], to develop a new palladium-13 wt%/chromium (PdCr) alloy. This PdCr alloy was selected by United Technologies Research Center (UTRC) under NASA contract to be the best candidate material for the high temperature strain gage [11]. It is structurally stable up to elevated temperatures and its apparent strain versus temperature characteristic is linear (Figure 4-10 (a)) repeatable and not sensitive to the rates of heating and cooling. Figure 4-11 (a) presents the pattern of a dynamic strain gage made of a PdCr thin film; the thickness of the PdCr is approximately 8 μm. The PdCr static strain gage (Figure 4-11 (b)) contains a platinum RTD to provide compensation for the linear effect of temperature on the resistance of PdCr. The Pt element, 5 μm thick, is located around the PdCr gage grid and is connected to the adjacent arm of a Wheatstone bridge circuit to minimize the temperature effect. The fabrication of thin film gages involves surface preparation, sputter-deposition, photolithography patterning and chemical etching techniques. The lead wires which connect to the measurement circuits are attached to the thin film gages by means of parallel gap welding.

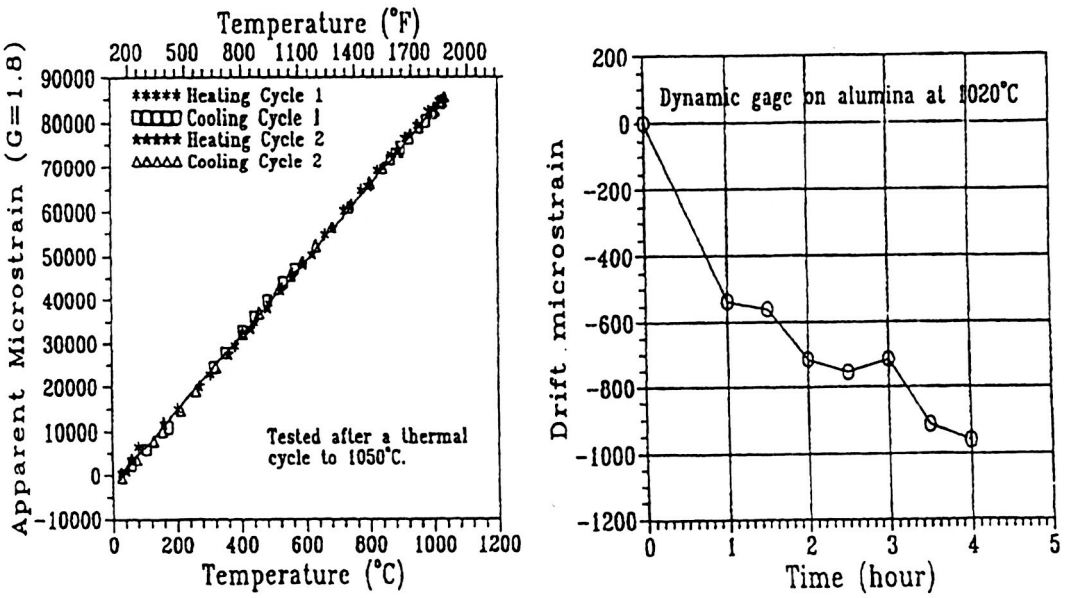

a) Apparent Strain

b) Drift Strain

ASC-1036

Figure 4-10. Apparent Microstrain Versus Temperature of a NASA Lewis Dynamic Pd/Cr Thin Film Strain Gage and Associated Drift in Microstrain as Function of Time

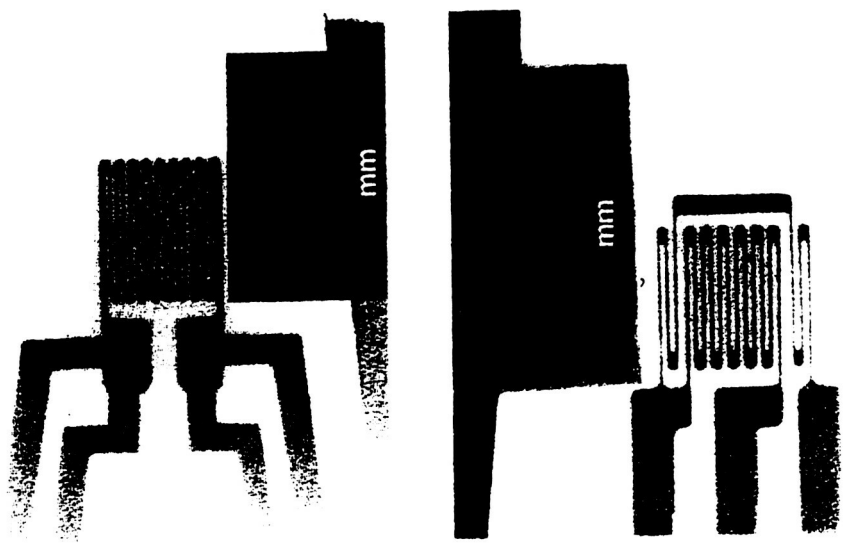

(a) Dynamic Gage

(b) Static Gage

ASC-1037

Figure 4-11. Pd/CR Thin Film Strain Gages From NASA Lewis Research Center, Cleveland, Measures Static and Dynamic Strain to 1,040°C

A portable version of a PdCr thin film gage (i.e., one fabricated on a transportable metal skin) is shown in Figures 4-12 (a) and 4-12 (b). The lead attachments required are evident in Figure 4-12 (b).

The apparent strain of a PdCr dynamic strain gage is stable and repeatable between thermal cycles to 1020°C (1870°F) (Figures 4-10 (a) and 4-10 (b)). The apparent strain sensitivity is approximately 85 με/°C. The drift stain of the gage at 1020°C is approximately 250 με /hour [10].

The apparent strain of a PdCr static strain gage, Figure 4-13, is stable and repeatable within ±200 με with a sensitivity less than 3.5 με/°C in the entire temperature range after cycling to 1020°C. The apparent strain of this PdCr compensated thin film gage can be corrected to within ±200με if the uncertainty in temperature measurement is within 57°C. The mechanical response as measured by a Wheatstone bridge circuit is linear in both tension and compression application (Figure 4-14). Thin film PdCr static strain gages hold significant potential for application to monitor the health of CMC combustors in gas turbine engines.

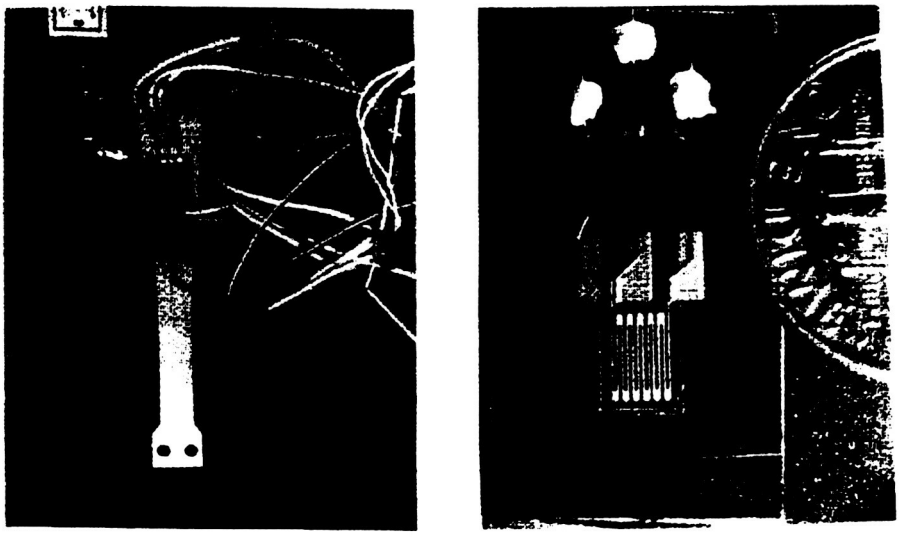

(a) Before welding to a substatic (b) After welding to a substatic

ASC-1035

Figure 4-12. A NASA Lewis Pd/Cr Thin Film Gage Made Portable by Application to a Metal Shim for Attachment by Welding

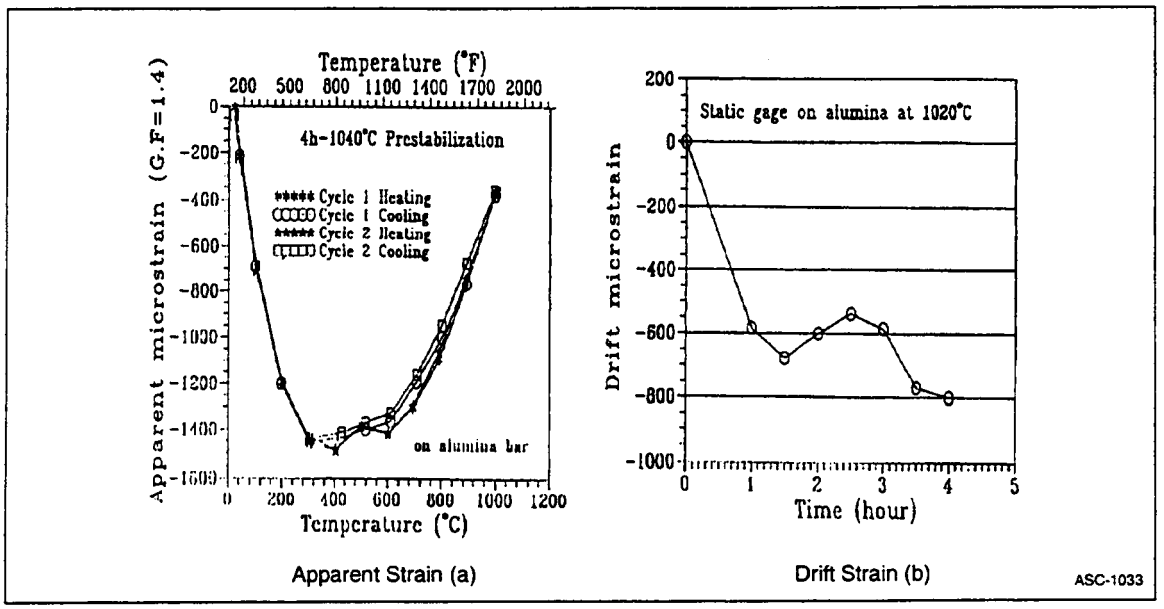

Figure 4-13. Static Pd/Cr Strain Gage Characteristics

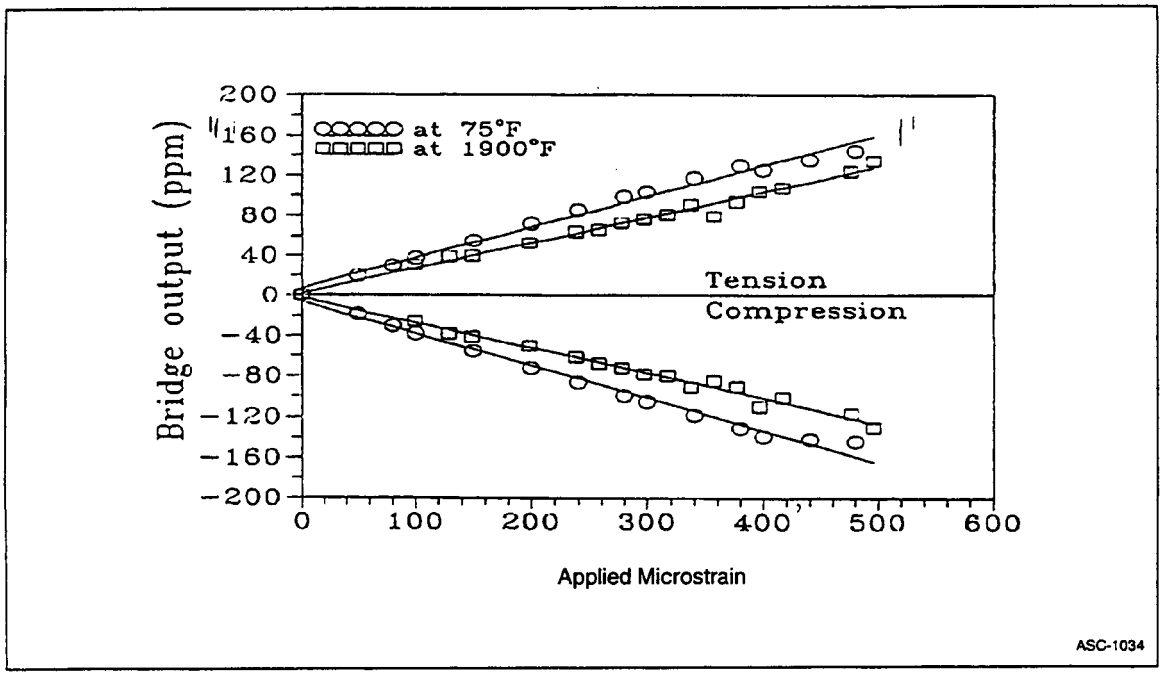

Figure 4-14. Linear Mechanical Strain Response in Tension and Compression

4.1.11 Radiation Pyrometry

AE has used optical pyrometry for a variety of testing requirements over a cross section of product lines, in both laboratory material evaluations and engine component testing. Single spot, single color and dual wavelength pyrometry have been used. Recently, an advanced high speed digital data acquisition system has been designed and employed for use in testing. Scanning 2D, 2 color pyrometry is in the development process. This technique is probably the best candidate for the measurements

required for computational code calibration. However, hardware constraints can limit accessibility to many of the hot section components in reverse flow engines (axial flow combustor engines are the most amenable in this regard). Emissivity variations on exposure of CMCs to elevated temperatures must be taken into account. Effort at NASA-LeRC is addressing this problem by providing a means of computationally handling these emissivity changes. Successful resolution of these problems would make optical pyrometry an important non intrusive means of temperature measurement. This holds great promise for the application of pyrometry to CMC temperature measurements.

4.1.12 Laser Induced Fluorescence (LIF)

LIF was developed by the DOE, and Los Alamos National Labs specifically as an alternative to the use of radiation pyrometry. It was recognized that the instability of the emmissivity for non metallic materials such as CMCs would be a formidable barrier to measurements on operational hardware. LIF uses a rare earth phosphor in a base oxide to measure temperature via a pulsed laser activation-decay time evaluation. Demonstration of the viability of LIF technology has been sponsored by the USAF/WPAFL. Primary demonstrator work at Allison Engine Co in Indianapolis, IN. is focused on LIF materials, such as europium doped yttrium oxide, applied to component surfaces via plasma spray or paint and fire processes. Among the critical aspects of phosphor application are that it must be strongly adherent to and uniformly dispersed on the substrate.

LIF temperature measurement technology is dependent on the availability of phosphors that will meet the temperature range of interest. (Figure 4-15) Adherence needs to be evaluated for each substrate/phosphor combination. The use and application of LIF as opposed to optical pyrometry may be a trade off depending on emissivity, material selection and hardware issues. Both require optical access to measure temperatures. LIF requires use of a probe, provision for the use of a laser to activate a phospor, and a means to measure phosphor decay time (Figures 4-16 and 4-17).

LIF probes can be used for both flowpath temperature measurements (Figure 4-16) or the phosphors can be applied directly to component surfaces to provide surface temperature measurements. LIF optical access and hardware constraints limit its applicability. Phosphor adherence, erosion, and durability are issues of merit for survivability.

4.1.13 Thermography

Optical thermography is a technology that is used extensively to provide thermal maps of components during development testing. It requires optical access to allow for camera viewing of the test location or article. Thermographic mapping is a very practical tool for rig and engine tests. Various off-the-shelf systems are available commercially. However, thermography is not suitable to provide feedback for control of an operating gas turbine engine.

4.1.14 Acoustic Emission

"Smart patches" containing an acoustic emission sensor in the form of a piezoelectric transducer, a rosette strain gage, and associated eleectronics on a flexible substrate have been employed by Northrup under Air Force contract WL=TR-93-3109 to detect flaw development at room temperatures in aluminum and graphite/epoxy composite panels. It was concluded that acoustic emission technology is promising but significant development is required before reliable analysis of geometrically complex structures can be made. Further, acoustic e4mission requires bulky equipment and significant operator expertise. Space limitations and elevated operating temperatures make it unrealistic to consider the use of acoustic emission sensors for health monitoring of CMC combustors.

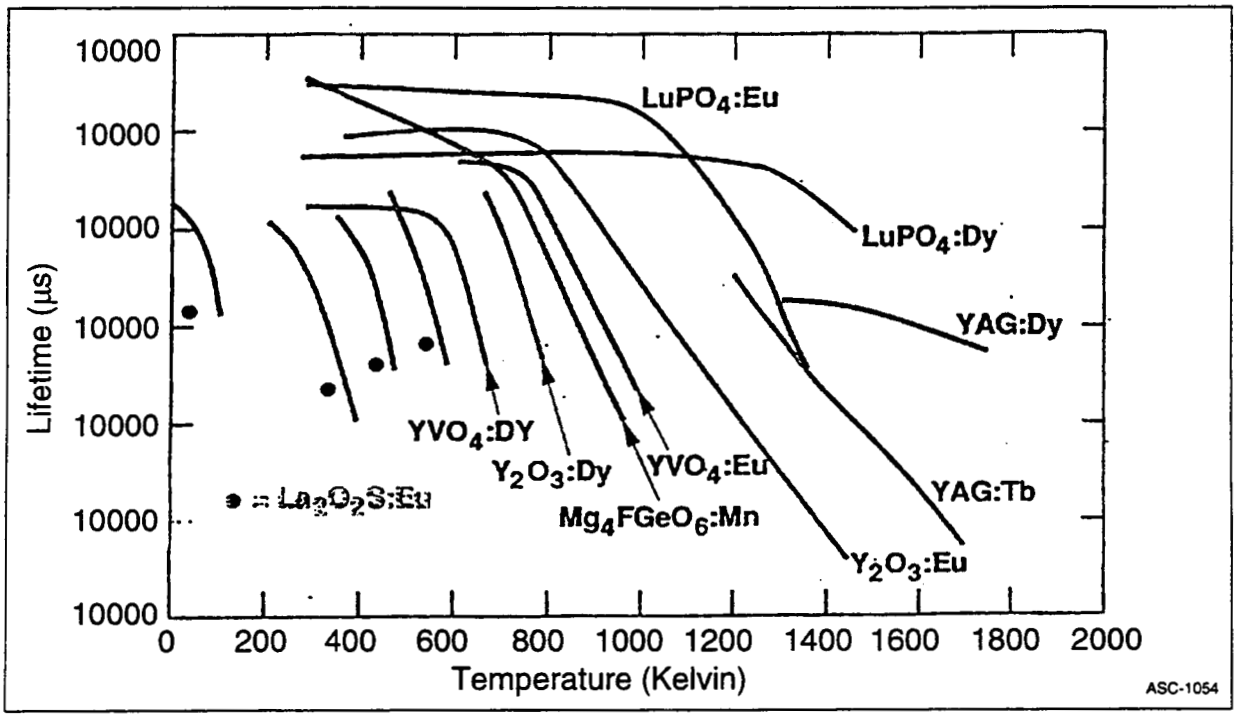

Figure 4-15. Lifetime of Various Phosphors as Functions of Temperature

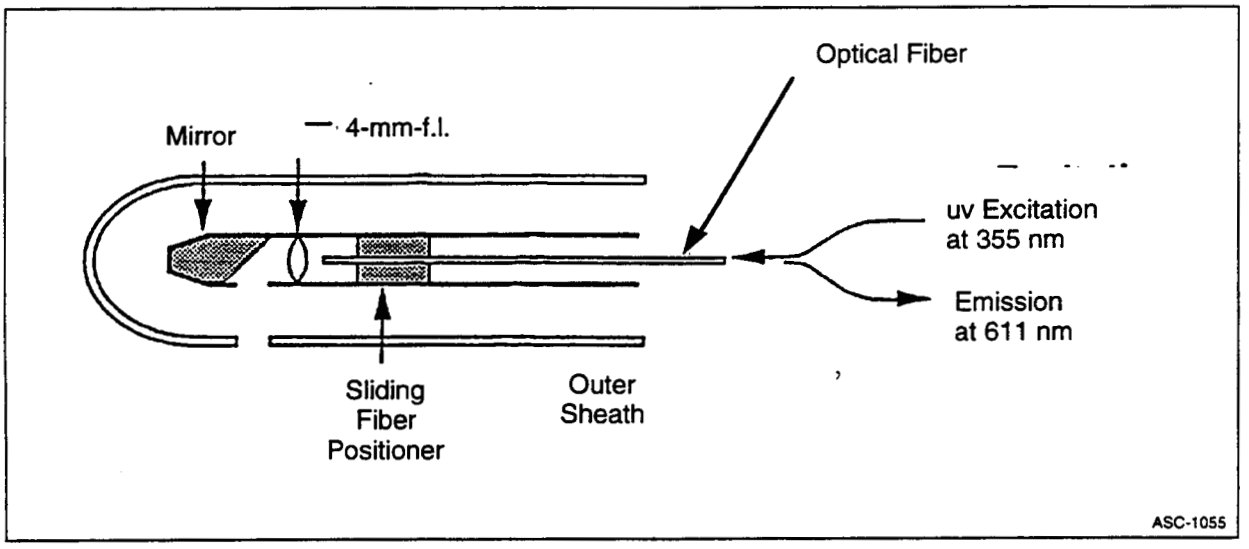

Figure 4-16. Laser Induced Fluorescence Probe

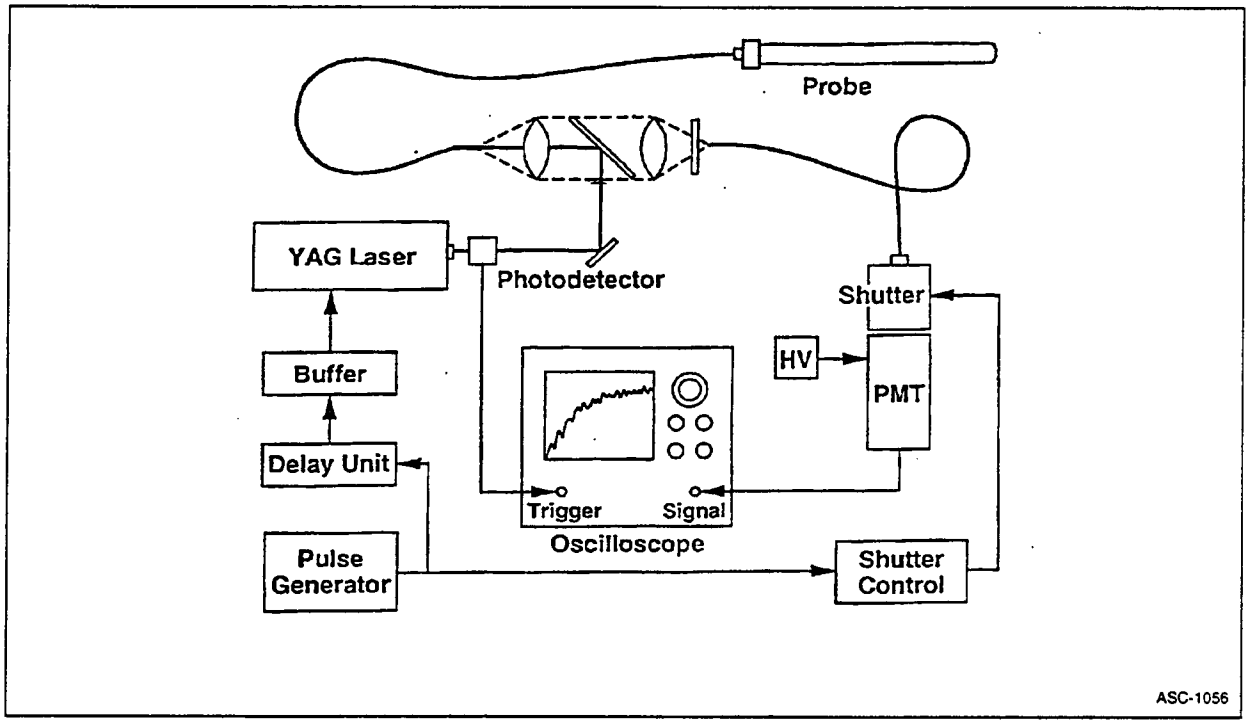

Figure 4-17. Laser Induced Fluorescence Sensor Schematic

4.1.15 ULTRASOUND

As with acoustic emission, ultrasound requires a contacting transducer, associated bulky equipment, and significant operator expertise. This plus elevated operating temperatures and limited space make it unrealistic to consider the use of ultrasound as a sensor mode for health monitoring of CMC combustors.

5.0 Material Selection

Currently available monolithic ceramic materials are not suitable for elevated temperature use in turbine engine combustors. This is the case primarily because their fracture toughness is well below acceptable values of 20 ksi $in^{1/2}$ or more as is evident in Table 5-1D. However, the fracture toughness of ceramic materials can be significantly improved by incorporating recently developed high strength ceramic fibers with elongations to failure greater than that of bulk ceramics by a factor of at least two. The resulting ceramic matrix composites (CMC)s have fracture toughness values of 20 to 26 ksi $in^{1/2}$ making them attractive for elevated temperature use in turbine engine combustors. In particular, the use of CMCs is regarded as being potentially key to meeting the performance goals of the Integrated High Performance Turbine Engine Technology (IHPTET) Phase II gas turbine engine program.

Selection of a CMC material for use in a combustor liner is a task requiring intimate knowledge of combustor requirements and test facilities to characterize CMC candidates and verify their potential for application to a combustor liner. This is an undertaking best performed by a gas turbine engine manufacturer. As such a manufacturer with a strong interest in advanced turbine engine development, Allied-Signal Engines (AE) has devoted considerable effort towards CMC materials selection, characterization, and sub-element and sub-scale studies to support development of a full scale CMC combustor.

The CMC materials considered by AE for combustor use included SiC matrix composites with SiC and C fiber reinforcement, glass-ceramic matrix (calcium, lithium, and magnesium aluminosilicates) composites with both SiC and C fiber reinforcements, and alumina matrix composites with SiC fiber reinforcement. CMCs with C fiber reinforcement were ruled out for manned rated engines. The C fibers would be rapidly degraded by the hot oxidizing environment of a combustor should a crack occur in the matrix. Monofilament fibers such as Textron's SCS6 SiC fiber were not acceptable because their stiffness allows only a 1/4 in radius bend which limits preform preparation by braiding and weaving operations. Glass-ceramic matrix and alumina matrix composites were rejected because of manufacturability and temperature capability concerns. The SiC-matrix/SiC-fiber composites made with a carbon coated SiC (Nicalon) fiber and a chemical vapor infiltrated (CVI) SiC matrix by Du Pont Lanxide Composites Inc. (DPLC) were considered the optimum choice. The carbon coating on the SiC fiber provides a weak fiber-to-matrix interface bond that promotes fracture toughness.

An important aspect in the selection of a suitable CMC for combustor application was that of providing the best fiber architecture from the standpoints of thermal-mechanical capability of combustor liners and their manufacturability. To this end a fiber architecture study was initiated by AE that included detailed interaction with composite and preform suppliers and limited property testing. Detailed investigation of various weaves and braids led to the selection of either 2D or 3D braid as the optimum fiber architecture. Tensile tests and stress rupture tests (the critical design parameter) were performed along with thermal tests to measure thermal conductivity, expansion, emissivity, and specific heat at temperatures up to 2500°F.

The DPLC CMC material initially selected by AE for use in combustor sub-element testing was externally coated with Chromalloy RT-42 to provide oxidation protection. Testing of combustor sub-elements was conducted under aggressive simulated service conditions intended to deliberately damage the sub-elements so potential failure modes could be observed. Some localized cracks were initiated but the fibers held the combustor intact and global failure did not occur. The results were considered favorable in that reaching the goal of a high temperature ceramic combustor liner appeared achievable, requiring a reasonable level of improvement in SiC/SiC CMC material combined with simulation modeling to obtain a more detailed understanding of a CMC combustor. Thus SiC/SiC CMC

Table 5-1. Properties of Ceramic Materials with Potential for Combustor Applications - Part A

No. 1	Temp (F)	Temp (C)	Matrix	Fiber	% Fiber	%Porosity
1	70	21	---	Nicalon	100	---
2	70	21	---	Nicalon	100	---
3	1832	1000	---	Nicalon	100	---
4	2192	1200	---	Nicalon	100	---
5	70	21	---	Nicalon (12.3 wt% O)	100	---
6	70	21	---	Hi-Nicalon (0.5 wt% O)	100	---
7	70	21	---	~SiC Nicalon (<0.5 wt% O)	100	---
8	70	21	---	T300 C	100	---
9	70	21	---	NEXTEL	100	---
10	70	21	SiC (CVI process)	---	0	---
11	1832	1000	SiC (CVI process)	---	0	---
12	2192	1200	SiC (CVI process)	---	0	---
13	70	21	SiC (Process not given)	---	0	---
14	70	21	SiC (Sintered)	---	0	---
15	70	21	SiC (Reaction Bonded)	---	0	---
16	70	21	SiC (Nitride Bonded)	---	0	11.5
17	77	25	SiC (Silicate Bonded)	---	0	13
18	68	20	Al2O3	---	0	15
19	68	20	Al2O3	---	0	10
20	68	20	Al2O3	---	0	6
21	68	20	Al2O3	---	0	4
22	68	20	Al2O3	---	0	0.5
23	68	20	Al2O3	---	0	0.1
24	1832	1000	Al2O3	---	0	15
25	1832	1000	Al2O3	---	0	10
26	1832	1000	Al2O3	---	0	6
27	1832	1000	Al2O3	---	0	4
28	1832	1000	Al2O3	---	0	0.5
29	1832	1000	Al2O3	---	0	0.1
30	68	20	AlN	---	0	---
31	68	20	MgAl2O4	---	0	---
32	68	20	xAl2O3ySiO2	---	0	---
33	68	20	Al3(Mg,Fe)2Si5AlO18	---	0	---
34	68	20	SiN (ReactionBonded)	---	0	---
35	68	20	SiN (Hot Pressed)	---	0	---
36	77	25	Boron Carbide	---	0	---
37	70	21	Zirconia (MgO partial Stab.)	---	0	---
38	70	21	Zirconia (Y2O3 partial Stab.)	---	0	---
39	70	21	Zirconia (Y2O3 fully Stab.)	---	0	---
40	77	25	Al2O3	Nicalon	40	---
41	1832	1000	Al2O3	Nicalon	40	---
42	2192	1200	Al2O3	Nicalon	40	---
43	73	23	SiC	Nicalon	40	8 - 12
44	1000	538	SiC	Nicalon	40	8 - 12
45	1830	1000	SiC	Nicalon	40	8 - 12

Table 5-1. Properties of Ceramic Materials with Potential for Combustor Applications - Part B

No.	Temp (F)	Temp (C)	Matrix	Fiber	D (lbs/in3)	E (MSI)
1	70	21	---	Nicalon	0.093	29.01
2	70	21	---	Nicalon	0.0921	27.4
3	1832	1000	---	Nicalon	---	21.8
4	2192	1200	---	Nicalon	---	18.3
5	70	21	---	Nicalon (12.3 wt% O)	---	31.91
6	70	21	---	Hi-Nicalon (0.5 wt% O)	---	39.16
7	70	21	---	~SiC Nicalon (<0.5 wt% O)	---	58.06
8	70	21	---	T300 C	0.065	31.91
9	70	21	---	NEXTEL	0.112	30
10	70	21	SiC (CVI process)	---	0.1156	54
11	1832	1000	SiC (CVI process)	---	---	54
12	2192	1200	SiC (CVI process)	---	---	54
13	70	21	SiC (Process not given)	---	0.1163	50.76
14	70	21	SiC (Sintered)	---	0.11	58
15	70	21	SiC (Reaction Bonded)	---	0.11	57
16	70	21	SiC (Nitride Bonded)	---	0.09	22
17	77	25	SiC (Silicate Bonded)	---	0.093	13.2
18	68	20	Al2O3	---	0.123	32
19	68	20	Al2O3	---	0.13	40
20	68	20	Al2O3	---	0.1335	44
21	68	20	Al2O3	---	0.1343	44
22	68	20	Al2O3	---	0.14	54
23	68	20	Al2O3	---	0.143	56
24	1832	1000	Al2O3	---	---	---
25	1832	1000	Al2O3	---	---	---
26	1832	1000	Al2O3	---	---	---
27	1832	1000	Al2O3	---	---	---
28	1832	1000	Al2O3	---	---	---
29	1832	1000	Al2O3	---	---	---
30	68	20	AlN	---	0.12	43
31	68	20	MgAl2O4	---	0.13	37
32	68	20	xAl2O3ySiO2	---	0.1	22
33	68	20	Al3(Mg,Fe)2Si5AlO18	---	0.09	12
34	68	20	SiN (ReactionBonded)	---	0.09	26
35	68	20	SiN (Hot Pressed)	---	0.12	45
36	77	25	Boron Carbide	---	0.087	42
37	70	21	Zirconia (MgO partial Stab.)	---	0.21	29
38	70	21	Zirconia (Y2O3 partial Stab.)	---	0.22	29
39	70	21	Zirconia (Y2O3 fully Stab.)	---	0.2	25
40	77	25	Al2O3	Nicalon	0.1	17.8
41	1832	1000	Al2O3	Nicalon	0.1	---
42	2192	1200	Al2O3	Nicalon	0.1	---
43	73	23	SiC	Nicalon	0.083	20.5
44	1000	538	SiC	Nicalon	---	22
45	1830	1000	SiC	Nicalon	---	21

Table 5-1. Properties of Ceramic Materials with Potential for Combustor Applications - Part C

No.	Temp (F)	Temp (C)	Matrix	Fiber	Ts (ksi)	Elong(%)
1	70	21	---	Nicalon	---	1.5
2	70	21	---	Nicalon	435	1.59
3	1832	1000	---	Nicalon	---	---
4	2192	1200	---	Nicalon	---	---
5	70	21	---	Nicalon (12.3 wt% O)	435	1.36
6	70	21	---	Hi-Nicalon (0.5 wt% O)	406	1.04
7	70	21	---	~SiC Nicalon (<0.5 wt% O)	435	0.75
8	70	21	---	T300 C	---	1.5
9	70	21	---	NEXTEL	250	---
10	70	21	SiC (CVI process)	---	2	0.0037
11	1832	1000	SiC (CVI process)	---	---	---
12	2192	1200	SiC (CVI process)	---	---	---
13	70	21	SiC (Process not given)	---	51	0.1
14	70	21	SiC (Sintered)	---	---	---
15	70	21	SiC (Reaction Bonded)	---	44.5	0.08
16	70	21	SiC (Nitride Bonded)	---	3	0.014
17	77	25	SiC (Silicate Bonded)	---	1	0.0075
18	68	20	Al2O3	---	22	0.69
19	68	20	Al2O3	---	32	0.80
20	68	20	Al2O3	---	28	0.64
21	68	20	Al2O3	---	28	0.64
22	68	20	Al2O3	---	38	0.70
23	68	20	Al2O3	---	45	0.80
24	1832	1000	Al2O3	---	---	---
25	1832	1000	Al2O3	---	15	---
26	1832	1000	Al2O3	---	15	---
27	1832	1000	Al2O3	---	14	---
28	1832	1000	Al2O3	---	---	---
29	1832	1000	Al2O3	---	32	---
30	68	20	AlN	---	---	---
31	68	20	MgAl2O4	---	---	---
32	68	20	xAl2O3ySiO2	---	---	---
33	68	20	Al3(Mg,Fe)2Si5AlO18	---	---	---
34	68	20	SiN (ReactionBonded)	---	---	---
35	68	20	SiN (Hot Pressed)	---	---	---
36	77	25	Boron Carbide	---	22.5	0.054
37	70	21	Zirconia (MgO partial Stab.)	---	51	0.18
38	70	21	Zirconia (Y2O3 partial Stab.)	---	---	---
39	70	21	Zirconia (Y2O3 fully Stab.)	---	---	---
40	77	25	Al2O3	Nicalon	41	---
41	1832	1000	Al2O3	Nicalon	---	---
42	2192	1200	Al2O3	Nicalon	---	---
43	73	23	SiC	Nicalon	33	0.41
44	1000	538	SiC	Nicalon	37	0.51
45	1830	1000	SiC	Nicalon	36.6	0.61

Table 5-1. Properties of Ceramic Materials with Potential for Combustor Applications - Part D

No.	Temp (F)	Temp (C)	Matrix	Fiber	CTE (in/F)	K1c
1	70	21	---	Nicalon	1.67E-06	---
2	70	21	---	Nicalon	2.10E-06	---
3	1832	1000	---	Nicalon	2.20E-06	---
4	2192	1200	---	Nicalon	2.30E-06	---
5	70	21	---	Nicalon (12.3 wt% O)	0.0000032	---
6	70	21	---	Hi-Nicalon (0.5 wt% O)	0.0000035	---
7	70	21	---	~SiC Nicalon (<0.5 wt% O)	---	---
8	70	21	---	T300 C	0.0/15.06E-06	---
9	70	21	---	NEXTEL	---	---
10	70	21	SiC (CVI process)	---	0.0000024	---
11	1832	1000	SiC (CVI process)	---	0.0000026	---
12	2192	1200	SiC (CVI process)	---	0.0000026	---
13	70	21	SiC (Process not given)	---	0.00000256	---
14	70	21	SiC (Sintered)	---	0.0000024	3
15	70	21	SiC (Reaction Bonded)	---	0.0000024	4
16	70	21	SiC (Nitride Bonded)	---	0.0000022	---
17	77	25	SiC (Silicate Bonded)	---	0.0000024	---
18	68	20	Al2O3	---	0.000004	3.5
19	68	20	Al2O3	---	0.0000045	3.5
20	68	20	Al2O3	---	0.0000046	4.5
21	68	20	Al2O3	---	0.0000046	4.5
22	68	20	Al2O3	---	0.0000046	4.5
23	68	20	Al2O3	---	0.0000047	4.5
24	1832	1000	Al2O3	---	---	---
25	1832	1000	Al2O3	---	---	---
26	1832	1000	Al2O3	---	---	---
27	1832	1000	Al2O3	---	---	---
28	1832	1000	Al2O3	---	---	---
29	1832	1000	Al2O3	---	---	---
30	68	20	AlN	---	0.0000032	---
31	68	20	MgAl2O4	---	0.0000044	---
32	68	20	xAl2O3ySiO2	---	0.0000029	2
33	68	20	Al3(Mg,Fe)2Si5AlO18	---	0.0000009	---
34	68	20	SiN (ReactionBonded)	---	0.0000017	3.5
35	68	20	SiN (Hot Pressed)	---	0.0000017	6
36	77	25	Boron Carbide	---	0.00000173	3.4
37	70	21	Zirconia (MgO partial Stab.)	---	0.0000056	11
38	70	21	Zirconia (Y2O3 partial Stab.)	---	0.0000057	13
39	70	21	Zirconia (Y2O3 fully Stab.)	---	0.0000058	3
40	77	25	Al2O3	Nicalon	0.0000032	26
41	1832	1000	Al2O3	Nicalon	---	21.5
42	2192	1200	Al2O3	Nicalon	---	21.5
43	73	23	SiC	Nicalon	0.0000028	22
44	1000	538	SiC	Nicalon	0.0000028	---
45	1830	1000	SiC	Nicalon	0.0000029	---

Table 5-1. Properties of Ceramic Materials with Potential for Combustor Applications - Part E

No.	Temp (F)	Temp (C)	Matrix	Fiber	Tmax (F)
1	70	21	---	Nicalon	---
2	70	21	---	Nicalon	---
3	1832	1000	---	Nicalon	---
4	2192	1200	---	Nicalon	---
5	70	21	---	Nicalon (12.3 wt% O)	2552
6	70	21	---	Hi-Nicalon (0.5 wt% O)	3272
7	70	21	---	~SiC Nicalon (<0.5 wt% O)	2732
8	70	21	---	T300 C	---
9	70	21	---	NEXTEL	2600
10	70	21	SiC (CVI process)	---	---
11	1832	1000	SiC (CVI process)	---	---
12	2192	1200	SiC (CVI process)	---	---
13	70	21	SiC (Process not given)	---	---
14	70	21	SiC (Sintered)	---	3000
15	70	21	SiC (Reaction Bonded)	---	2550
16	70	21	SiC (Nitride Bonded)	---	2900
17	77	25	SiC (Silicate Bonded)	---	2900
18	68	20	Al2O3	---	2552
19	68	20	Al2O3	---	2732
20	68	20	Al2O3	---	3092
21	68	20	Al2O3	---	3092
22	68	20	Al2O3	---	3182
23	68	20	Al2O3	---	3452
24	1832	1000	Al2O3	---	2552
25	1832	1000	Al2O3	---	2732
26	1832	1000	Al2O3	---	3092
27	1832	1000	Al2O3	---	3092
28	1832	1000	Al2O3	---	3182
29	1832	1000	Al2O3	---	3452
30	68	20	AlN	---	---
31	68	20	MgAl2O4	---	2000
32	68	20	xAl2O3ySiO2	---	3100
33	68	20	Al3(Mg,Fe)2Si5AlO18	---	2500
34	68	20	SiN (ReactionBonded)	---	2552
35	68	20	SiN (Hot Pressed)	---	2192
36	77	25	Boron Carbide	---	1000
37	70	21	Zirconia (MgO partial Stab.)	---	932
38	70	21	Zirconia (Y2O3 partial Stab.)	---	4350
39	70	21	Zirconia (Y2O3 fully Stab.)	---	4350
40	77	25	Al2O3	Nicalon	---
41	1832	1000	Al2O3	Nicalon	---
42	2192	1200	Al2O3	Nicalon	---
43	73	23	SiC	Nicalon	2200
44	1000	538	SiC	Nicalon	2200
45	1830	1000	SiC	Nicalon	2200

Table 5-1. Properties of Ceramic Materials with Potential for Combustor Applications - Part F

No.	Temp (F)	Temp (C)	Matrix	Fiber	
1	70	21	---	Nicalon	
2	70	21	---	Nicalon	
3	1832	1000	---	Nicalon	
4	2192	1200	---	Nicalon	
5	70	21	---	Nicalon (12.3 wt% O)	
6	70	21	---	Hi-Nicalon (0.5 wt% O)	
7	70	21	---	~SiC Nicalon (<0.5 wt% O)	Near Stoichometric SiC
8	70	21	---	T300 C	
9	70	21	---	NEXTEL	
10	70	21	SiC (CVI process)	---	CVI = Chemical Vapor Infiltration
11	1832	1000	SiC (CVI process)	---	
12	2192	1200	SiC (CVI process)	---	
13	70	21	SiC (Process not given)	---	
14	70	21	SiC (Sintered)	---	
15	70	21	SiC (Reaction Bonded)	---	
16	70	21	SiC (Nitride Bonded)	---	
17	77	25	SiC (Silicate Bonded)	---	
18	68	20	Al2O3	---	
19	68	20	Al2O3	---	
20	68	20	Al2O3	---	
21	68	20	Al2O3	---	
22	68	20	Al2O3	---	
23	68	20	Al2O3	---	
24	1832	1000	Al2O3	---	Porosity assumed same as a 68F
25	1832	1000	Al2O3	---	Porosity assumed same as a 68F
26	1832	1000	Al2O3	---	Porosity assumed same as a 68F
27	1832	1000	Al2O3	---	Porosity assumed same as a 68F
28	1832	1000	Al2O3	---	Porosity assumed same as a 68F
29	1832	1000	Al2O3	---	Porosity assumed same as a 68F
30	68	20	AlN	---	
31	68	20	MgAl2O4	---	Spinel
32	68	20	xAl2O3ySiO2	---	Mullite
33	68	20	Al3(Mg,Fe)2Si5AlO18	---	Cordierite
34	68	20	SiN (ReactionBonded)	---	
35	68	20	SiN (Hot Pressed)	---	
36	77	25	Boron Carbide	---	
37	70	21	Zirconia (MgO partial Stab.)	---	
38	70	21	Zirconia (Y2O3 partial Stab.)	---	
39	70	21	Zirconia (Y2O3 fully Stab.)	---	
40	77	25	Al2O3	Nicalon	8 plies, 0/90 2-D preform layup
41	1832	1000	Al2O3	Nicalon	8 plies, 0/90 2-D preform layup
42	2192	1200	Al2O3	Nicalon	8 plies, 0/90 2-D preform layup
43	73	23	SiC	Nicalon	0/90 2-D plain weave composites
44	1000	538	SiC	Nicalon	0/90 2-D plain weave composites
45	1830	1000	SiC	Nicalon	0/90 2-D plain weave composites

material made from braided Nicalon fiber embedded in a CVI SiC matrix was considered to be the optimum choice for application to a gas turbine combustor liner. However, it was recognized that improvements in this material system - particularly in resistance to thermal crack development - were required coupled with health monitoring to assure reliable performance in a combustor liner.

Recently, DPLC has made available an enhanced SiC/SiC CMC that has a long life (up to 2200°F in oxidizing environments) under moderate stresses without an external protective coating. This enhanced SiC/SiC CMC contains an additive that reacts with oxygen to seal matrix cracks as they develop. It is projected to sustain 30 percent less thermal stress than the unenhanced material. An evaluation of the high temperature mechanical properties of enhanced SiC/SiC CMC material made by Dupont Lanoxide for AE has been made [12]. The SiC/SiC CMC material tested was reinforced with Nicalon fiber tows woven into a triaxial, two-diemensional braid with tows at 0, 60, and -60 (or 120) degrees orientation. Tensile stress-strain results are presented in Figures 5-1 through 5-4 and Table 5-2. Elongations at failure range from 0.38 percent at room temperature to 0.94 percent at 2000°F. Tensile strengths are near 120 mpa (17.4 ksi) which is well below an estimated strength of 106 ksi based on fiber vomume alone with an assumed fiber strength of 400 ksi. This suggess serious fiber degradation can occur during composite fabrication.

A full scale CMC combustor made of enhanced SiC/SiC CMC material has now been successfully rig tested by AE (under Navy and JTAGG contract [13].) for 14 hours at 1700°F (cold side temperature - no reliable sensor is available to measure the hot side). No cracks developed. Although these results are very encouraging, the life of this material is still not sufficient for use in a production engine. This situation is currently being addressed by a long life materials development effort being conducted by NASA for the Enabling Propulsion Materials Program and by the Fiber Consortium consisting of all of the aerospace gas turbine engine companies. Thus, a final decision on selection of a CMC material suitable for combustor application is not presently available. However, enhanced SiC/SiC CMCs are prime candidates and are selected for the purposes of the effort of this report.

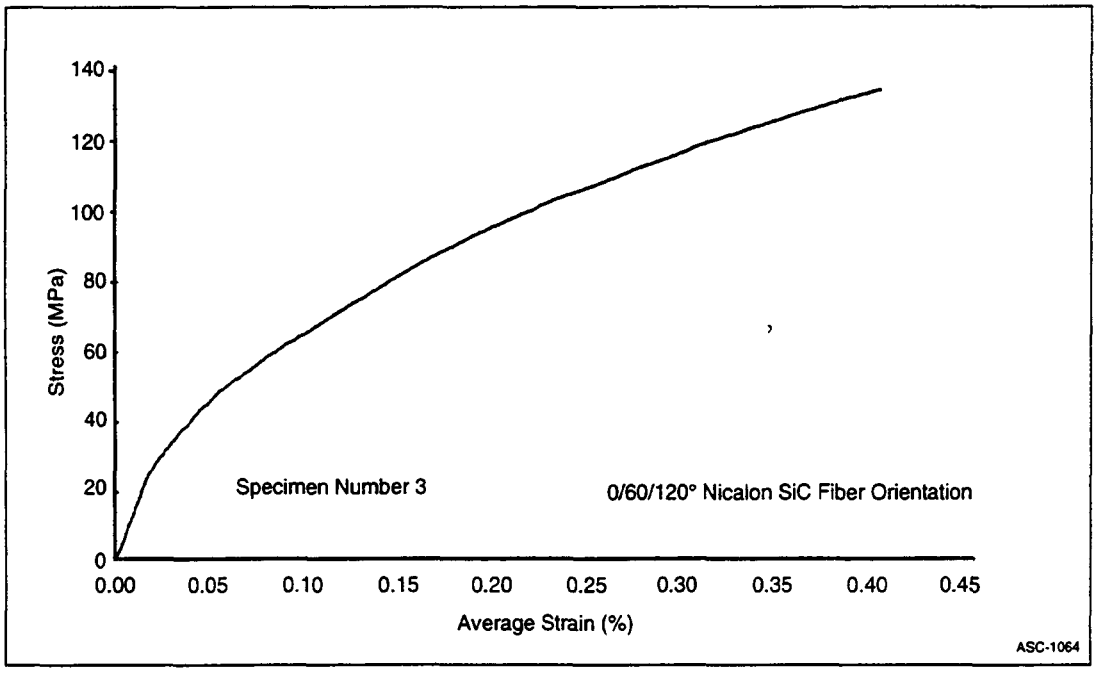

Figure 5-1. Room Temperature Stress Strain Curve for Enhanced SiC/SiC CMC

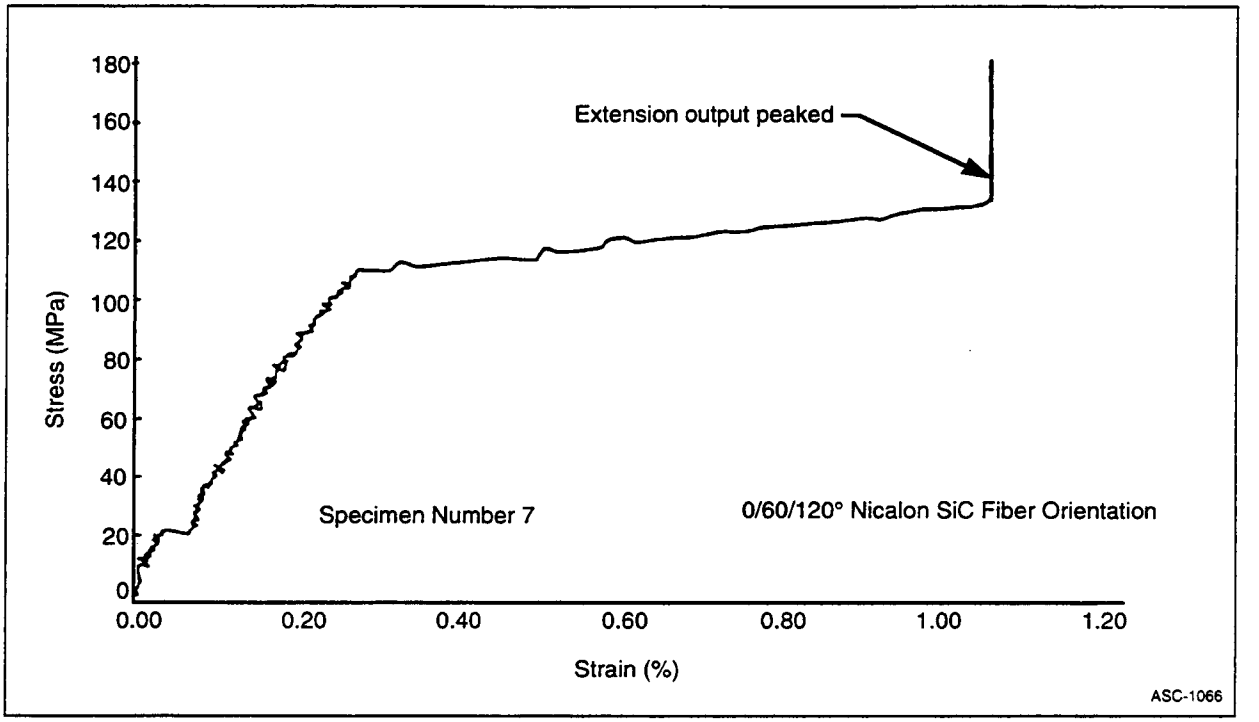

Figure 5-2. Stress Strain Cr Enhanced SiC/SiC CMC at 815°C (1500°F) in Air

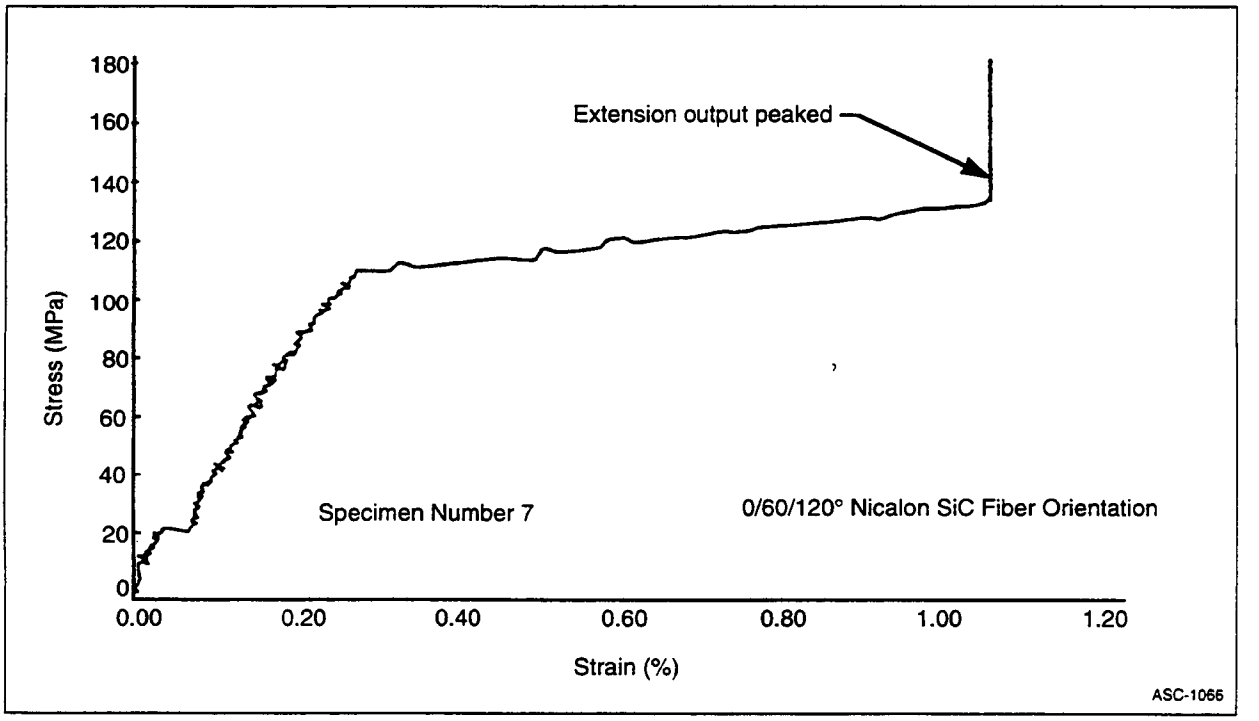

Figure 5-3. Stress Strain Curve for Enhanced SiC/SiC CMC at 1090°C (2000°F) in Air

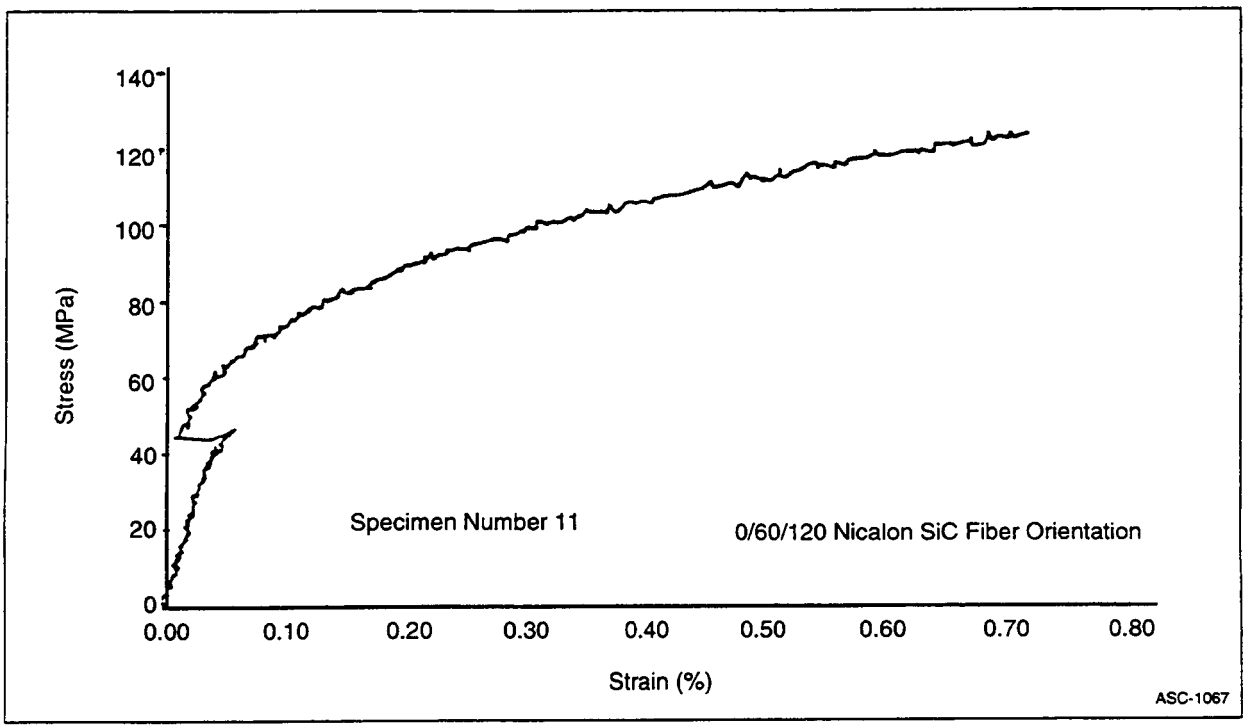

Figure 5-4. Stress Strain Cr Enhanced SiC/SiC CMC at 1370°C (2500°F) in Air

Table 5-2. High Temperature Properties of SiC/SiC Composite Made for AE by DuPont Lanxide

No.	T °C (°F)	E Gpa (Mpsi)	cγ Mpa (ksi)	εγ %	σ_ Mpa (ksi)	ε_ %
1-3	24 (75)	134±17 (19.4±2.5)	24±9 (3.5±2.0)	0.02±0.01	141±9 (20.4±1.3)	0.38±0.01
4-6	815 (1500)	84±8 (12±1)	38±14(5.5±2.0)	0.04±0.02	162±12(23.5±1.7)	0.52±0.08
7-9	1094 (2000)	48+(7.0 ±0.6)	83±54(12±8)	0.18±0.12	169±12(24.5±1.7)	0.94±0.28
11	1371(2500)	88 (13)	46 (6.7)	0.06	121 (17.5)	0.69

Further testing of CMC combustor is planned by AE for 1996. Current plans are for use of 0.003-inch diameter wire, Type K thermocouples transitioned to Inconel sheathed hardwire and attached to the combustor wall with AE's silicide cement. The results of new testing will be taken into consideration in the modelling.

5.1 CMC MATERIAL CHARACTERIZATION

The SiC/SiC CMC material selected for use in ceramic combustors is in the process of being more or less rapidly up-graded so that testing to characterize this material has encompassed progressively improved versions of this material. The progression has been from Nicalon™/SIC to Nicalon™/Enhanced-SIC to Hi Nicalon™/Enhanced-SIC. As a consequence data from any one version is limited making it prudent to present data from all four versions in order to provide a more complete view of the SiC/SiC CMC material.

5.1.1 Nicalon™ Standard SIC

Upon selection of the 2-D triaxial braided SIC/SIC as the combustor material, mechanical tests were conducted on Nicalon™/SIC CMC coupons. These tests were focused on in-plane fast fracture and strain rupture at temperatures up to 2500 F to provide basic material properties such as stiffeness, short term

strength , and stress rupture (the critical design parameter). The inplane stiffeness, and strength versus temperature are shown in Figure 5-5 for the 0° direction of a laminate with 40 fiber volume percent (FVP). As shown in the Figure, strength and stiffeness stay fairly constant up to about 2200F and then drop off rapidly.

Thermal conductivity and expansion tests were conducted up to 2500F. The results, shown in Figure 5-6, are used in simulations relative to making calculations involving heat transfer; e.g., calculations of temperature gradient induced combustor stresses. hot spot locations, and energy losses.

5.1.2 HI Nicalon SiC Fiber/ Enhanced SIC CMC

Nippon Carbon has developed a high heat-resistant silicon carbide fiber"HI-NICALON", which retains high mechanical properties after 1500° C exposure in an inert atmosphere and is flexible even after 2000° C exposure. It features: (1) continuous fiber tow with small diameter filaments, flexible and weavable; (2) excellent mechanical properties, high tensile strength with high tensile modulus; and (3) excellent thermal and chemical stability. Hi-Nicalon™ fiber reinforced SiC matrix CMCs are expected to have: (1) use temperature to 1400° C (2550°F), (2) excellent thermal shock

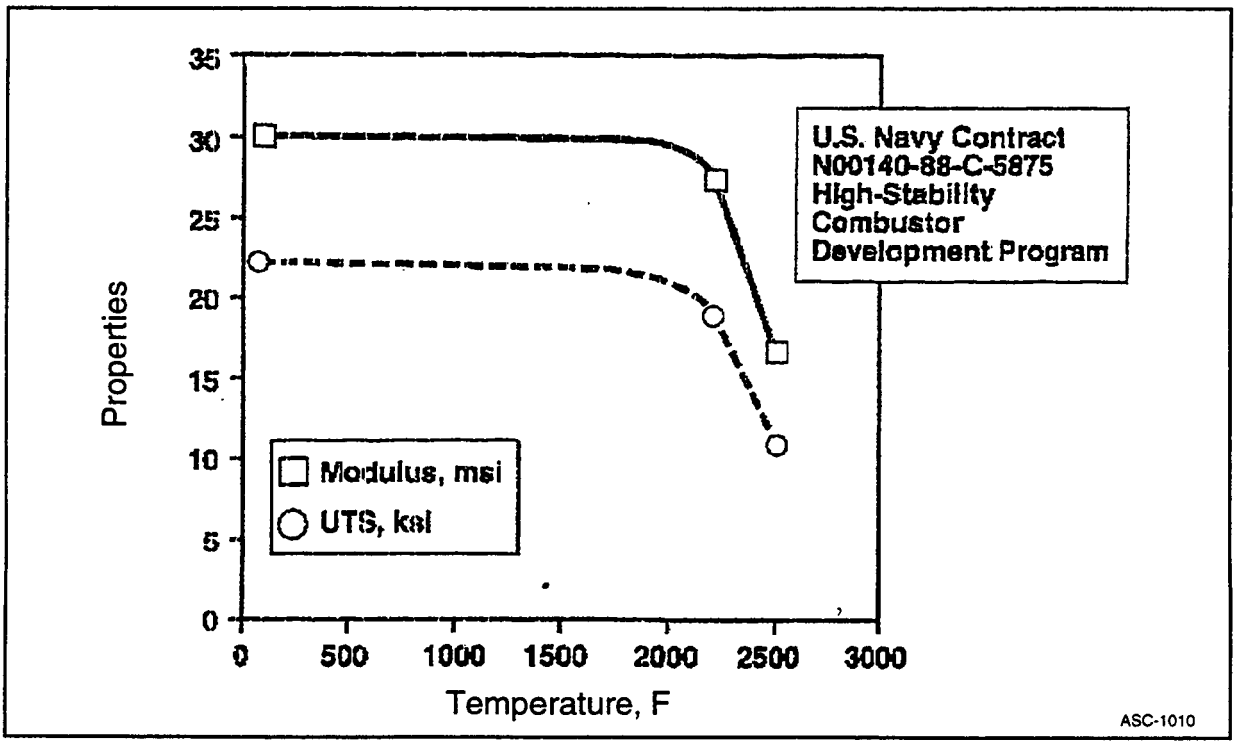

Figure 5-5. Mechanical Tensile Test Results at Room and Elevated Temperatures on 2-D Triaxial Braided SiC/SiC CMC With 40% Nicalon™ SiC Fiber

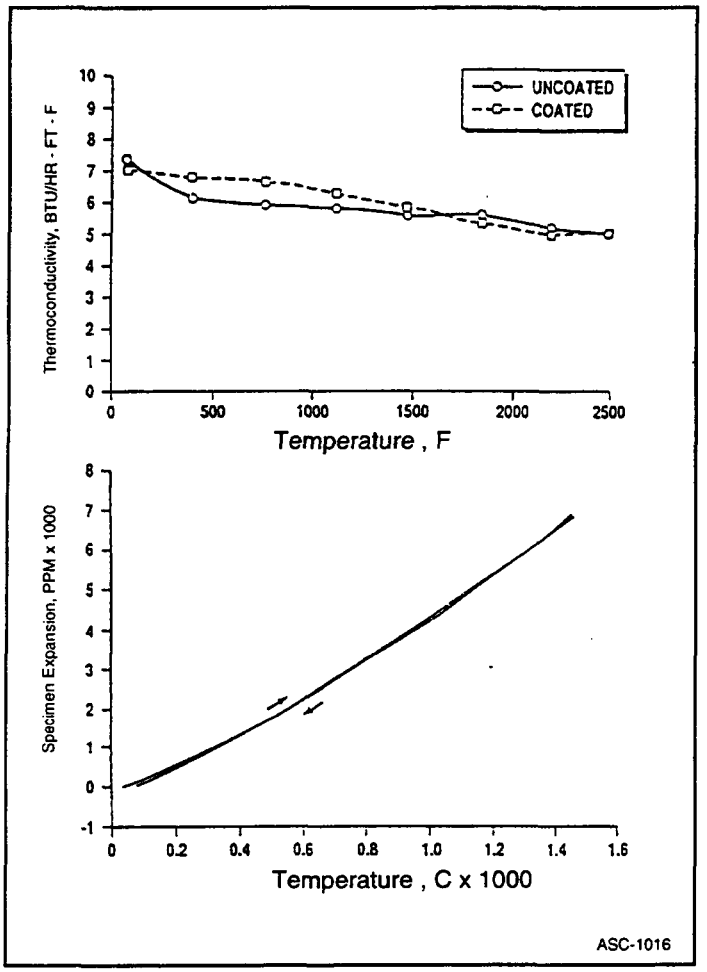

Figure 5-6. Through-Thickness Thermal Conductivity and Expansion for the Standard Nicalon/SiC Material

resistance, (3) high strength and toughness at room and elevated temperatures, and (4) improved oxidative stability.

The enhanced SiC/SiC CMC material system developed by Dupont Lanxide has 40 percent Nicalon ™ Fiber in a SiC CVI matrix and a porosity of 8 to12 percent. It has a Lower Modulus and Higher Strain Tolerance compared to the unenhanced SiC/SiC material and a long life in ≤ 2200°F oxidizing environments at moderate stresses without an external protection coating. With coatings a higher stress level is attainable.

Room temperature and elevated temperature mechanical properties of Hi-SiC/SiC are showns in Figures 5-7 through 5-11 and in Tables 5-3 through 5-5. As tensile stress is increased enhanced SIC/SIC CMC exhibit elastic behavior to a strain of about 0.05 percent beyond which significant micro cracking begins in the matrix forcing load transfer to adjacent fibers and initiating non linear stress-strain behavior (Figure 5-7).

Stress rupture and low cycle fatiigue properties are presented in Figures 5-8, 5-9, 5-10 and Table 5-5. Ultimate and linear elastic limit stresses are presented in Figure 5-11 as a function of temperature.

More mechanical tensile properties at elevated temperatures are currently being generated at DuPont and will be reported when they become available.

Table 5-3. Comparison of SiC/SiC CMC Materials Available From DuPont Lanoxide

Ambient Temperature	**Nicalon™/SiC**	**HiNic/Sic**	**Nicalon™/E-SiC**	**Hi-Nic/E-SiC**
Density (g/cc)	2.5	2.7	2.35	2.6
Ambient				
Tensile Strength (ksi)	28	31	33	23*
Elongation(%)	0.22	0.23	0.4	0.14*
Modulus (MSI)	33.7	38.6	20	32
Elastic Limit Stress (ksi)	11	13	8	15
Elastic Limit Strain	0.033	0.034	0.039	0.047
Elastic Strength (ksi) S:D - 30:1	40	48	50	62
Elevated Temperature	**1000°C (1830°F)**	**No Data Available**	**1000°C (1830°F)**	**1300°C (2370°)F**
Tensile Strength (Ksi)	34.6		37	
Elongation (%)	0.35		0.6	
Modulus (MSI)	33.7		21	25
Elastic Limit Stress (ksi)	18		13	
Elastic Limit Strain (%)	0.053		0.080	

*Minimum value because of break in grip area during test

ASC-1027

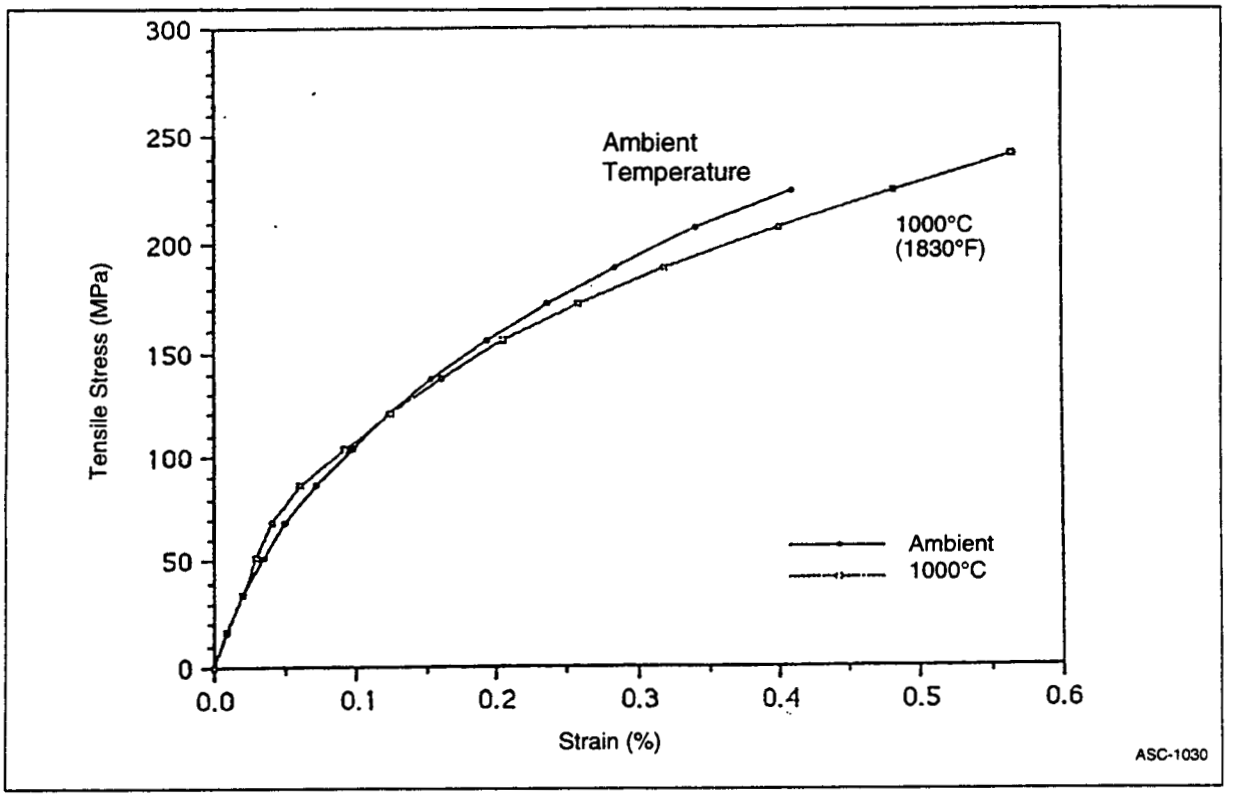

Figure 5-7. Enhanced Hi Nicalon/SiC Tensile Stress-Strain Behavior

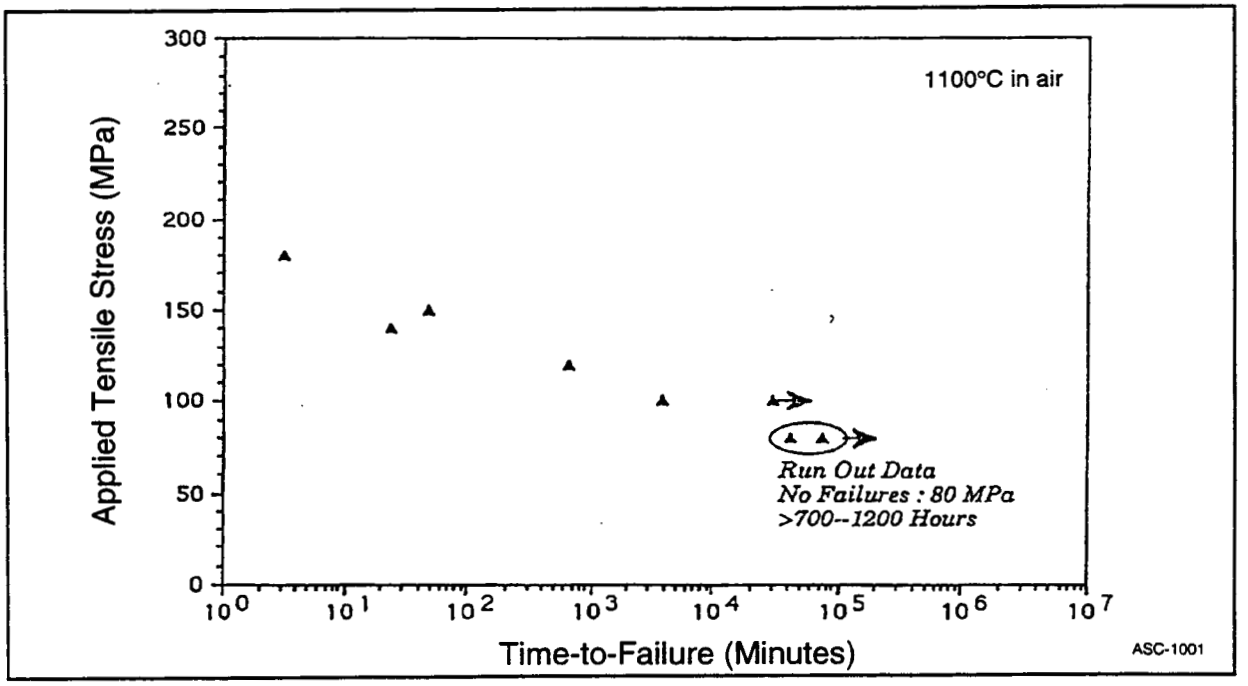

Figure 5-8. Enhanced Hi Nicalon/SiC: Low Cycle Fatigue

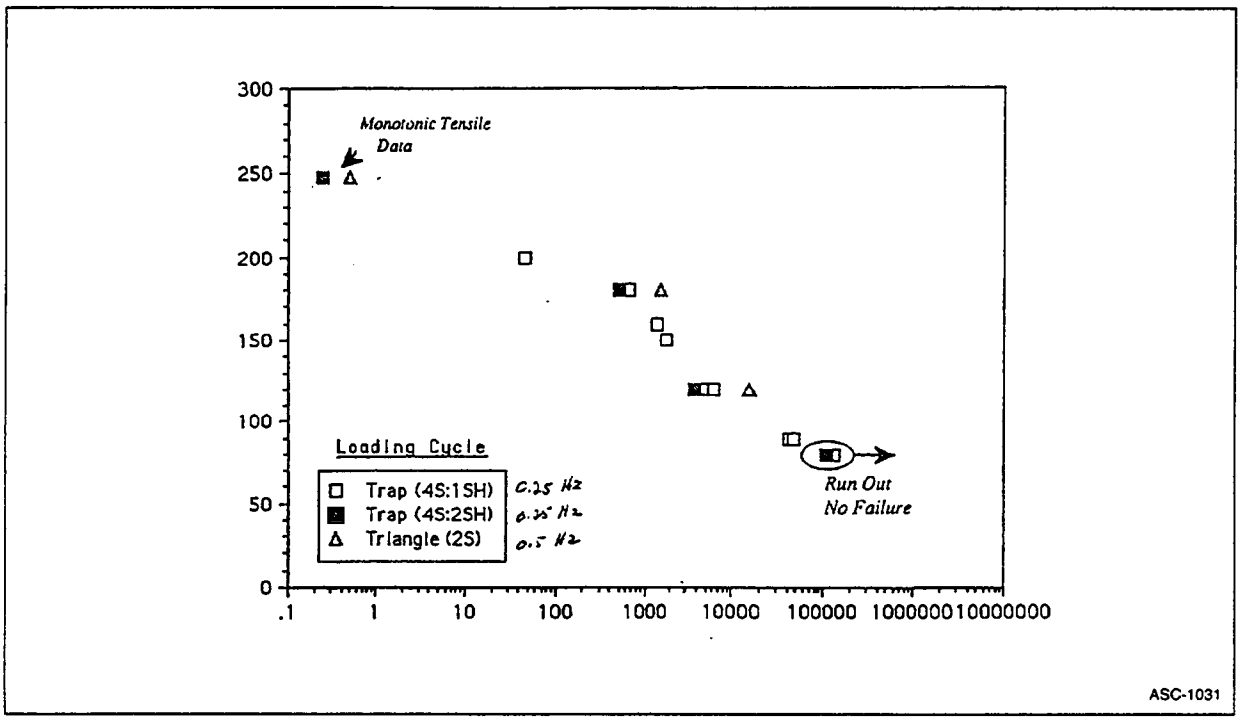

Figure 5-9. Enhanced SiC/SiC: Low Cycle Fatigue

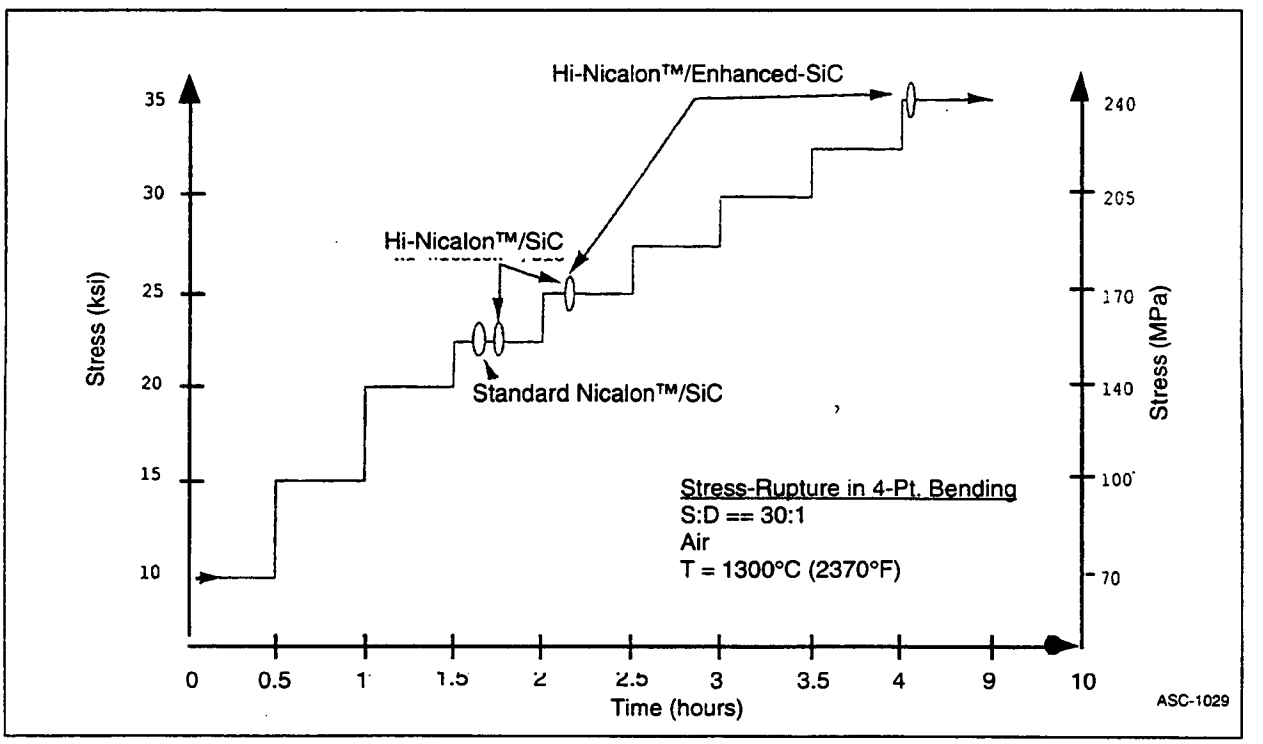

Figure 5-10. Stress-Staircase Evaluation

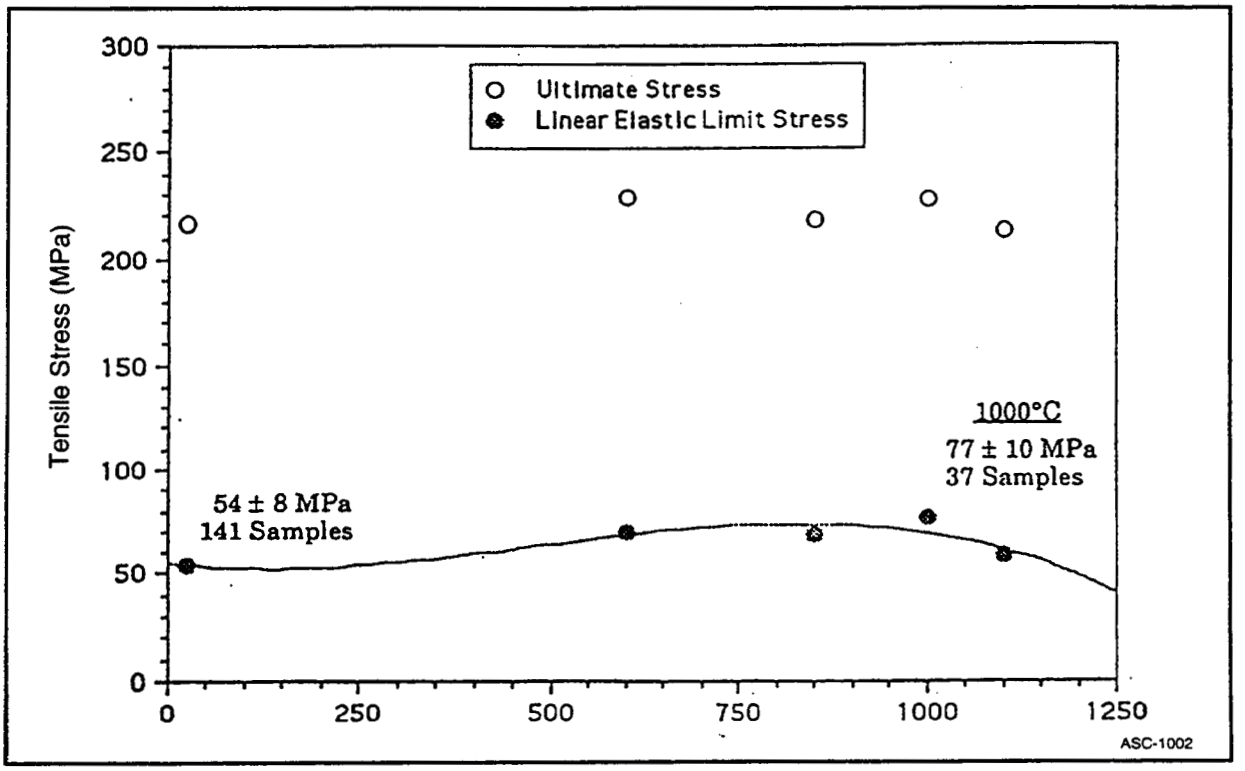

Figure 5-11. Linear Elastic Limits of Enhanced Hi Nicalon/SiC From Tensile Test

Table 5-4. Mechanical Properties of Enlanced SiC/SiC

		Average value	Standard deviation	Units	No. of tests
23ºC (73ºF)	Tensile Strength	217	20	Mpa	149
	Tensile Strain	0.42	0.05	%	146
	Tensile Modulus	140	18	Gpa	146
	Linear Elastic limit	54	8	Mpa	141
538ºC (1000ºF)	Tensile Strength	255		Mpa	3
	Tensile Strain	0.51		%	3
	Tensile Modulus	150		Gpa	3
	Linear Elastic Limit	72		MPa	3
1000ºC (1830ºF)	Tensile Strength	228	15	Mpa	42
	Tensile Strain	0.53	0.06	%	36
	Tensile Modulus	127	15	Gpa	41
	Linear Elastic Limit	77	10	MPa	37
23ºC (73ºF)	Compressive Strength	500	76	Mpa	39
	Compressive Modulus	145	19	GPa	39
	Flexure Strength	345		Mpa	6
	Interlaminar Shear	31	7	Mpa	47
	Interlaminar Tension	>13	0.7	Mpa	12

ASC-1002a

Test results are for 0°/90° 2D laminate plain weave composites.

Table 5-5. Enhanced SiC/SiC Stress-Rupture Results (Uncoated Samples, Tested in Air)

Load Type	Temperature(ºC)	Stress(MPa)	Lifetime(hrs)
Flexural	450	207	>300+
	600	207	>300+
	1000	207	>1000+
	1200	207	>300+
Tensile	1000	60	>300+
	1100	80	>1200+
	1200	80	>4500+
	1200	90	>1200+
	1200	100	60

* sample was pre-stressed to 138 Mpa prior to testing

5.2 SiC/SiC CMC COMBUSTOR TESTS

5.2.1 Subelement Tests

Allied Signal has tested two SiC/SiC CMC subelement combustors reinforced with 2D triaxial braided, carbon coated, Nicalon fiber [9]. These subelement combustors were cylindrical tubes approximately 3 inches in diameter and 6.3 inches long with a wall thickness of 0.08 inch. One subelement incorporated effusion cooling holes. Both subelements were coated with chromalloy RT42A for added protection from oxidation. Test conditions were aggressive in order to deliberately cause damage for study purposes, localized regions with temperatures greater than 2500°F were observed.

During testing, backside cooling air was used to control temperature gradients and combustor loading was simulated by a load applied by a thrust piston (Figure 5-12). Thermal paint stripes, applied to the hot (inside) and cold (outside) surfaces provided the data for the temperature profiles shown in Figure 5-13 and summarized in Table 5-6. The thickness temperature gradients remained fairly constant during the cycling. However, the thickness temperature gradient (650°F) of the effusion cooled subelement was considerably higher than the temperature gradient (370°F) of the non-effusion cooled subelement.

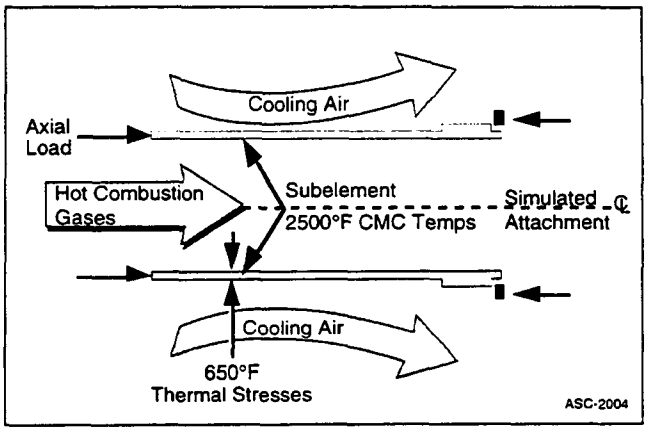

Figure 5-12. Combustor Subelement Testing

The observed temperature profiles (Figure 5-13) were utilized in a finite element analysis to calculate hoop and axial thermal stress gradients for the noneffusion cooled subelement. Simulation prediction of areas where stress levels would exceed the short term ultimate strength of the material (previously determined by coupon testing) were made. These were in excellent agreement with experimental results in that cracks were observed at the predicted locations in the noneffusion cooled subelement.

Table 5-6. Results From Subelement Testing

	Effusion Cooled	Noneffusion Cooled
Maximum material temp, F	2500	2500
Temp gradient F	650	370
Stead-state*, hours	15	15
Thermal cycling, hours	>6**	>6**
*Included about 3 hours for start-up and shutdown		
**12 cycles		

5.2.2 Full Scale Tests

Allied Signal has tested three full scale SiC/SiC CMC combustors for a small gas turbine engine (Figure 5-14). As with the subelement combustor testing, thermal paint data coupled with optical and thermocouple temperature measurements was utilized to map a temperature profile as shown for a unit section in Figure 5-15. In addition, real-time thermography was used in some runs to obtain thermal maps (Figure 5-16). Thermal gradient stresses were then calculated using the experimentally determined temperature profile maps. For the first two combustors, hoop stress values were predicted to exceed the mechanical properties at the aft end where cracks developed. Reduced hoop mechanical properties were used for the analyses because hoop fibers were skewed to the axial direction of the combustors.

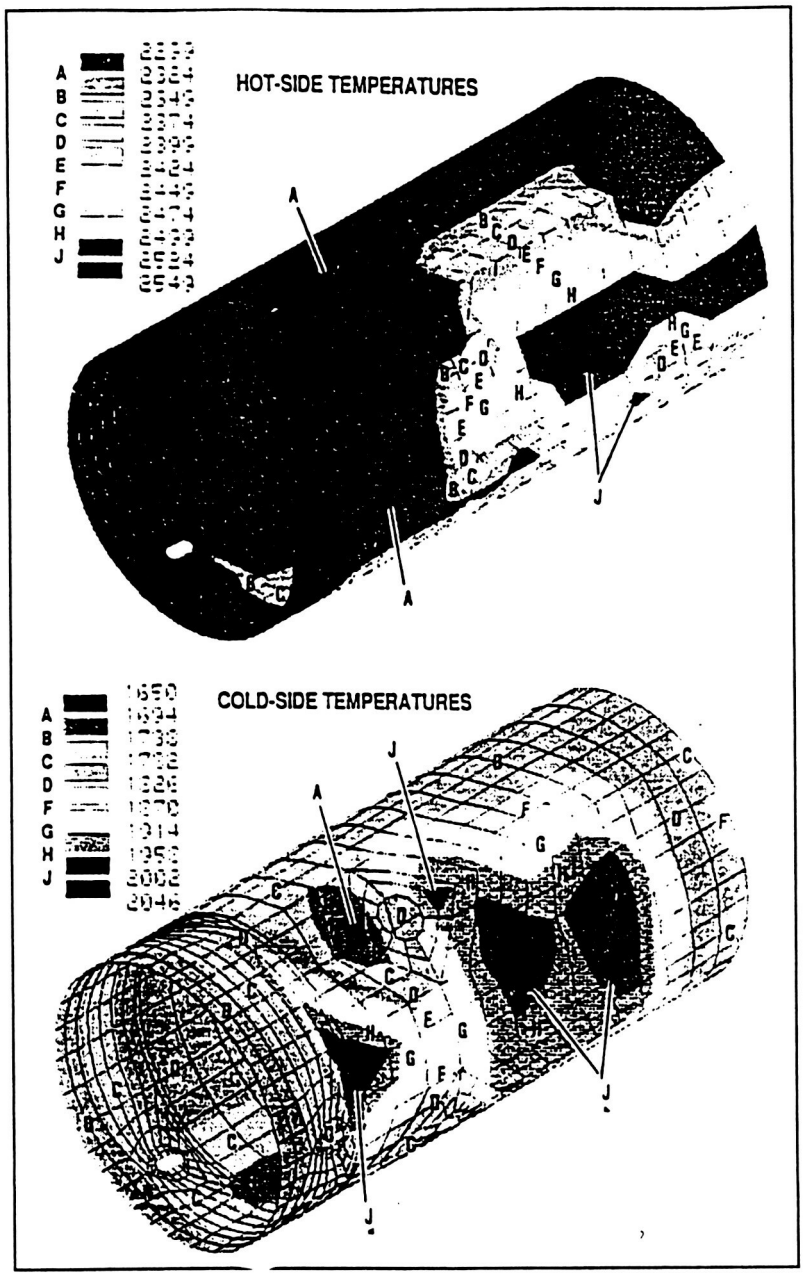

Figure 5-13. The Cold- Hot-Side Surface Temperatures of the Model Were Mapped From the Uncooled Subelement Thermal Paint Data

Additional hoop fiber tows were used at the aft end of the third combustor to give higher strength in the hoop direction. No cracks were observed in this combustor after 14 hours of testing.

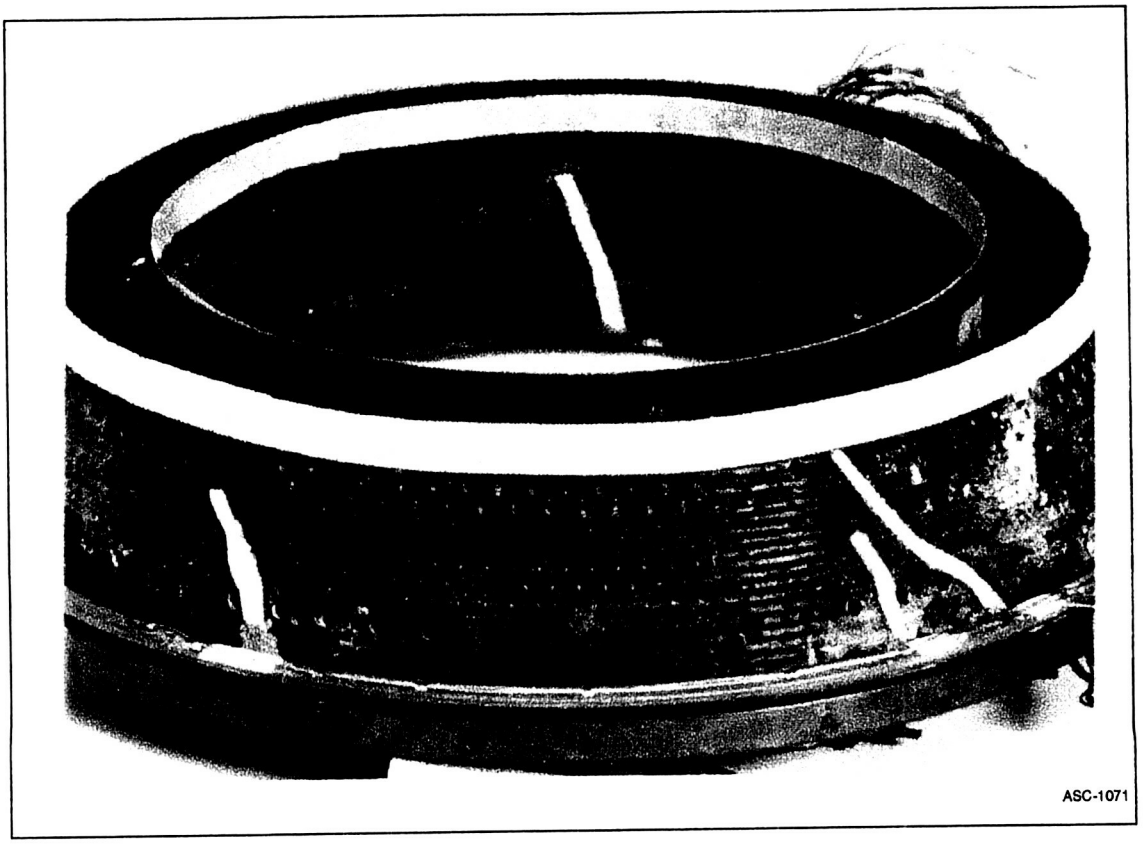

Figure 5-14. A Full Scale Experimental SiC/SiC CMC Small Gas Turbine Engine Combustor Tested by AE

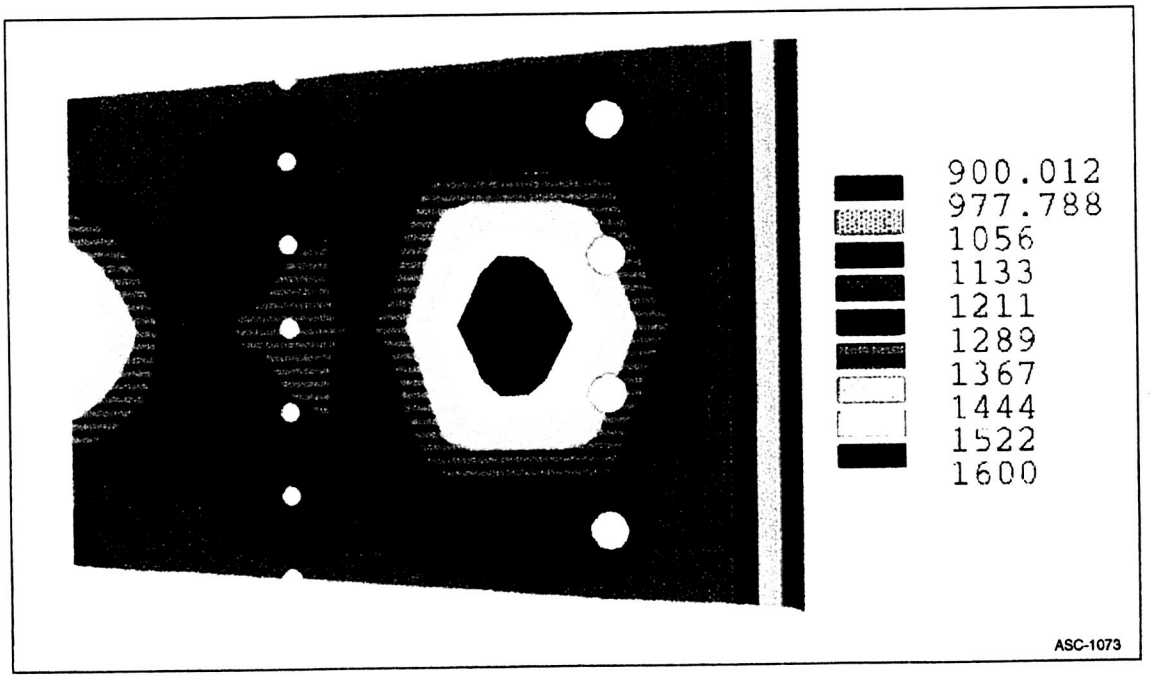

Figure 5-15. Thermal Paint Temperature Profile Map of a Unit Section of Tested SiC/SiC CMC, Combustor of Figure 5-14

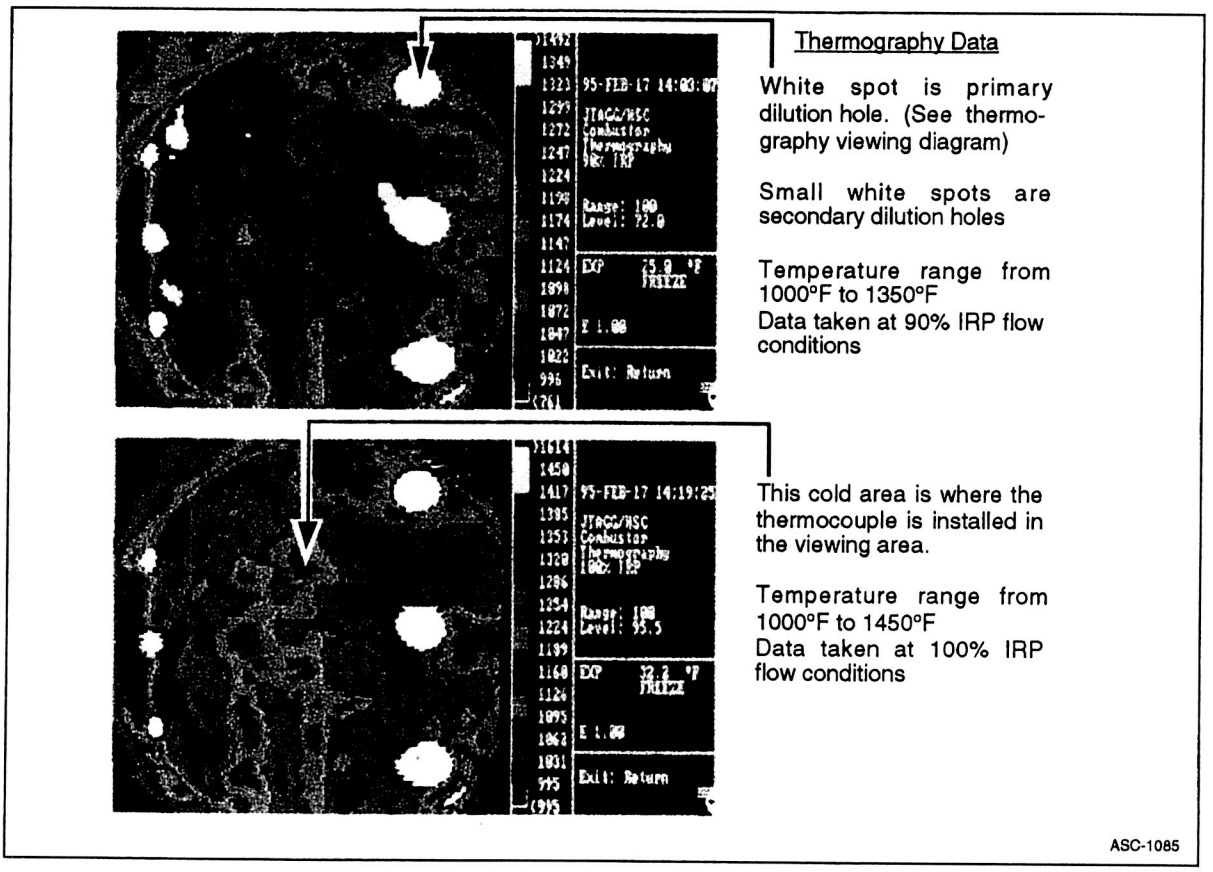

Figure 5-16. Thermography Data Obtained in Real-Time by AE During Full Scale SiC/SiC CMC Combustor Testing

6.0 Multidisciplinary Computer Code Development for Stochastic Analysis of CMC Composite Smart Structure

Alpha STAR has developed a system that integrates existing specialty codes and methodologies to perform probabilistic simulation of high temperature composite structural response, as shown in Figure in Figure 6-1. This system capitalizes on the computational speed of parallel computing hardware and is intended to meet the demands for an analytical engineering tool for design of advanced aerospace structures.

The integrated analysis tool was demonstrated by detailed verification and benchmark studies of an array of applications. This portion of the study was divided into four categories, each of which require the application of specialized techniques and methodologies. These categories are:

1. Structural Analysis Methods utilizing Laminate Theory and Micromechanics of MMCs
2. Probabilistic Analysis for Structural Reliability and Materials Strength Simulation
3. Domain Decomposition and Parallel Transformation Methods
4. Dynamic load balancing and optimization to minimize the Computer Processing Unit (CPU) calculations

6.1 AN INTEGRATED MULTI-DISCIPLINARY CONSTITUENT MATERIAL STRENGTH AND RISK ASSESSMENT ANALYSIS

Current methods of structural and materials probabilistic analysis primarily tend to fall into categories of simulation, perturbation and reliability. Each of these categories has specific areas for which their application is best suited. In some cases they can be implemented concurrently to perform a desired analysis. One such capability allows integrated structural analysis using distribution estimation for micro-level uncertainty in a micromechanics approach to evaluate the stochastic variation of constituent material properties and strengths subjected to primitive variables.

Alpha STAR has recognized a unique opportunity to integrate PROMISS [14], CEMCAN [15], and NESSUS [16] codes presently integrated in a modified HITCAN (High Temperature Composite ANalyzer) into its GENOA code to provide a user friendly code that can be used to determine stresses, strains, displacements, creep, and fatigue responses to mechanical and thermal loading applications with concurrent reliability assessments. A flow chart showing the calculation sequence in which the codes are used is shown in Figure 6-2. The CEMCAN code uses microproperty inputs to calculate properties of CMC plies and laminates. The laminate properties are then input to NESSUS, a finite element analysis (FEA) code to calculate composite stresses, strains, displacements, and reaction forces. The stress outputs from the NESSUS FEA are compared to the previous outputs and iterations are made by updating stress inputs to CEMCAN until convergence within prescribed limits is achieved.

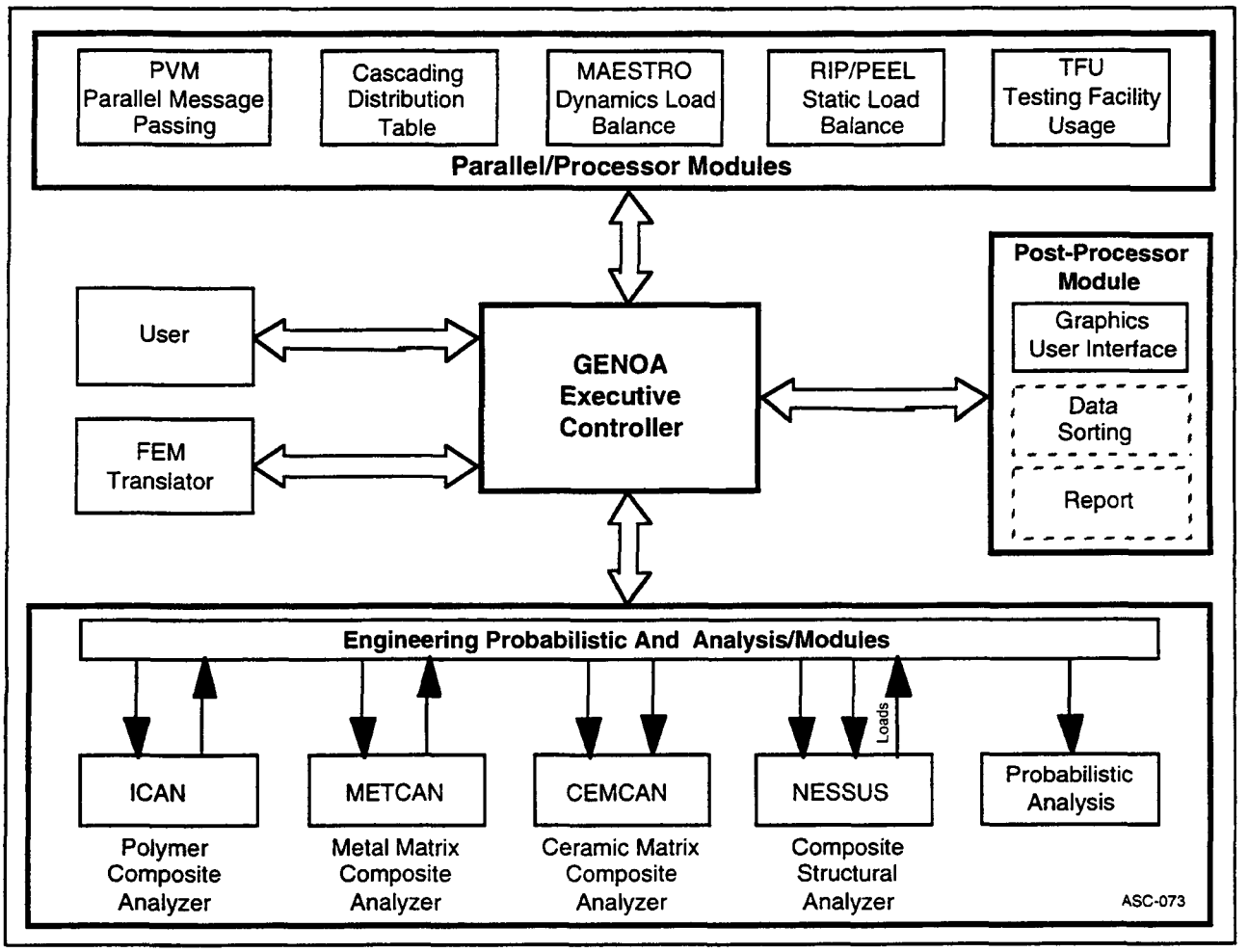

Figure 6-1. Architecture of GENOA Parallel Software System

Probabilistic micro-level analysis employing distribution estimation and simulation has been demonstrated. Boyce, et. al. [17] have developed a code known as PROMISS (Probabilistic Material Strength Simulator). Their approach centers on the application of a general phenomenological constitutive relationship for composite materials utilizing maximum likelihood estimations as the basis for stochastic variation of constituent properties subjected to various primitive variables.

Composite micromechanics analysis is performed by combination of NESSUS and CEMCAN codes. A schematic of the codes iterative structure is shown in Figure 6-2. NESSUS is responsible for the finite element analysis where CEMCAN calculates micromechanic response of the composite structure. The micromechanics formulation in CEMCAN is based on a unit cell or representative volume element (RVE) which assumes that fibers are arranged in square array pattern. The unit cell consist of fiber, matrix, and interface between the constituents. The unit cell in CEMCAN analysis is further subdivided into several slices and simplified micromechanics equations are applied to each slice to get the equivalent slice properties in terms of constituent properties. These are subsequently integrated to obtain the equivalent unit cell or ply properties by the application of the laminate theory in a way equivalent to obtaining homogenized composite properties from ply properties. The modeling details of the substructured representative element is shown in the flow chart under CEMCAN in Figure 6-3. As shown the left side of the chart illustrates the various steps involved in the synthesis of the properties from slice to laminate level, while the right side of the chart illustrates the various steps involved in the decomposition of the response from laminate to ply, to slice and then to microstresses. This novel modeling technique has been referred to as a fiber sub-structuring technique and has been

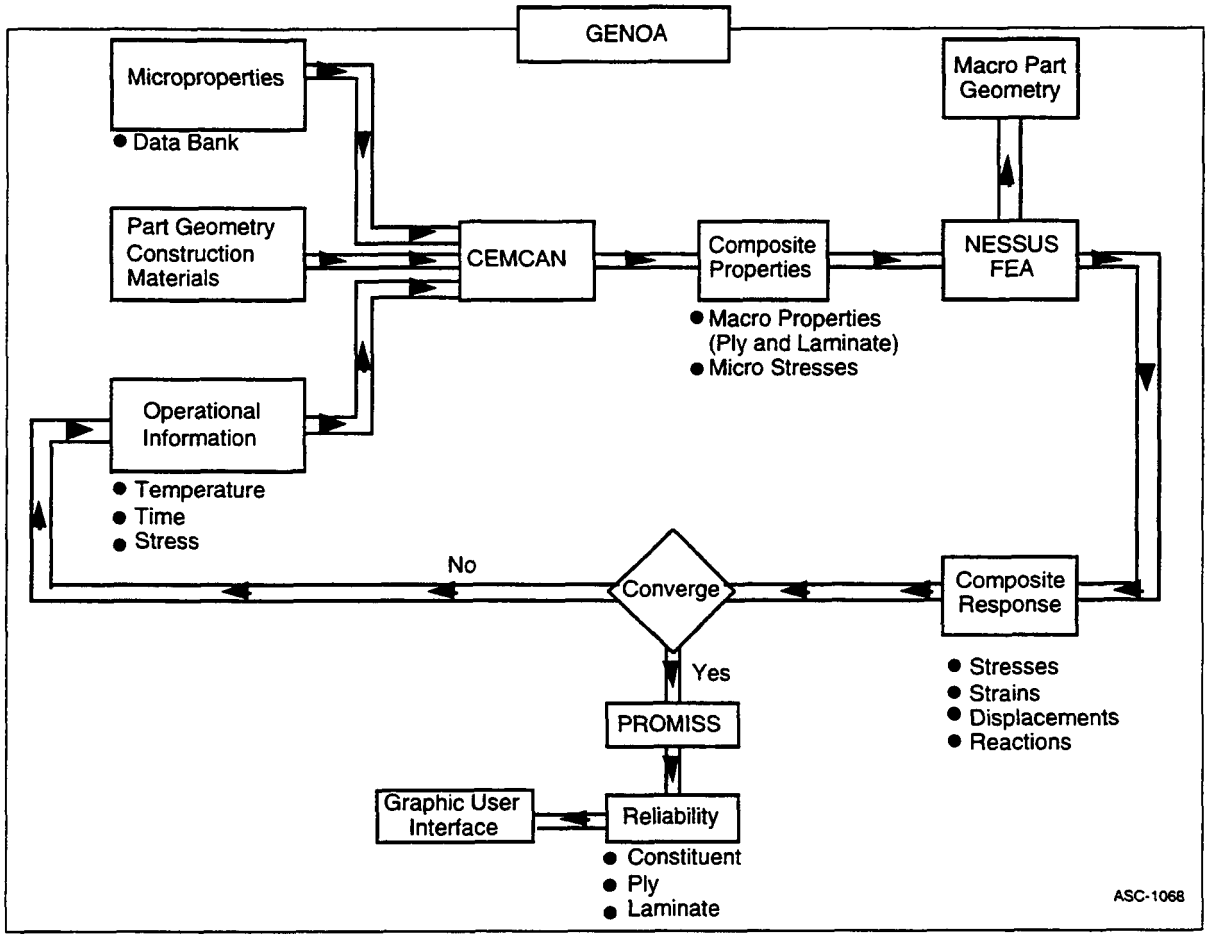

Figure 6-2. Illustration of GENOA Integrated Stochastic Analysis Package

implemented into the CEMCAN (Ceramic Matrix Composite ANalyzer) for analyzing and predicting the behavior of ceramic matrix composites. Such a technique allows for a more accurate micro-mechanical representation of interfacial conditions, and provides a greater detail of stress distribution within a ply. It is to be noted that the fiber/matrix interface plays an important role in toughening mechanisms such as fiber debonding, fiber pull out and crack deflection and therefore must be a significant feature of CMC modeling.

6.1.1 Modularization Of HITCAN: A Source For Baseline Analytical Capabilities

HITCAN is modularized (Table 6-1) to perform iterative local, and global modeling while achieving computational efficiency by using dynamic allocation of memory. The modularization is directed to: 1) maximize the size of the iterative problem that can be solved, 2) easily utilize and adopt other material simulators such as CEMCAN, ICAN. etc., 3) implement mixed material models within the same FE model, 4) integrate the NESSUS parallel FEM solver into HITCAN, and 5) to ease setting up the control information to perform a HITCAN simulation.

In order to perform a modular integration with HITCAN, a three stage approach is taken . The first stage copies the deck initialization data from the NESSUS panel which performs parallel FEM analysis. The second stage copies the initialization deck from the CEMCAN panel (Figure 6-1) and initiates the actual parallel analysis using CEMCAN. The third stage sets up the HITCAN control file

with the necessary information to begin the iterative analysis. The steps taken in this modularization are as follow:

Table 6-1. Input/Output Parameter Panel for High Temperature Composite ANalyzer (HITCAN)

HITCAN---High Temperature Composite ANalyzer ---HITCAN		
This code performs integration and iteration between finite element and material constituents		
1	CEMCAN	– Set CEMCAN Option Control Parameters
2	NESCNTL	– Set NESSUS Option Control Parameters
3	HITCNTL	– Set HITCAN Option Control Parameters
4	DSNAMES	– Define CEMCAN File Names
5	DSNAMES	– Define NESSUS File Names
6	DSNAMES	– Define HITCAN File Names
C	CHECK	– Check File Names Without Execution
E	EXEC	– Executive HITCAN Module
Select One Of The Available Options By Number/Letter		
		ASC-203

STAGE 1 NESSUS Initialization: by the Executive controller

1. Start the Peel algorithm and partition the model into as many substructures as there are available processors.
2. Read the computer facility information from MAESTRO, e.g. the number of processors, rate of communication , and partition data from RIP and PEEL algorithms
3. Read the finite element model from PATRAN or GENOA FEM preprocess
4. Setup loads, boundary conditions and temperatures as physical parameters.
5. Create an initial NESSUS deck and send the initializing parameters to the HITCAN control deck.

STAGE 2 CEMCAN Initialization:

1. Make a system call to CEMCAN input deck (automatically performed by the executive controller).
2. Execute a system call to initialize CEMCAN (the number of mesh nodes, the number of parallel processors, and the distribution of CEMCAN runs among the processors).
3. Map the CEMCAN data for use in Stage 3.

STAGE 3 HITCAN Initialization

1. Initiate the HITCAN program (using input from STAGES 1, and 2) for assembly of an iterative job.
2. Perform parallel CEMCAN analysis and generate laminate data for NESUSS FEM.
3. Use parallel processing to obtain a NESSUS FEM solution for the stresses and strains.
4. BASED ON HITCAN executive control data continue NESSUS/CEMCAN iteration, and check for convergence.
5. Return to HITCAN to perform response computations and post processing.

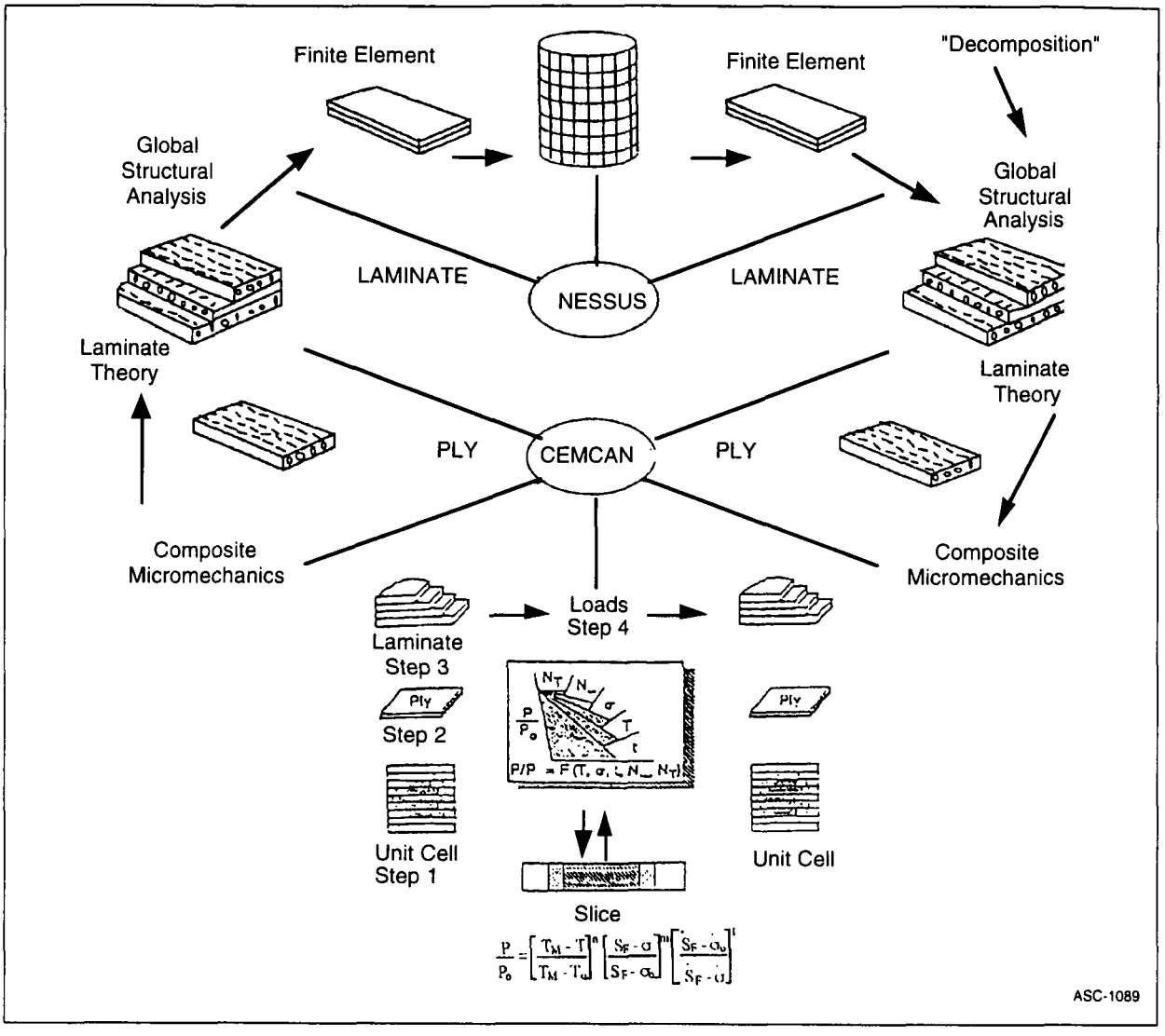

Figure 6-3. Illustration of the Computational Iterative Procedure Utilized by HITCAN to Perform Composite Micromechanics Within a Finite Element-Based Analysis.

6.1.2 CEMCAN Integration For GENOA

The nonlinear version of Ceramic Matrix Composites ANalyzer (CEMCAN) under development at NASA/LeRC was integrated as part of the GENOA system. The CEMCAN code incorporates various levels of composite mechanics models (substructuring) to allow a comprehensive point analysis of composite behavior . The CEMCAN control program is written to interact with the executor and build the control file for the CEMCAN module.

In the application of CEMCAN to CMC material the volume element or unit cell is assumed to be arranged in a regular pattern. The unit cell consists of fiber, matrix and interphase. By applying the micromechanics equations which are based on a mechanics of materials approach to the unit cell, the equivalent properties for the ply are obtained. The interphase is treated as a separate constituent with distinct properties. Thus, it can either represent a zone formed due to a chemical reaction between the fiber and the matrix or a fiber coating provided intentionally to prevent such a reaction.

The CEMCAN application to a ceramic matrix uses a volume element subdivided into several slices with separate micromechanics equations for each slice. Results from these slices are subsequently integrated to obtain ply properties. Figures 6-4 and 6-5 demonstrate the graphical the vertical and horizontal slicing by CEMCAN for stress calculation in the time domain. Ply stress can be plotted in the 11, 22, 33, 12, 13, and 23 directions

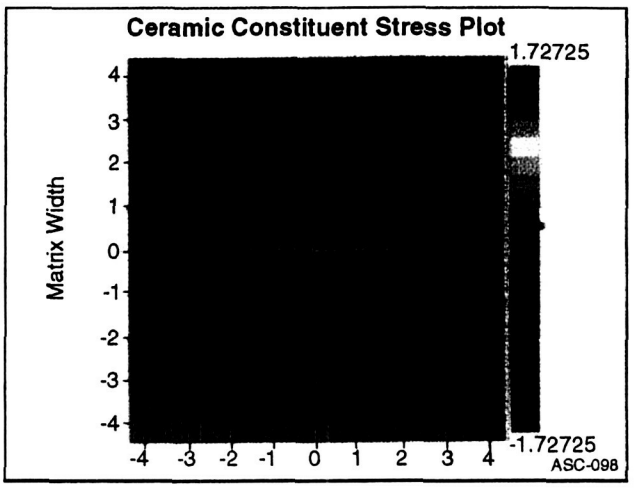

Figure 6-4. Ceramic Constituent Stress Plot - YY Slice

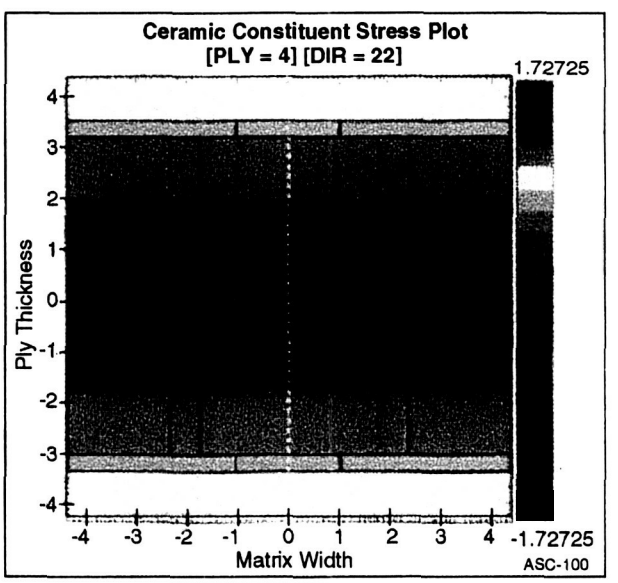

Figure 6-5. Ceramic Constituent Stress Plot - XX Slice

6.1.3 PROMISS Integrated With CEMCAN

PROMISS integration with the CEMCAN module provides the capability to perform probabilistic materials strength simulation in place of the deterministic form of the multifactor law for the fiber, interface and matrix. Evaluation of the CMC constituent material strengths and risk assessment is performed by a new subroutine, CEMPRO. CEMPRO extracts information (Table 6-2) from the CEMCAN data bank, and the CEMCAN simulation output for each ply at each node following every load increment.

Alpha STAR efforts focused on integrating probabilistic materials strength simulation for the following: 1) ply stress, 2) individual slice stress, 3) matrix stress, 4) fiber stress, and 5) interface stress in the 11, 22, 33, 12, 13, and 23 directions.

Material property data is passed through from the data bank to provide the current, ultimate, reference and empirical constant values. The form of the constitutive strength degradation equation used for the ceramic composite analysis is given as:

$$\frac{P}{P_o} = \left[\frac{T_F - T}{T_F - T_o}\right]^n \left[\frac{S_F - \sigma}{S_F - \sigma_o}\right]^m \left[\frac{S_F - \dot{\sigma}}{S_F - \dot{\sigma}_o}\right]^l \left[\frac{\dot{T}_F - \dot{T}}{\dot{T}_F - \dot{T}_o}\right]^k \left[\frac{R_F - R}{R_F - R_o}\right]^p \left[\frac{N_{MF} - N_M}{N_{MF} - N_{Mo}}\right]^q \left[\frac{N_{TF} - N_T}{N_{TF} - N_{To}}\right]^r \left[\frac{t_F - t}{t_F - t_o}\right]^s \quad (1)$$

P-property; T-temperature; S-strength; R-metallurgical reaction; N-number of cycles; D-diameter; d-stress; t-time; over dot-rate; subscripts: O-reference; F-final; M-mechanical; T-thermal

The equation provides a multifactor interaction relationship (MFIR) assumed to represent the various factors which influence in-situ constituent material behavior. As expressed, this relationship takes into account:

- Effects that proceed gradually until final stages where progression is rapid.
- The in situ behavior of fiber, matrix, interphase, coating
- The role of primitive variables (PV)
- Constituent properties in terms of PV
- Room-temperature reference property values.
- Continuous interphase growth
- Simultaneous interaction of all primitive variables

and is:

- Adaptable to new materials
- Amenable to verification inclusive of all properties
- Readily adaptable to incremental computational simulation

Within each primitive variable term the current, ultimate and reference values and the empirical material parameters may be modeled as either, normal, lognormal, or Wiebull random variables. Simulation is used to generate a set of realizations for normalized random strength, S/S_o, from a set of primitive variables and empirical material constants. Maximum penalized likelihood is used to generate an estimate for the probability density function (PDF) of normalized strength, from a set of realizations of normalized strength. Integration of the PDF yields the cumulative distribution function (CDF). Plot files are produced both the PDF and the CDF. PROMISS also provides information on S/S_O statistics (mean, variance, standard deviation and coefficient of variation), Figure 6-6 illustrates the procedure in performing material reliability assessment.

A graphic user interface (GUI) is provided to allow direct input to PROMISS of the analytical results of CEMCAN. The GUI provides the user the following capabilities: 1) Interactive preparation of input data for PROMISS from unit cell material constituent analysis by CEMCAN, 2) Interactive selection of the ply, subregion, within unit cell, time step, and the stress direction in performing probabilistic failure analysis, and 3) graphical display of the failure probability distributions, i.e. PDF, and CDF. The procedure to evaluate the constituent material and risk assessment for strengths of material systems is depicted in Table 6-2. Also, many uncertainties and perturbations in the constituent properties of fiber, matrix, interface, and fabrication variables can be simulated. These constituent properties are illustrated in Table 6-3.

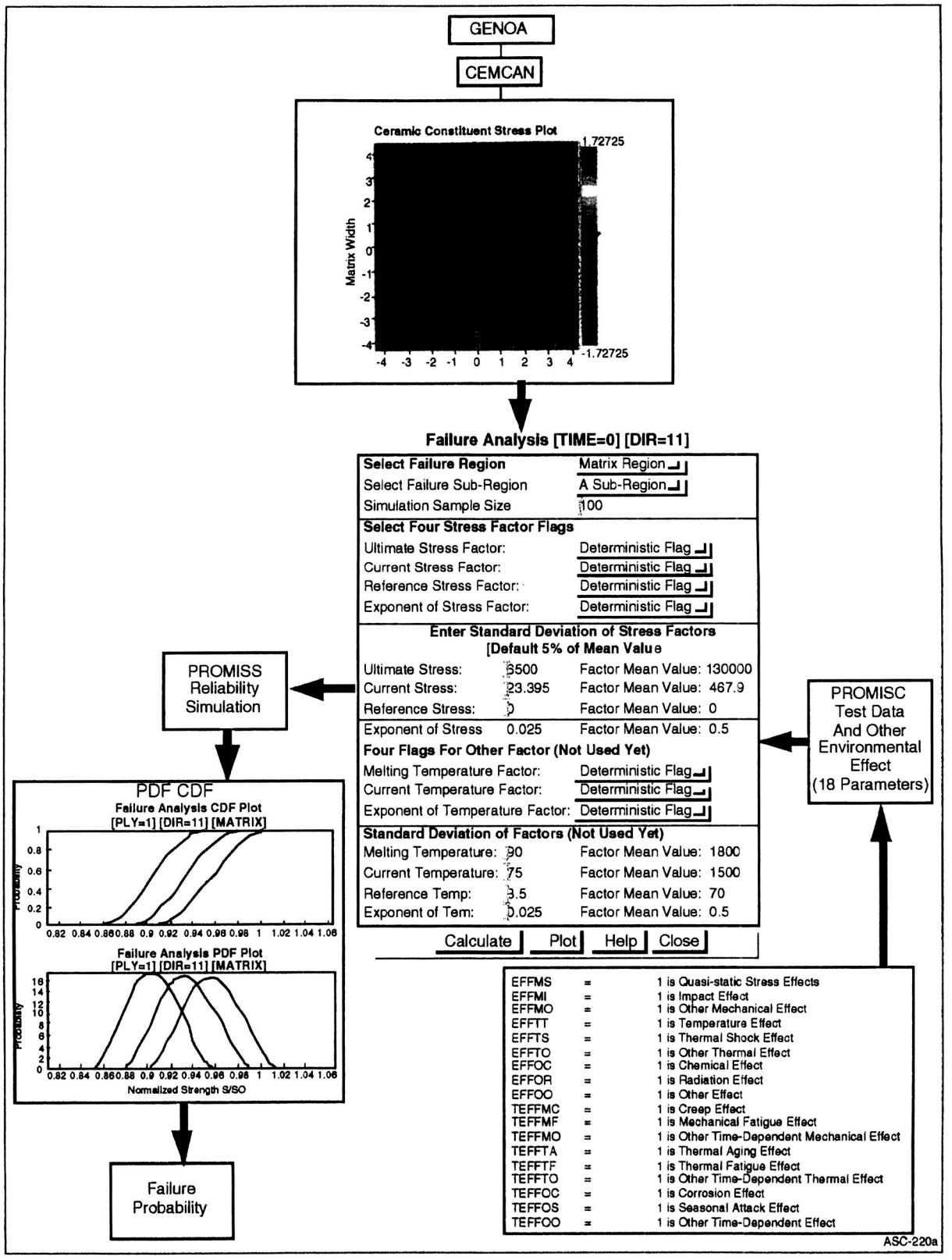

Figure 6-6. Procedure For Assessment of Material Reliability

Table 6-2. Procedure of Interactive Material Risk Assessment

READ Constituent DATA for failure assessment From GRAPHICS (GUI)
STEP 1: A-Select time step; B-Select Ply Number for failure assessment; C-Select the probability of failure (fiber, or Matrix, or Interface) due to stress in "11", "22", "33", "12", "13", "23"
STEP 2: Select deterministic variable, or random Variable with normal distribution, or random variable with lognormal distribution, or random variable with Weibull distribution from GUI
STEP 3: Program to Calculate or USER Input: STANDARD DEVIATION of Selected four primitive variables (A_i, A_{iF}, and A_{io})and ai the empirical material constant from GUI
READ DATA From Constituent DATA BANK
STEP 4: Read Material data from CEMCAN.IN file; Extract Material data for Matrix, Fiber, and Interface; Read Melting Temperature of fiber, and Matrix; Read Fiber Tensile and Shear Strength; Read Exponent of stress and temperature
READ STORED DATA From Constituent SIMULATION
STEP 5: Read fiber stress for each subregion [C]; Read MATRIX stress and temperature for each subregion [A or B or C]; Read INTERFACE stress and temperature for each subregion [B or C]
X11/MOTIF POST PROCESSOR PLOTS
STEP 6: Prepare data input for PROMISS, Execute PROMISS, Generate PDF, CDF; Generate Post Processor PDF, and CDF Graphics and save the plots for STEP 7.
STEP 7: Repeat step 1 through 3 to perform sensitivity analysis; Re Generate Post Processor PDF, and CDF Graphics. Create failure probability plots

Table 6-3. Uncertainties In The Constituent Properties

FIBER	MATRIX	FABRICATION VARIABLE
Normal Modulus E_{f11}	Normal ModulusE_m	Fiber volume ratio, K_f
Normal Modulus E_{f22}	Poisson's ratio, v_m	Void volume ratio, k_v
Poisson's ratio, v_{12}	Tensile Strength, S_{mT}	Ply Thickness, t_i
Poisson's ratio, v_{23}	Compressive Strength, S_{mC}	Orientation angle θ
Shear Modulus, G_{f12}	Shear Strength, S_{mS}	
Shear Modulus, G_{f23}		
Tensile Strength, S_{fT}		
Compressive Strength, S_{fC}		

6.1.4 Probabilistic Analysis in GENOA

The assessment of reliability of material strength is performed by the PROMISS code. Ceramic Matrix Composite (CMC), material strength and risk assessment analysis for each ply at each node following every load increment is performed by integration of PROMISS within CEMCAN. Probabilistic materials strength simulation is performed in place of the deterministic form of the multifactor law for the fiber, interface and matrix. This assessment utilizes the NASA data banks available for the CEMCAN and PROMISS codes.

The probabilistic assessment of the strength is calculated by PROMISS code. Modifications are made to interactively generate sensitivity of primitive parameters from CEMCAN in order to simulate the distribution of the matrix and fiber, and interface for specific subregions of the material microstress. With the ability to save the perturbed distribution in the Fail Probplot subroutine, the randomness in

the calculated ply stress/modulus, by constituent modulus, volume fraction, etc. from CEMCAN is simulated from the anticipated respective probabilistic distributions.

The calculated stress distributions from CEMCAN are saved in a file at time t with the ply information needed to perform risk assessment in the subroutine PROBPLOT. This subroutine plots the appropriate CDF and PDF using PROMISS with degraded constituent material strengths. A realization of the probability of failure is performed by finding the intercept of the three probability densities functions and adding the common populations so that the sum can be compared to the cumulative distribution function of degraded strength. The result is then used as an estimated probability of failure for the specific subregion of the material.

6.1.5 Micromechanical Risk Assessment

In order to perform a micromechanical risk assessment, a point in the multi-level iterative analysis must be chosen such that enough information is present to provide a comprehensive evaluation of probable failure. With respect to a probabilistic CEMCAN analysis, this point follows each realization of ply and constituent material strength degradation. Risk assessment also requires that a failure mode be used which is representative of a realistic situation which would cause probable failure. For the purposes of evaluating probable failure in CMC composites, a failure mode can be defined for both the ply-level and the constituent-level in the analysis. At the constituent-level, the failure mode represents a probable event which would initiate failure in the form of crack growth or local yielding. This mode is then defined as the event that a particular microstress is greater than the corresponding constituent material strength. The probability of constituent failure initiation is then calculated by:

$$P_f(i,j,k) = \int f_{\sigma_{ijk}}(x)\, F_{S_{ijk}}(x)\, dx$$

where $f_{\sigma_{ijk}}$ is the probability density function of the normalized microstress, σ/S_o, at the ith structural node, the jth ply and the kth constituent material. $F_{S_{ijk}}$ is the cumulative distribution function for the degraded strength, S/S_o, at the ith structural node, the jth ply and the kth constituent material. At the ply-level, the failure mode represents a greater risk of catastrophic failure. This mode is defined as the event when a ply stress is greater than the corresponding ply strength. Graphically, the assessment of risk can be shown as the overlap of the probability density functions for the stress and strength (illustrated in Figure 6-7).

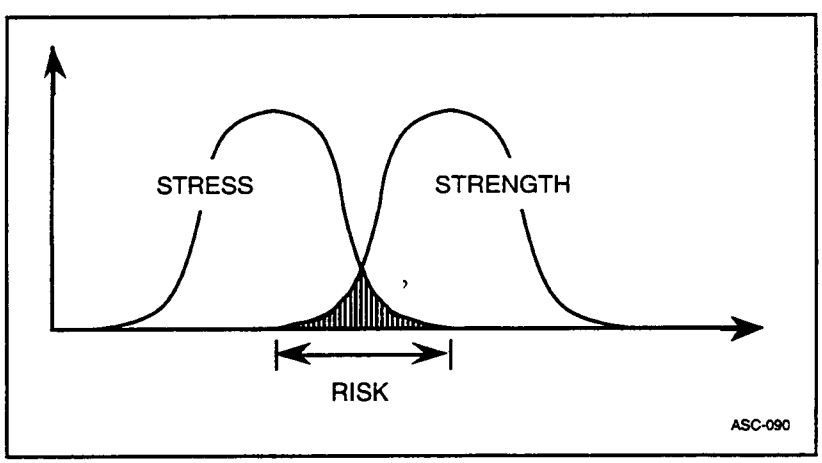

Figure 6-7. Illustration Of The Overlapping Probability Densities Functions Representative Of The Probable Event Of Failure.

It is anticipated to be feasible to perform risk assessment at each structural node, for each ply and ply strength, as well as each constituent and constituent material strength. With this type of analytical capability, the design of new aerospace structures and components could push the limits of new

composite material systems. The use of over-bearing design allowable would become a method of the past. The ability to assess micromechanical damage would also provide a unique tool for validating and upgrading numerous mechanism-based methodologies. In short, an analytical tool providing this type of detailed structural and material response, would represent an innovative step forward in the design process of aerospace structures.

6.1.6 Integration Of Environmental And Test Data With A Stochastic Simulation

Test data can be merged into a unified simulation analysis by using PROMISS analysis . Statistical scatter of experimentally observed properties can be explained by reasonable statistical distribution of input parameters in composite micromechanics and laminate theory predictive models (refer to Figure 6-6).

(It is important to note that other uncertainties can also be included at this level in the micromechanics analysis. An example is the probabilistic treatment of the ply alignment or misalignment q_l which is used to calculate the ply transformation matrix $[R_l]$. Small variations in the values of this matrix could have wide spread effect on the predicted behavior of the composite and could account for many of the geometric uncertainties associated with laminated composites.)

Once the various densities and distributions have been simulated, they must be stored for subsequent analyses. One feasible method is to store the probability densities and cumulative distributions of each variable as a probability array indexed in such a way that a pseudo-random number can rapidly extract a value from the realization. This method is utilized by PROMISS and has only one drawback; it consumes a large amount of memory when dealing with large arrays of variables.

6.1.7 NESSUS: 3-D Inelastic Finite Element Analysis

The NESSUS program implements an innovative mixed finite element procedure which is intended to improve accuracy and diversity in modeling capability [18]. The parallel version of NESSUS is integrated with the Alpha STAR Multi Frontal Algorithm (AMF). The AMF allows the user to simulate combination of elements within the same finite element analysis to permit the use of beam, and shell elements as the mixed element capability. This allows the finite element user to run large models beyond the limitation of local processors to make static analysis of three types of inelastic constitutive models: 1) simplified plasticity, 2) conventional plasticity, and 3) an advanced viscoplasticity.

The NESSUS program was originally written in FORTRAN using static allocation of memory that is hard coded before compilation time. This means code recompiling is necessary for different sizes of input models. GENOA instead uses dynamic memory allocation supported in " C" language and passes the allocated memory to the other parts of the code written in FORTRAN. The optimization module of MAESTRO dynamically calculates the amount of memory needed based on the specifications of the model, number of processors, and their capabilities. If there is not enough memory for some processor, the whole process can be stopped and run again for a new configuration.

The iterative finite element solution procedure of HITCAN-NESSUS is illustrated by the flow diagram shown in Figure 6-8. Matrices [K] and [F] are the conventional finite element stiffness matrix and load vector, respectively. Other conventional finite element matrices appearing in this flow diagram are [B], [D], and [Q], the strain-displacement matrix, the stress-strain matrix and the diagonalized inner product of shape functions respectively. All quantities involved in the computation are evaluated as nodal vectors. Values for stresses, strains and displacements are obtained at nodes by the nodal strain recovery calculation and the residual load correction shown in the flow diagram.

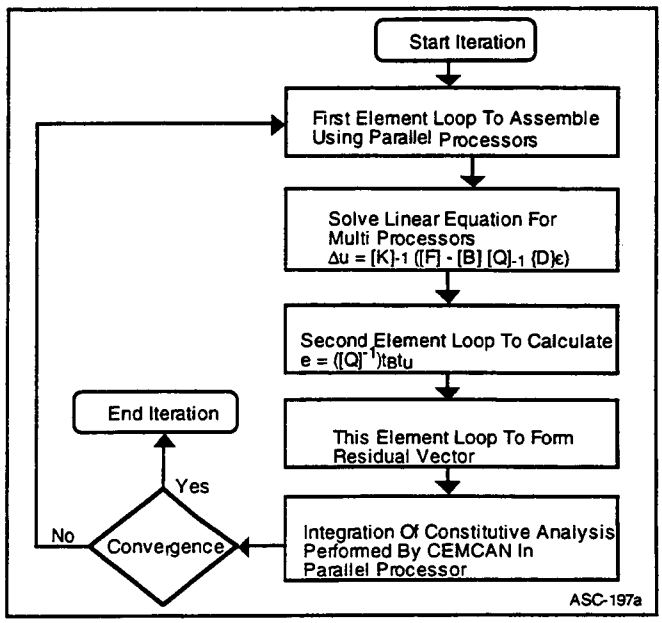

Figure 6-8. Iterative Method Utilized By HITCAN To Perform Nonlinear Structural Analysis.

Iterative solutions are utilized by NESSUS even when solving for a purely elastic response. An iterative solution of elastic response, compared to the standard displacement method, produces improved stress results.. In path-dependent inelastic calculations, such improved response increases the accuracy of analyzing the behavior of a composite structure at high temperatures.

6.2 TEMPERATURE AND STRAIN DISTRIBUTION IN A CMC COMBUSTOR

A parametric mapping technique extensively developed by Alpha STAR for NASA/LaRC [19] can be integrated into the GENOA simulation code to provide the capability of real time mapping of surface and through the wall thickness temperature and strain distributions of an operating CMC combustor (provided that sensor data from representative locations is available). The proposed parametric mapping technique provides a means of transforming thermal and structural deformation between CFD grids and structural cells. This concept is based on a non-aligned interface interpolation scheme. As illustrated in Figure 6-9, the CFD grid mesh and structural nodal points can be interchangeably transformed from one domain on to the other through parametric mapping. Each of the receiving points is searched and located within the donor domain. This searching algorithm is formulated for a 3-dimensional general surface which will require the point to lie within the cell's projection plane with a minimum normal distance from the projected surface. Once the receiving point is located on donor face, its location will be expressed in terms of the parametric variable (α,β) in the donor face.

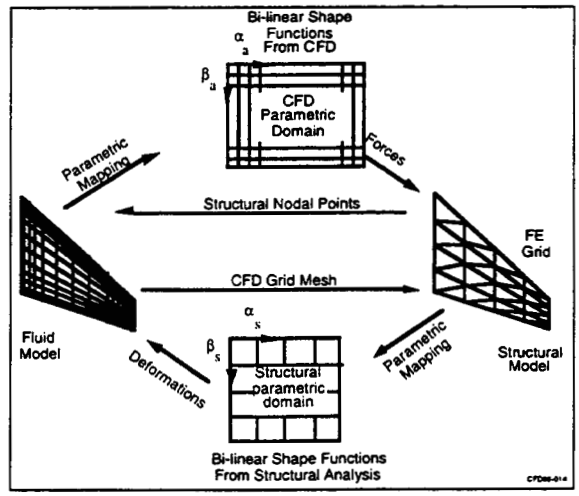

Figure 6-9. Parametric Mapping Technique Couples With Bi-Linear Shape Function Interpolation Provides an Efficient and Robust Means of Data Communication

Since the CFD grids and structural cells will be riding on the flexible surface of their fixed relative locations, the searching and mapping procedures are required only once at the beginning of the run and will be stored in the memory. The bi-linear shape function of each donor cell is formed at each time step to account for the changes of the airloads and deformations. This algorithm, offers the advantages of being efficient, robust, and applicable to multiple-component configurations.

6.3 COMPUTATIONAL SIMULATION OF CMC CREEP BEHAVIOR

An important consideration to assure the successful application of high-temperature ceramic composites in aircraft engine hot structures is creep performance. The traditional approach for evaluating creep performance is long term testing in representative stress and temperature environments. Data obtained from these tests is subsequently used in conjunction with empirical relationships to design ceramic composites to resist the sustained temperature and stress. However, this approach is generally costly and time consuming because it requires a relatively large number of tests to reliably determine critical combinations of stresses and temperatures which will cause creep in hot composite structures.

Computational simulation supplemented with a few strategically selected experiments is an alternative approach. This approach has the potential to substantially reduce the number of tests and yet provides the reliable information needed to accurately describe creep. The CEMCAN computer code has been modified to perform creep analysis. CEMCAN is similar to METCAN [20] which has a novel MFIR for representing the high temperature nonlinear behavior of materials.

The approach for upgrading CEMCAN for creep consists of modifying the time term of equation 6.1 by substitution of $(1-\sigma_t/S_F t_F)^s$ for the time expression. The calibration of the modified CEMCAN consists of selecting t_f and the exponent to match the experimental data. Figure 6-10 shows the fit achieved by

modified CEMCAN to stress-rupture test results obtained by DuPont on enhanced Hi-Nicalon/SiC ceramic corresponding to exponents in MFIR are selected to reproduce the test data.

In the absence of test data, it is presently recommended that t_F be selected to meet an acceptable limit on the degradation of a specific constituent property. This can be done by expressing the acceptable degradation in the specific property as a ratio in the MFIR and then solve the relationship for t_F.

As a results of upgrading:

- CEMCAN can rapidly simulate the effect of stress and temperature levels (creep) on time dependent behavior in high temperature ceramic composites.
- CEMCAN can be calibrated to simulate complex nonlinear behavior in specific high temperature ceramic composites where experimental data are available.
- Nonlinear behavior can be modeled by using the multi-factor interaction relationship.
- Significant effects of processing history on high temperature ceramic composite behavior and can be included in a simulation.
- CEMCAN can be used to select short term tests to assess long term behavior.

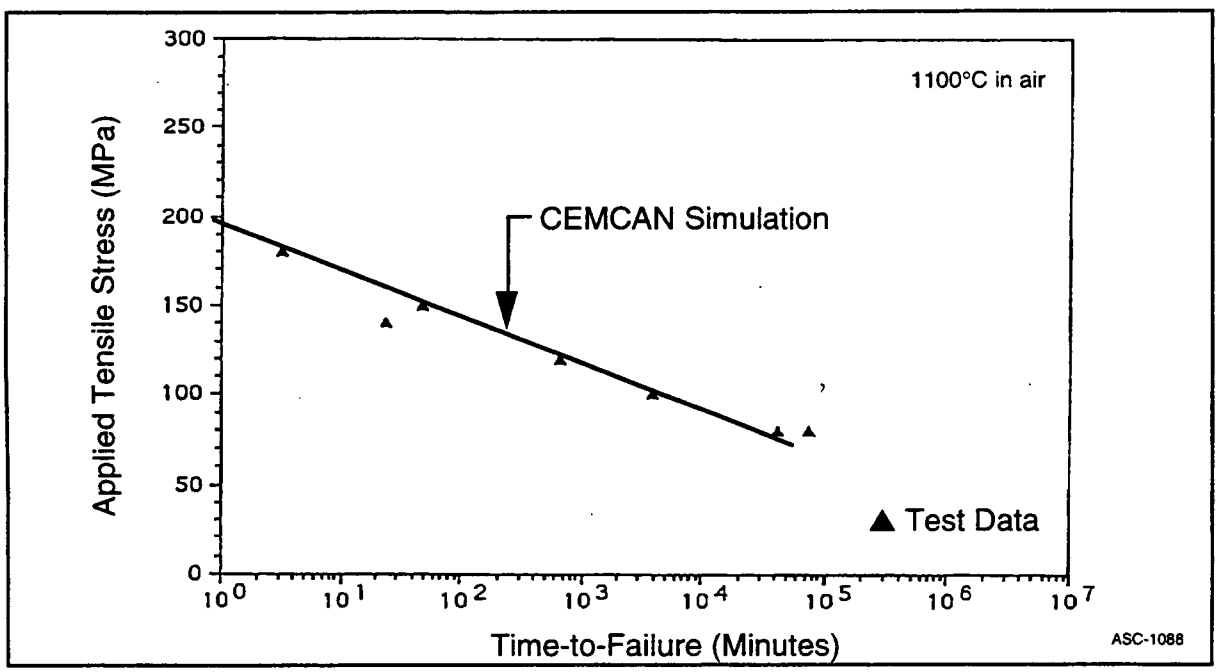

Figure 6-10. CEMCAN was Calibrated with Stress Rupture Test Results

7.0 Simulation And Model Verification

Thermal paint data from combustor tests and coupon tensile data obtained by Allied Signal on CMC combustor material was utilized by Alpha STAR in simulations to:

1. Calculate the stress distribution using GENOA code through the thickness direction of a combustor to provide superior stress distribution calculated by use of ANSYS code because ANSYS does not : a) take into account material degradation over time; b) uncertainties in material properties and geometric and thermal boundaries; and c) progressive damage failure due to crack initiation and growth.

2. Calculate the probability of failure, and predict combustor life (utilizing stress distribution results of Step 1).

3. Accurately preview performance of a specific combustor design and thereby reduce sub- and full-scale combustor design and test effort.

4. Assess the impact of embedding sensors in a CMC combustor

TASK 3 - SIMULATION AND MODEL DEVELOPMENT/VERIFICATION

1. Develop geometry and finite element model of a CMC combustor made by Allied Signal Aerospace

2. Perform linear and nonlinear finite element analysis using Alpha STAR and NASA codes, GENOA, NESSUS, CEMCAN (Ceramic Matrix Composite Analyzer) to predict the structural response under combined loading conditions.

3. Conduct probabilistic analysis of component performance operating on the basis of sensor input. This analysis includes identifying the uncertain primitive variables at constituent and ply levels and perturbing the variables to establish the probabilistic relationship between structural response and the primitive variables using PROMISS code.

4. Develop sensor influence coefficients: Define the necessary steps to enhance the existing CEMCAN to predict the structural response of the combustor with embedded sensors.

5. Modify the existing CMC data bank used by CEMCAN to account for the material property change due to embedded sensors.

6. Verify the numerical simulation model by comparing the simulation results with the test data obtained in Task II.

7.1 PREDICTION OF STRUCTURAL RESPONSE UNDER COMBINED LOADING

To better understand the failure mechanism of the combustor a finite element analysis (FEA) was performed on the noneffusion-cooled subelement. The analysis was performed using a commercial FEA (ANSYS) code in which observed temperature maps were used as input for the thermal stress analysis. The cold -and hot -side surface temperatures of the model were mapped from the uncooled subelement thermal paint data. Figure 7-1 shows the resulting cold-side thermal stresses in the form of normalized

axial and hoops stress plots. The areas identified by arrows indicate stress levels that exceed the short-term ultimate strength of the material. As evidenced from this figure axial stress near the hole and at the thick-to-thin transition area as well as high-hoop stress at the free edge were predicted to be high enough to crack the material. This prediction did in fact correspond to observed cracks at those locations in the noneffusion-cooled subelement (Figure 7-2).

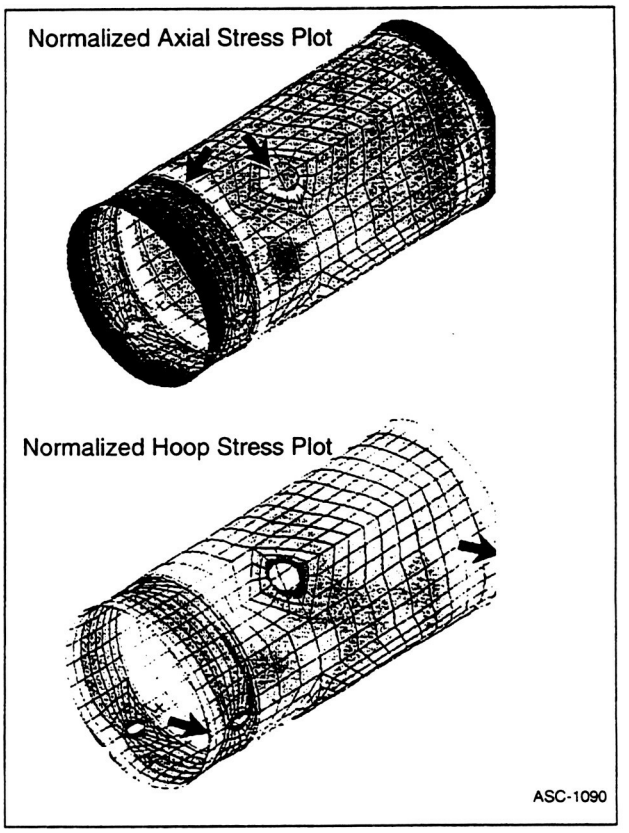

Figure 7-1. Cold-Side Thermal Stress

7.2 VERIFY NUMERICAL PROBABILISTIC SIMULATION MODEL WITH COUPON TEST DATA

In this section numerical simulations on test coupons are performed and the results are validated. Important parameters are identified and the effect of sensor on ply reliability is discussed.

7.2.1 Verification Of Composite Mechanics Analysis Based On The Coupon Test Results

The global material properties (E_x, E_y, E_z, G_{xy}, G_{xz}, G_{yz}, ρ, α_x, etc.) of eight layered braided composite of the combustor model at various temperatures are evaluated experimentally by Allied Signal Company. The material used was Nicalon fibers in Silicon Carbide matrix (SiC/SiC). The material properties of these constituents at three different temperatures are given in Section 5.0. The experimental values of composite elastic modulus and strength as functions of temperatures are shown in Figure 7-3. These properties are reduced as temperature is increased. At elevated temperatures, the reduction in material properties become more noticeable.

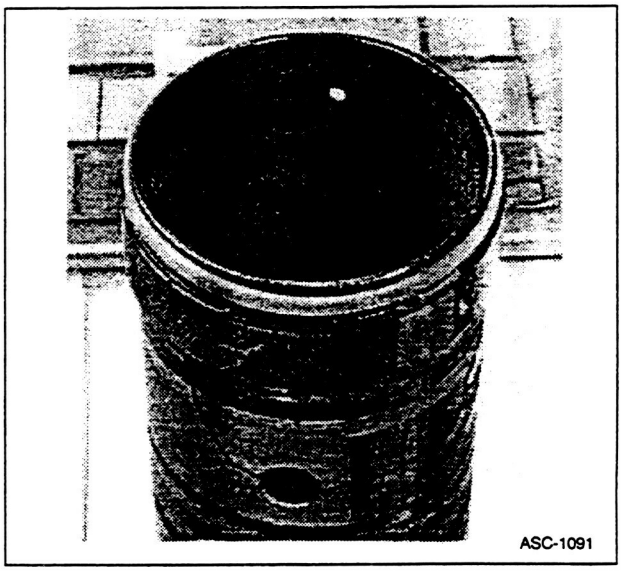

Figure 7-2. Uncooled Subelement Post Test Condition

At ASC, CEMCAN program is used to simulate SiC/SiC ceramic combustor model for various material porosity's at a wide range of temperatures. The calculated results are plotted in Figures 7-3 through 7-5

along with Allied Signal test results on material believed to have 10 percent to 12 percent porosity. The fiber volume for these simulations is 40 percent. The uncertainties in material properties provided room to calibrate the test results at room temperature. For example, the simulated results corresponding to 10 percent porosity best match the test results as shown in the figures. First, numerical simulations were performed to obtain composite properties at 70°F. At higher temperatures, the multifactor interaction relation (MFIR) embedded in CEMCAN was used to account for material degradations. The exponents in MFIR are calculated from the test results. The exponents calculation requires values of material properties at two different temperatures. According to MFIR the reduction in property P due to temperature T is given by

$$\frac{p_c}{P_0} = \left(\frac{T_m - T_c}{T_m - T_0} \right)^n \tag{7.1}$$

where subscripts *o*, *c*, and *m* refer to initial, current, and melting (final) values. After some algebraic manipulations, equation (6.1) can be reduced to an expression for exponent n:

$$n = \frac{\ell n(P_c) - \ell n(P_0)}{\ell n(T_m - T_c) - \ell n(T_m - T_o)} \tag{7.2}$$

To calculate the exponent n, values of the specific property at initial and current temperatures are plugged in Equation (7.2). With proper degradation exponents CEMCAN is run over the target temperature range of 70°F to 2500°F.

Figure 7-3 demonstrates that there is a good correlation for the modulus of elasticity in longitudinal direction (E_x). Similarly, Figure 7-4 demonstrates good agreement between simulated E_y and test results. The transverse modulus of elasticity E_z (shown in Figure 7-5) is not as close to the test results as E_x and E_y are. This is due to the weave in the material. However, all elasticity modulus reduce with an increase in fiber volume ratio. This is expected since matrix is more stiff than the fiber. Furthermore, due to weave, CEMCAN overestimated the in-plane poison ratio.

Traditional computational approaches are deterministic and thus, do not account for uncertainties associated with composite structures and materials. The strength values for materials, particularly for brittle materials, may depend on the size and distribution of flaws and therefore, maximum stress criterion of failure alone becomes inaccurate in predicting the strength of such materials. A statistical/probabilistic analysis can be carried out to accurately account for the effect of flaw size and distribution on the strength of a constituent. Uncertainties in several constituent properties and applied temperatures can be accounted for in predicting the structural response and reliability. CEMCAN was modified to work with GENOA's executive controller to make CEMCAN results suitable for input to the PROMISS code to provide probabilities of in service thermo-mechanical failures of ceramic composite (1) fiber, (2) interface, (3) matrix, (4) lamina, and (5) laminate components.

The integrated combination of CEMCAN and PROMISS is called CEMPRO. CEMCAN calculates all micro and composite stresses. These stresses along with material properties are sent to PROMISS for probabilistic analysis. A typical output of CEMPRO for the ceramic combustor is plotted in Figures 7-6a and 7-6b. These figures show the probability density function (PDF) and the cumulative distribution function (CDF) for a SiC/SiC laminate at 2500°F. The horizontal axis in both the PDF and CDF plots represent strength. The mean reduction strength is reduced 0.87 or 87 percent of the baseline value. The CDF in Figure 7-6b also shows reliability. For example, the probability of strength to fall under 73 percent of its baseline value (S_o) is 10 percent. This implies that 90 percent of the times the strength is

greater than 73 percent of S_o. Once the reliability of layers are calculated system reliability of the entire combustor structure can be evaluated.

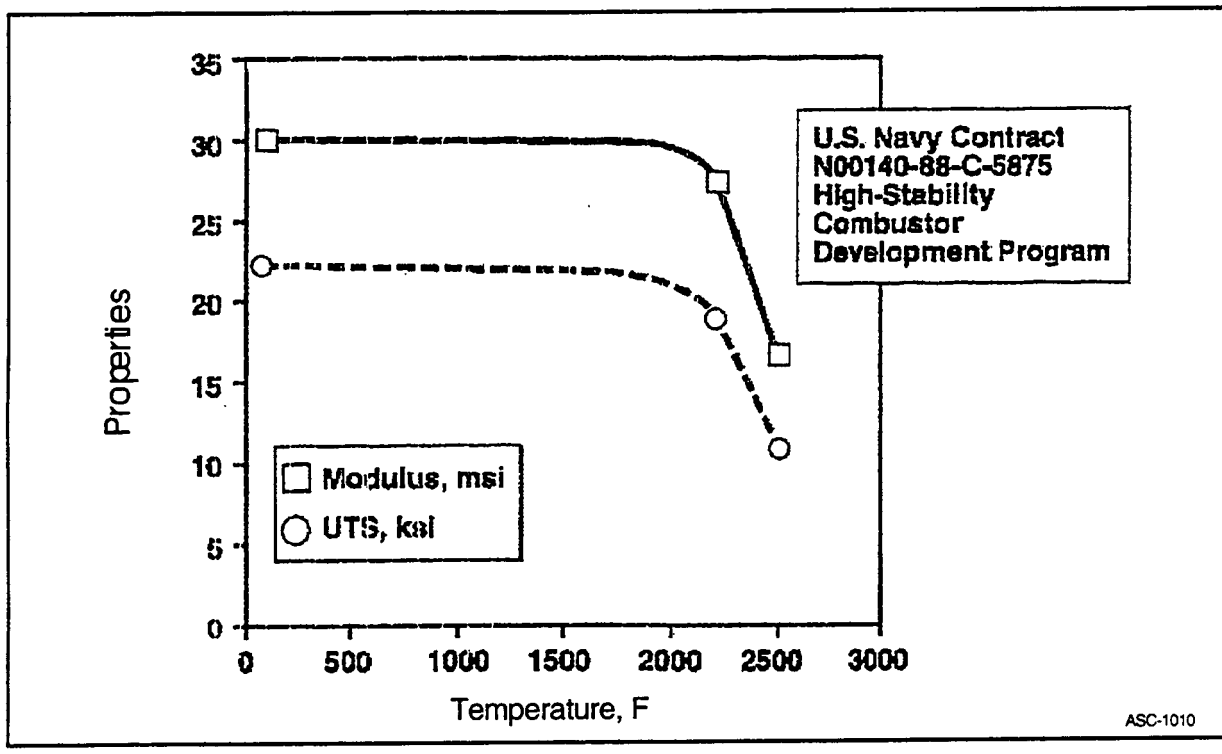

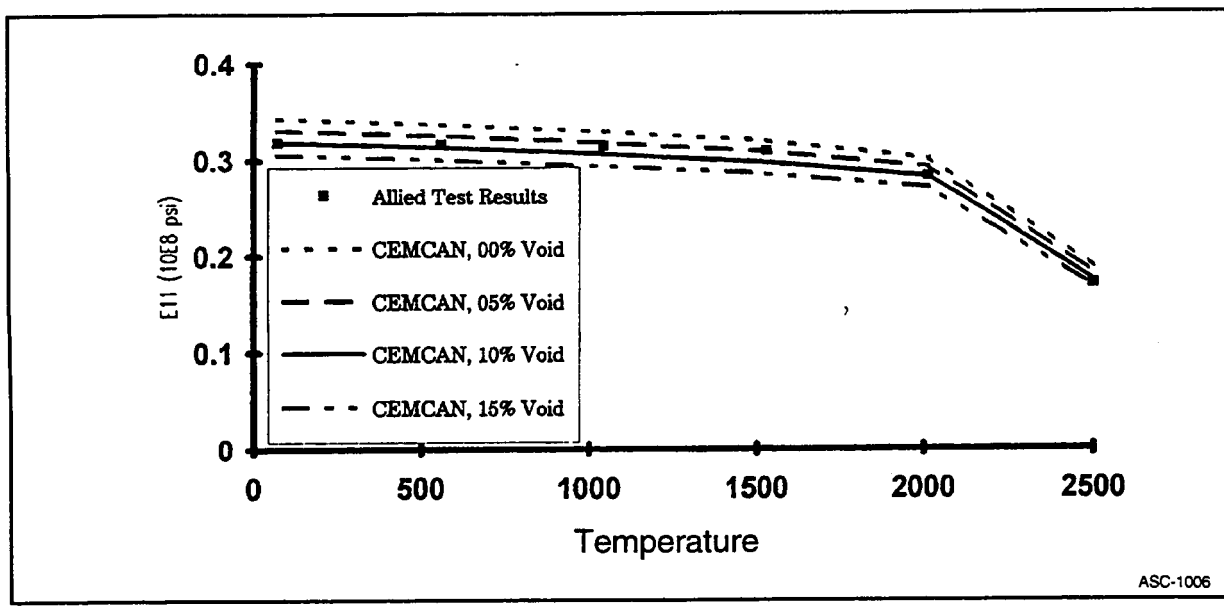

Figure 7-3. Influence of Porosity and Temperature on Composite Elastic Modulus E_{11}

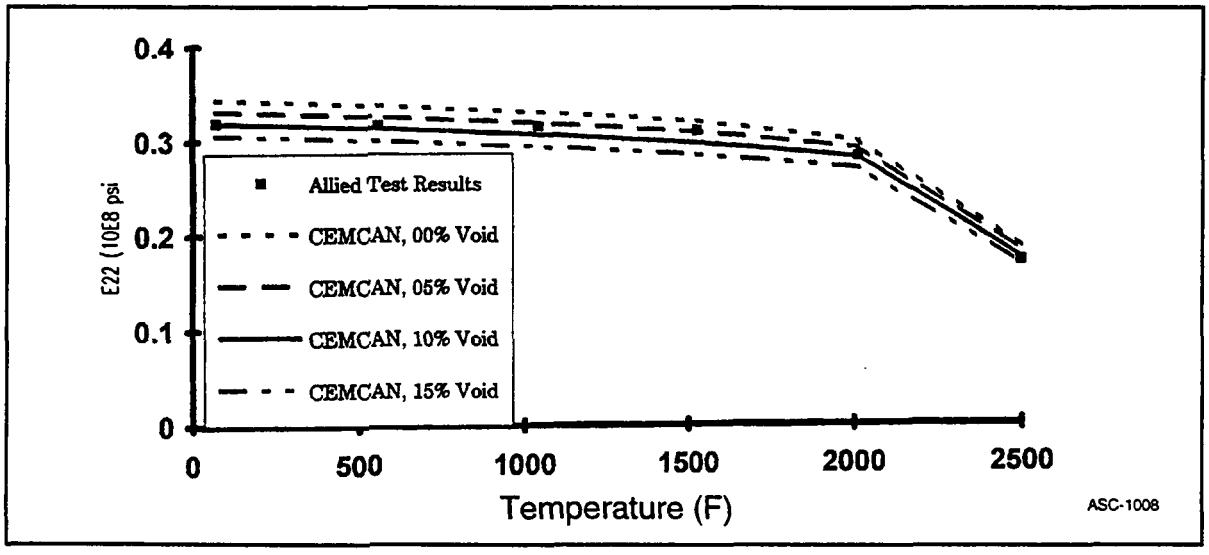

Figure 7-4. Influence of Porosity and Temperature on Composite Elastic Modulus E_{22}

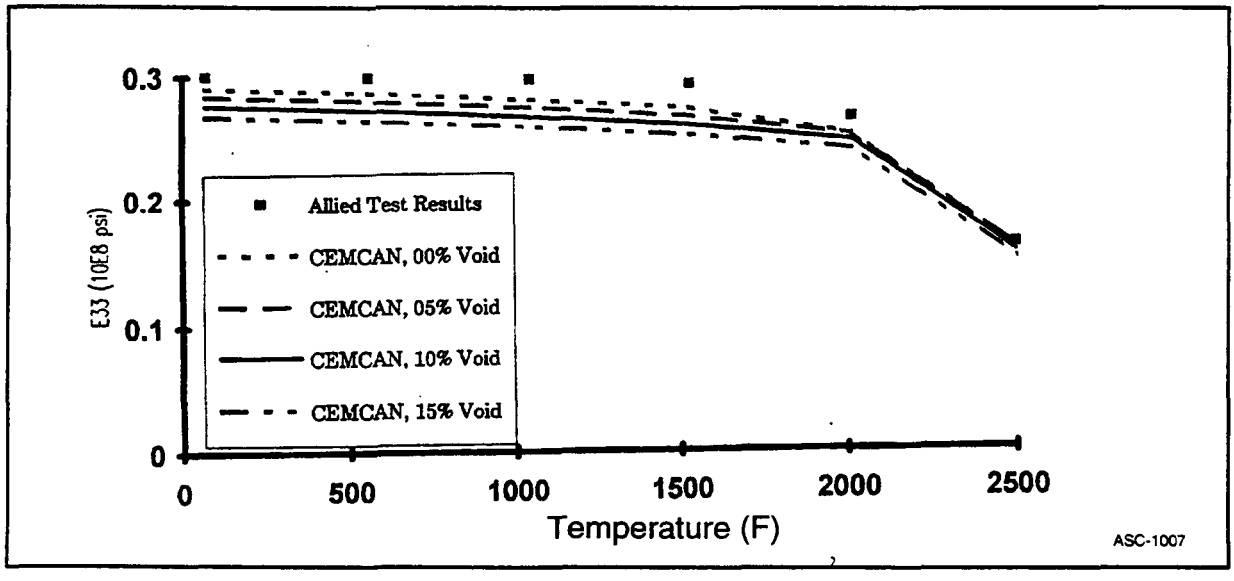

Figure 7-5. Influence of Porosity and Temperature on Composite Elastic Modulus E_{33}

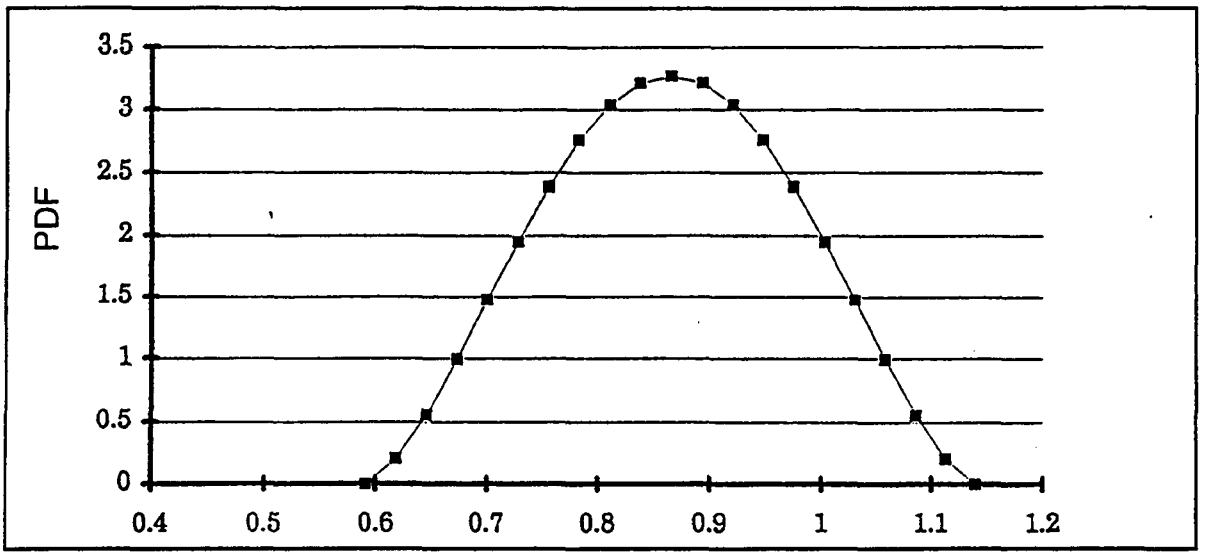

Figure 7-6a. Probability Density Function For Sic/Sic (0/±60) 24 Laminate Ply Thickness 0.08 Inunder Thermal Load Of 2500 F

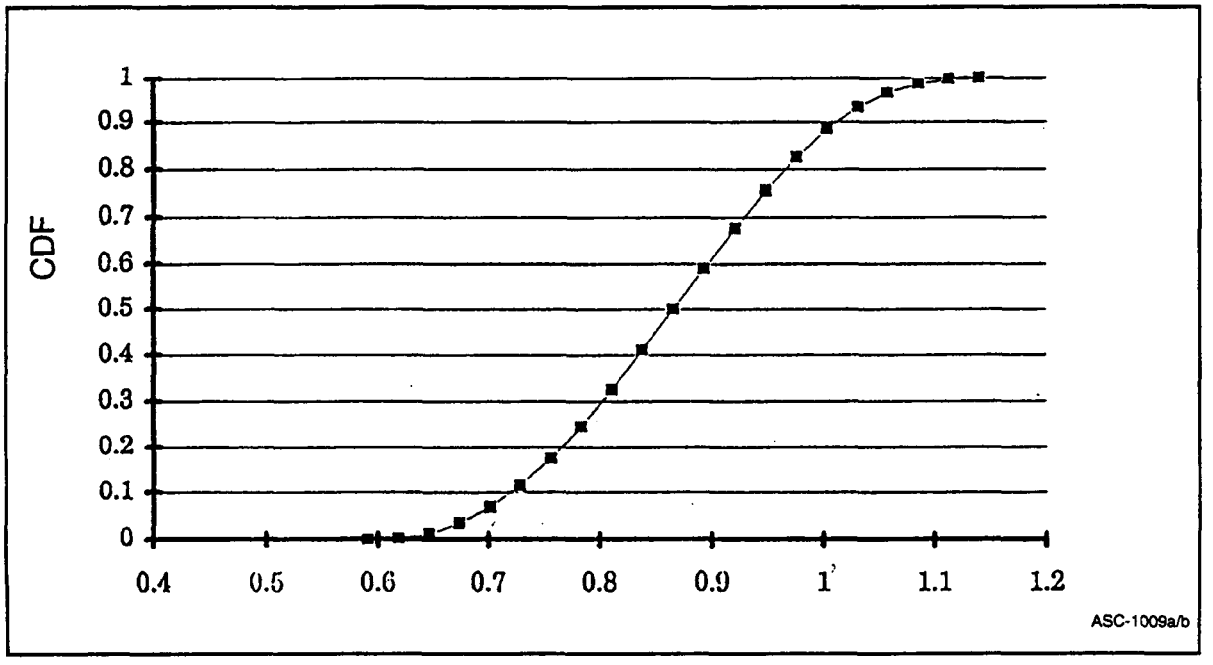

Figure 7-6b. Cumulative Distribution Function for SiC/SiC (0/+60) 24 Laminate Ply Thickness 0.08-in. Under Thermal Load of 2500°F

7.2.2 Finite Element Analysis

HITCAN code is used to simulate tensile test for the entire bone shape structure of composite coupon model shown in Figure 7-7. The resulting axial and transverse stress contours are shown in Figures 7-8 and 7-9, respectively. The loading is axial and symmetric. The axial stresses are not completely symmetric because composite layers are not symmetrically stacked. The area around the four corners are highly stressed as expected. PROMISS code is implemented to further investigate the reliability of the test coupon. The reliability of the top layer due to tensile longitudinal stress in test coupon is

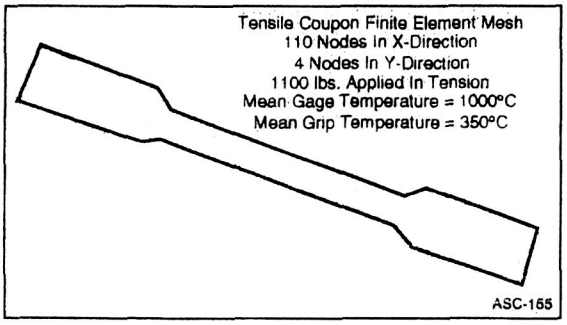

Figure 7-7. Composite Tensile Coupon Model Used to Demonstrate the Preliminary Probabilistic Analysis Capability of PROMISS Integrated With HITCAN

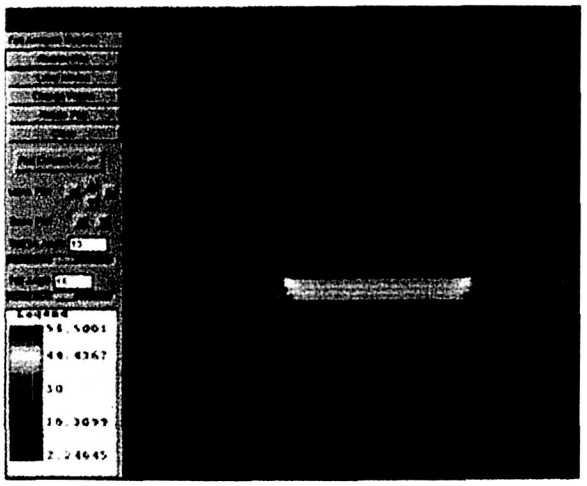

ASC-1092

Figure 7-8. Axial Stress Contour Plot for Coupon Test Model

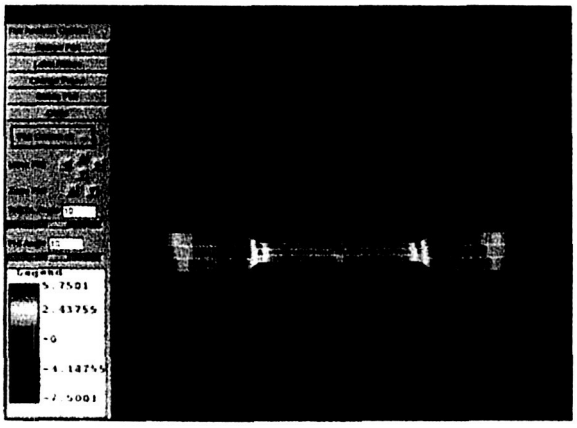

ASC-1093

Figure 7-9. Transverse Stress Contour Plot for Coupon Test Model

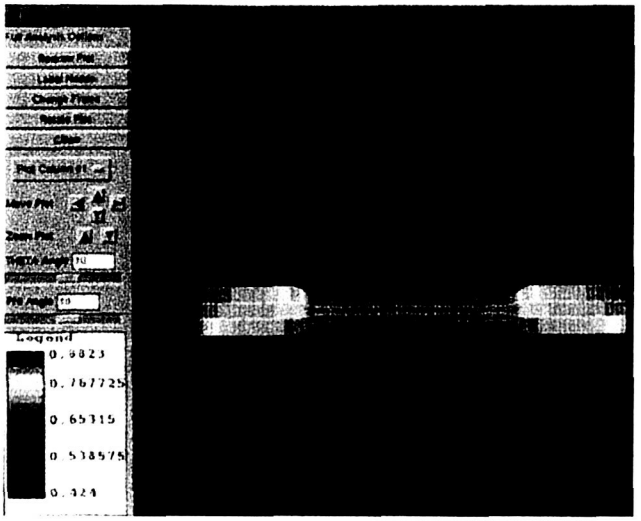

ASC-1094

Figure 7-10. Reliability Contour Plot for Top Layer of the Coupon Test Model

shown in Figure 7-10 as a contour plot. Obviously, the four corner neck areas are the least reliable areas due to high local stresses. Conversely, the raised areas next to necks have high reliability due to low local stresses. The successful numerical simulation of the test coupon stress distribution coupled with a reliability prediction mapping favorably demonstrates the potential of the GENOA software system to simulate an entire CMC combustor. This would allow significant reduction in expensive developmental testing as well as provide the basis for health monitoring of an operating CMC combustor.

7.2.3 Identification Of Important Parameters By Means Of Sensitivity Analysis

The stress in 0° fiber direction of a ply in the hottest section of the combustor is used to obtain a cumulative distribution function (CDF) for a combustor model under thermal loading only. Figure 7-11 shows the CDF of the ratio of the strength, S, to a baseline value, S_o. Figure 7-11 also shows that the strength CDF shift to the left, means that the strength under thermal loads drop as temperature increases. At temperature equal to 1800 F, 2000 F, and 2200 F, the respective mean strength is 80 percent, 75 percent and 73 percent of the initial strength of the structure. Also the respective strength for 0.99 reliability are 70 percent, 65 percent, and 62 percent of initial strength as shown

in Figure 7-12. Perturbation analysis was performed to calculate the sensitivity of response with respect to thermal load, and various fiber and matrix properties. The strength sensitivity at 0.99 reliability is shown in Figure 7-13. As shown in Figure 7-13, the strength is most sensitive to fiber volume ratio (FVR), normal modulus of fiber (E_f), and temperature.

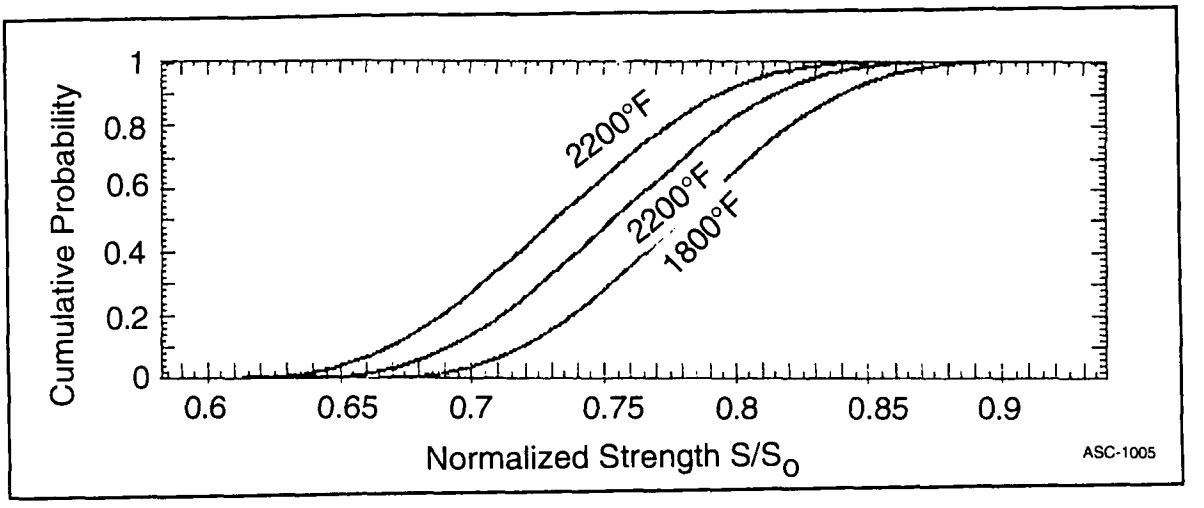

Figure 7-11. Cumulative Distribution Function (CDF) for the Strength Ply With the Highest Temperature

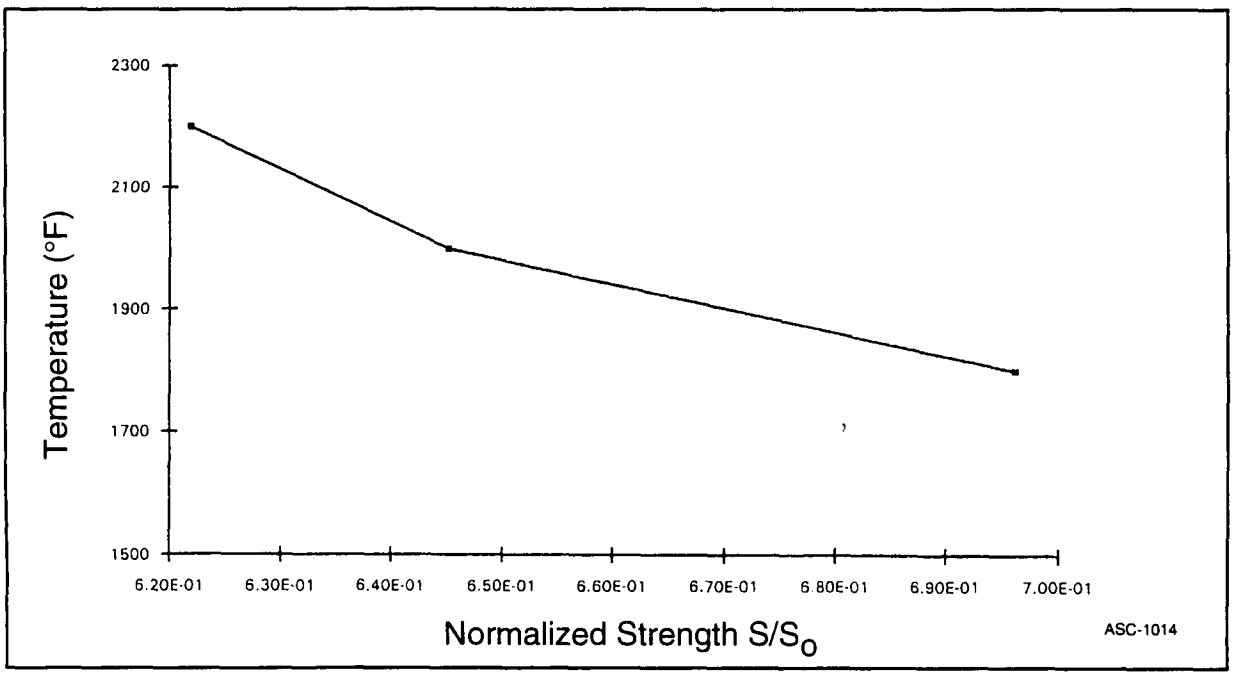

Figure 7-12. Strength Variation for 0.99 Reliability

In order to calculate the strength degradations, we use CEMCAN to evaluate the initial strength in longitudinal (material 11) and transverse (material 22) directions for composite layers of the ceramic combustor. In the simulation of initial strength, an incremental axial load in a particular direction is

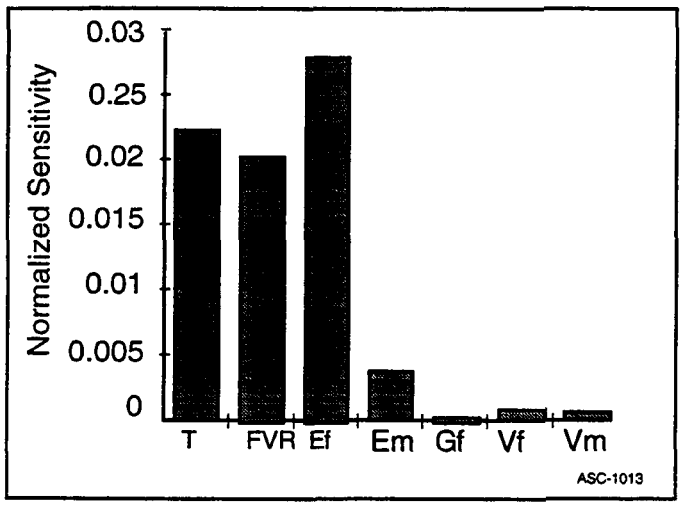

Figure 7-13. Strength Sensitivity at 0.99 Reliability for Coupon Test Model

applied to a layer. As the load is increased, the strain in the loaded direction is calculated by CEMCAN. The strength at a particular direction is the stress at which a jump of several order of magnitude in strain appears. As such, the calculated tensile strength are 6 and 2 ksi in material 11- and 22-direction. These low values show that the layers are very brittle.

CEMPRO is used to calculate the probabilistic strength degradation due to stresses in longitudinal (11) and transverse (22) directions. Weibull distribution is assumed in all probabilistic analysis. The effect of temperature on Cumulative Distribution Function (CDF) for hottest ply of the hottest section is shown in Figure 7-14. At that section the temperatures at cold and hot sides are 1600 °F and 1800 °F, respectively. Furthermore, it is assumed that variation of temperature through thickness is linear. Figure 7-14 also shows that a 5 percent increase (decrease) in temperatures shift CDF to the left (right) showing reduction (increase) in strength reliability. The corresponding strength sensitivity at 0.99 reliability is plotted in Figure 7-15. As shown, the strength sensitivity is more affected by longitudinal stress than transverse stress.

The sensitivity of strength with respect to fiber volume ratio (FVR), fiber modulus (E_{11f}), and matrix modulus (E_m) are also calculated. These sensitivities due to longitudinal and transverse stresses are normalized and plotted in Figure 7-16 for comparison. The results show that not only the longitudinal stress has great effect on the strength, but also that the strength is most sensitive to fiber modulus, temperature and fiber volume ratio.

7.2.4 Effect Of Incorporating Sensors On Ply Reliability

The effect of potential sensors imbedded in composite structure of the ceramic combustor and the distortion of structure due to insertion of sensors was investigated. A sensor embedded in aluminum oxide is inserted in ceramic combustor under the top layer (Figure 7-17). The results of CEMCAN and CEMPRO simulations are plotted in Figure 7-18. Both CDF curves are shifted to the left showing that the insertion of sensor lowers the strength reliability. The degradation is very large for the curve corresponding to transverse stress (22-direction). This is due to combination of the fact that insertion of sensor has shifted the transverse stress in the layer from compressive stress to tensile stress, and the fact that the material is very brittle. The reduction in reliability may be decreased by decreasing the sensor thickness. For example, the sensor thickness is assumed to be decreased by 75 percent and the simulation results are plotted in Figure 7-19. Clearly, the shifts in CDF curves are reduced. Therefore, reliability distortion due to insertion of sensors is less for thin sensors.

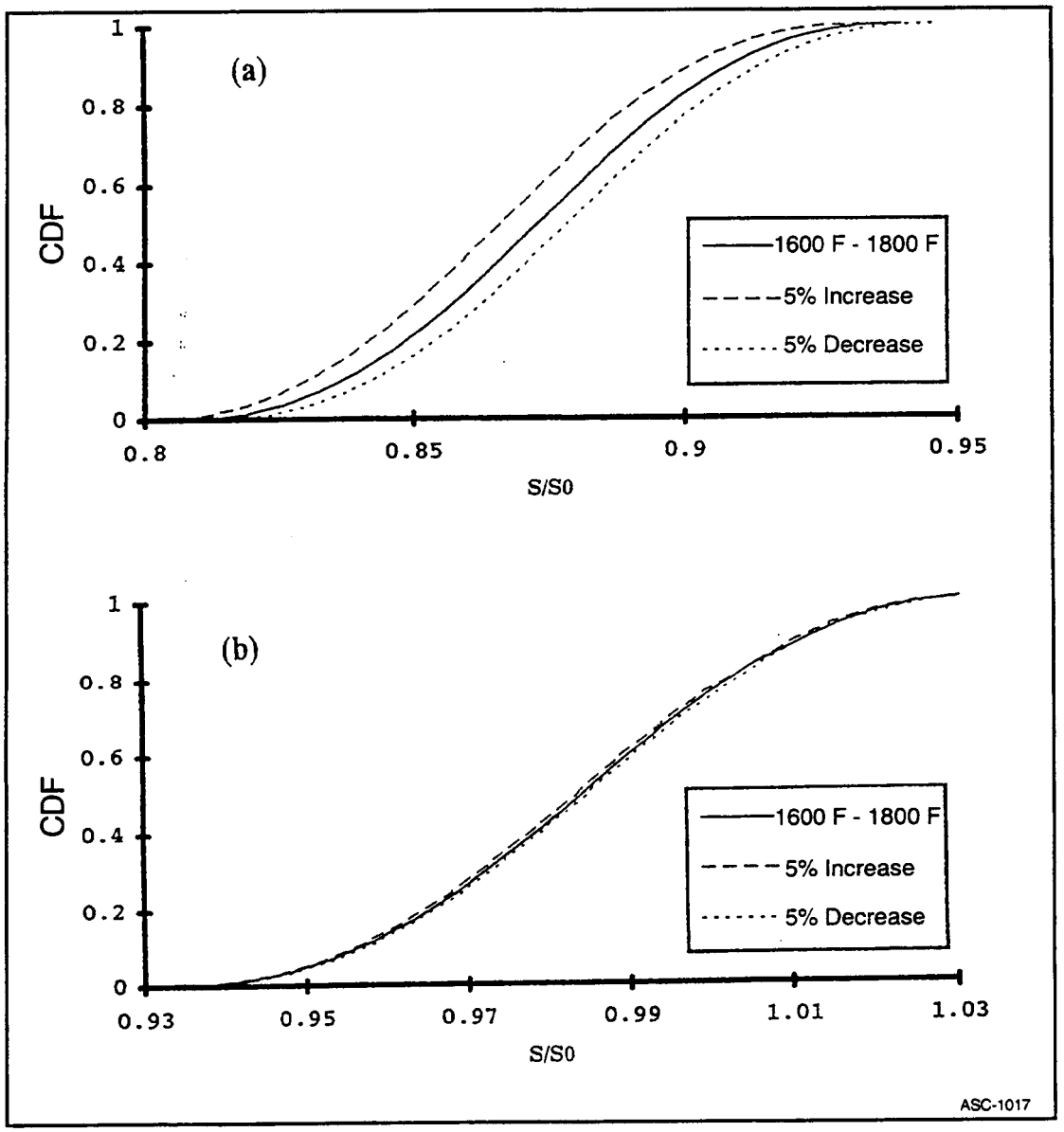

Figure 7-14. The Effect of Temperature on Cumulative Distribution Function Due to (a) Longitudinal Stress (11), and (b) Transverse Stress (22)

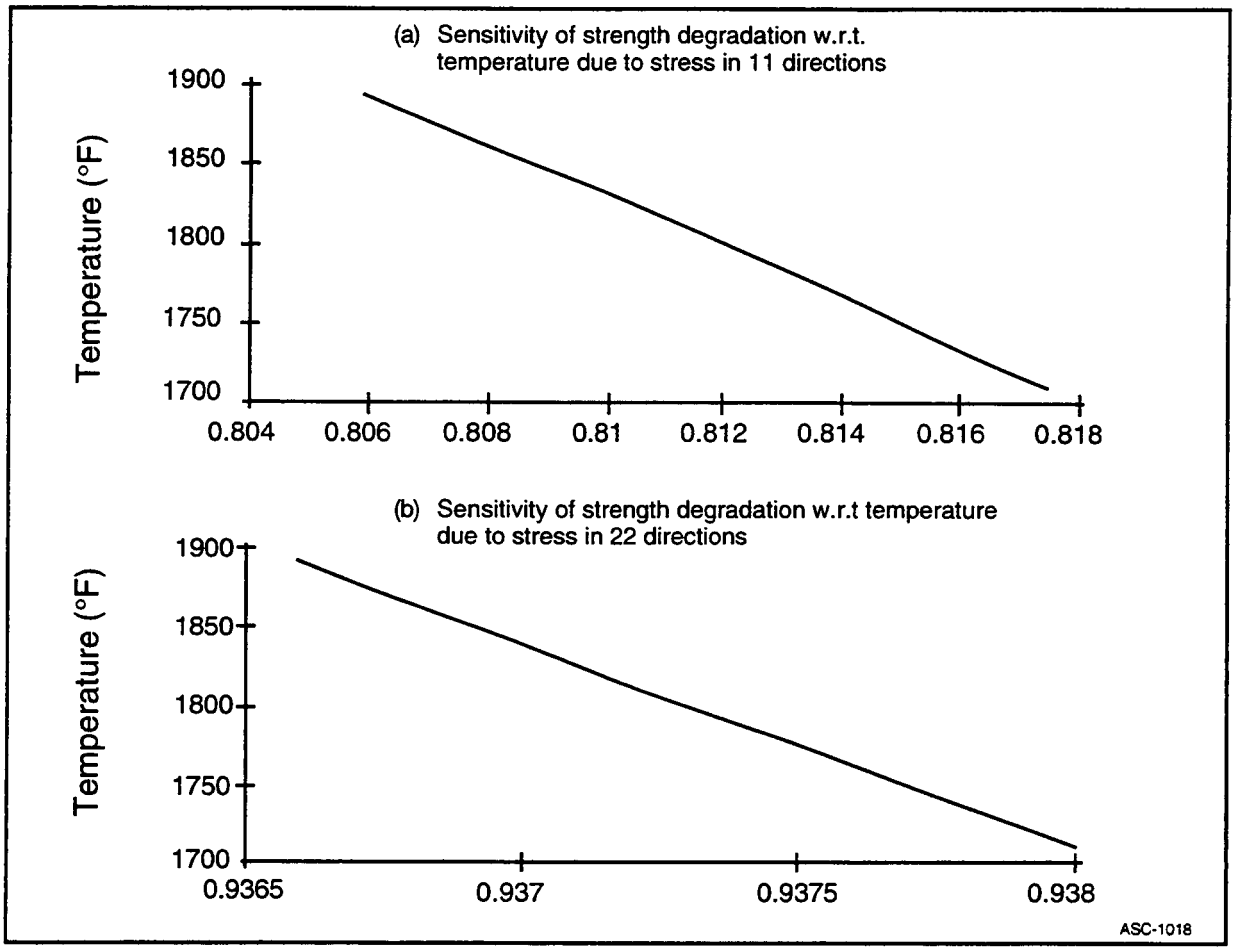

Figure 7-15. The Sensitivity of Strength With Respect to Temperature at 0.99 Reliability Due to (a) Longitudinal Stress (11), and (b) Transverse Stress (22)

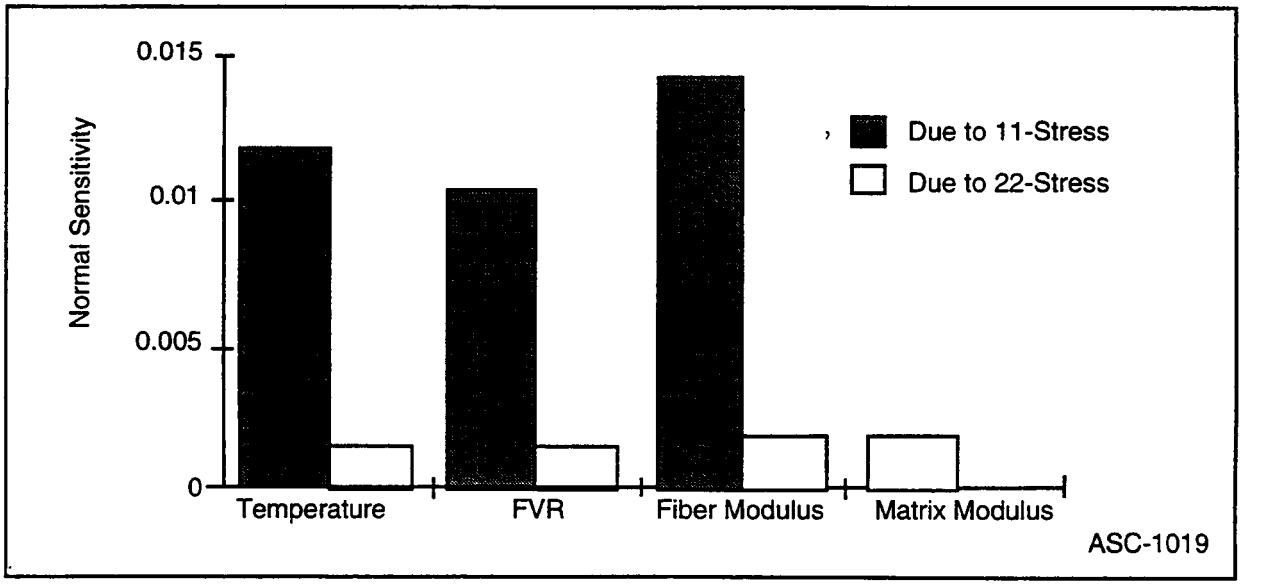

Figure 7-16. The Strength Sensitivity of First Ply With Respect to Various Parameters of SiC/SiC at 0.99 Reliability Due to Longitudinal (11) and Transverse (22) Stresses

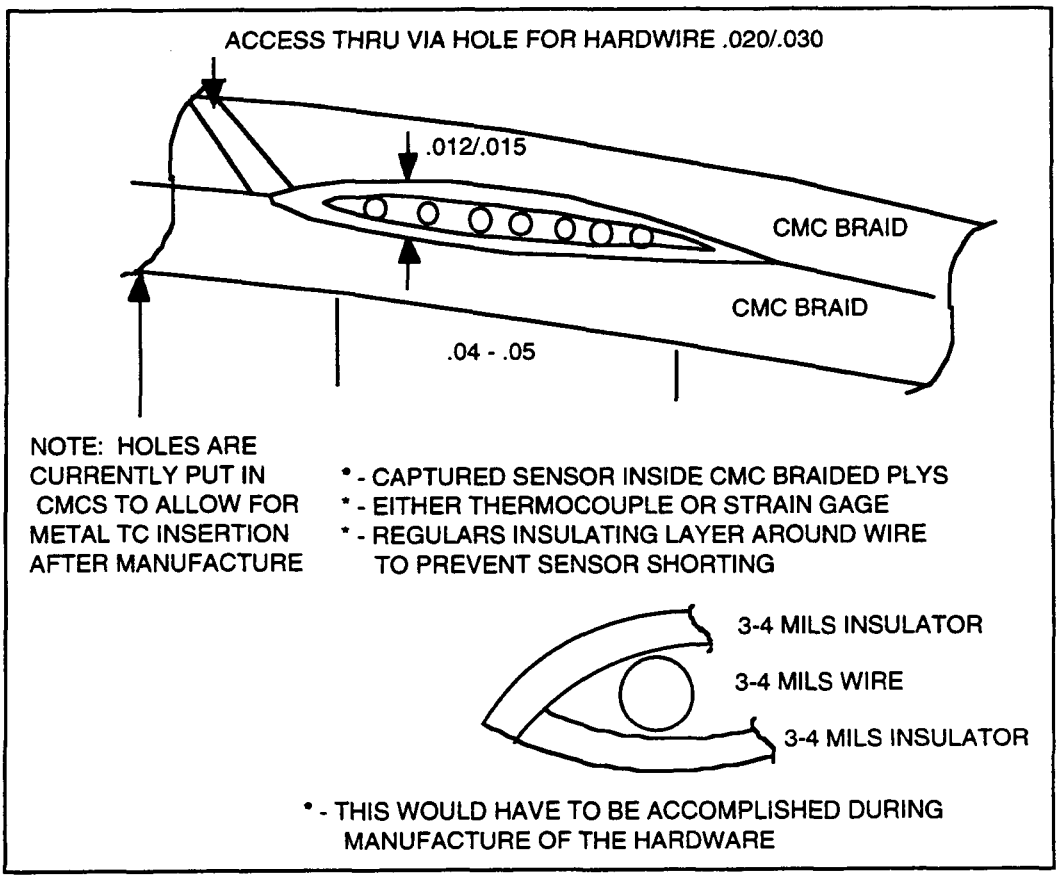

Figure 7-17. Allied Signal Technique of Sensor Insertion in CMC Combustor

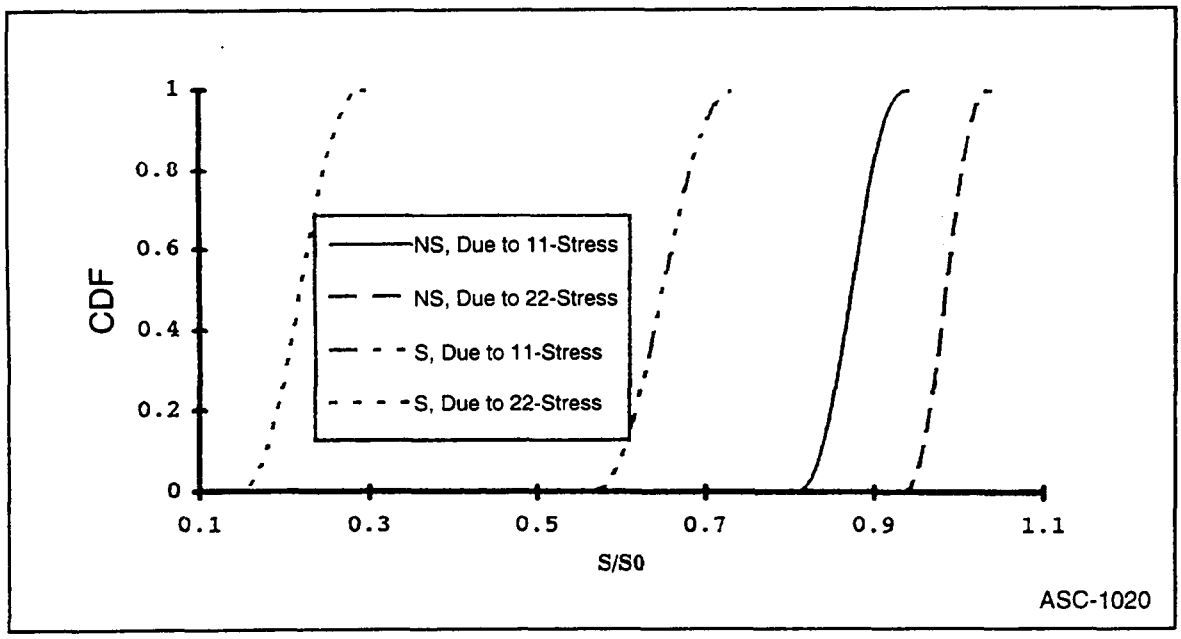

Figure 7-18. The Effect of Sensor on Cumulative Distribution Functions - NS = Without Sensor; S = With Sensor

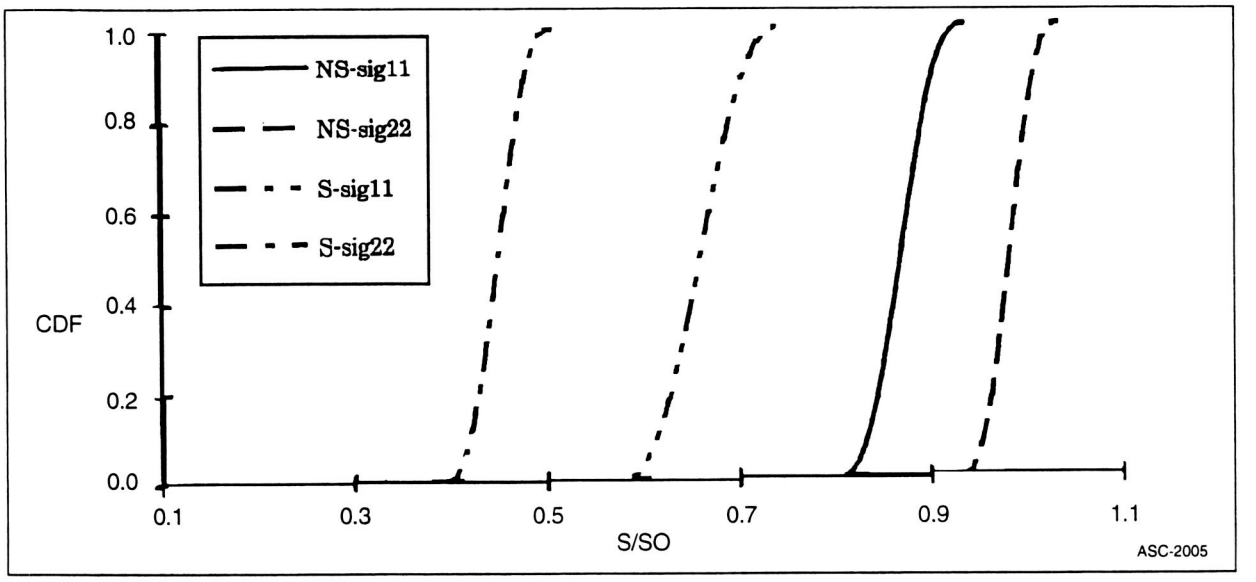

Figure 7-19. The Effect of the Sensor on Cumulative Distribution Function - NS = Without Sensor; S = With Sensor

7.3 STRUCTURAL RELIABILITY OF CMC COMBUSTOR

In this section stresses, strains, and reliability of the CMC combustor is calculated. Both deterministic and probabilistic analysis are performed for the combustor with and without insertion of sensors. Due to existing symmetries, only one twentieth forth (equivalence of 15 degrees hoop) of the CMC combustor structure, as shown in Figure 7-20, is used to perform all numerical simulations.

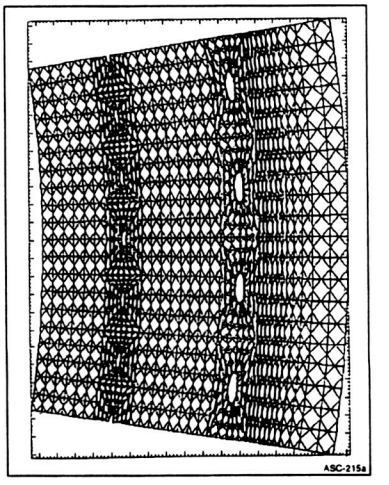

Figure 7-20. A Generic Finite Element Model of CMC Combustor (1188 Quad Elements, 1334 Nodes, 8004 DOF)

7.3.1 CMC Combustor Without Sensors

GENOA software system is used to investigate structural response and integrity of the CMC combustor. First we studied the combuster without insertion of any sensors. The stress, strain, and deflection at each node (and even each layer) of the combustor structure under thermal and mechanical loading (internal pressure) conditions are calculated. Figure 7-21 illustrate the resulting contour stresses several directions. As seen, all the stresses around the holes are large.

The contour plot for 99 percent reliability (probability density function) of the top layer of structure in several directions due to service loading is shown in Figure 7-22. As shown, in there is variations in the reliability level.

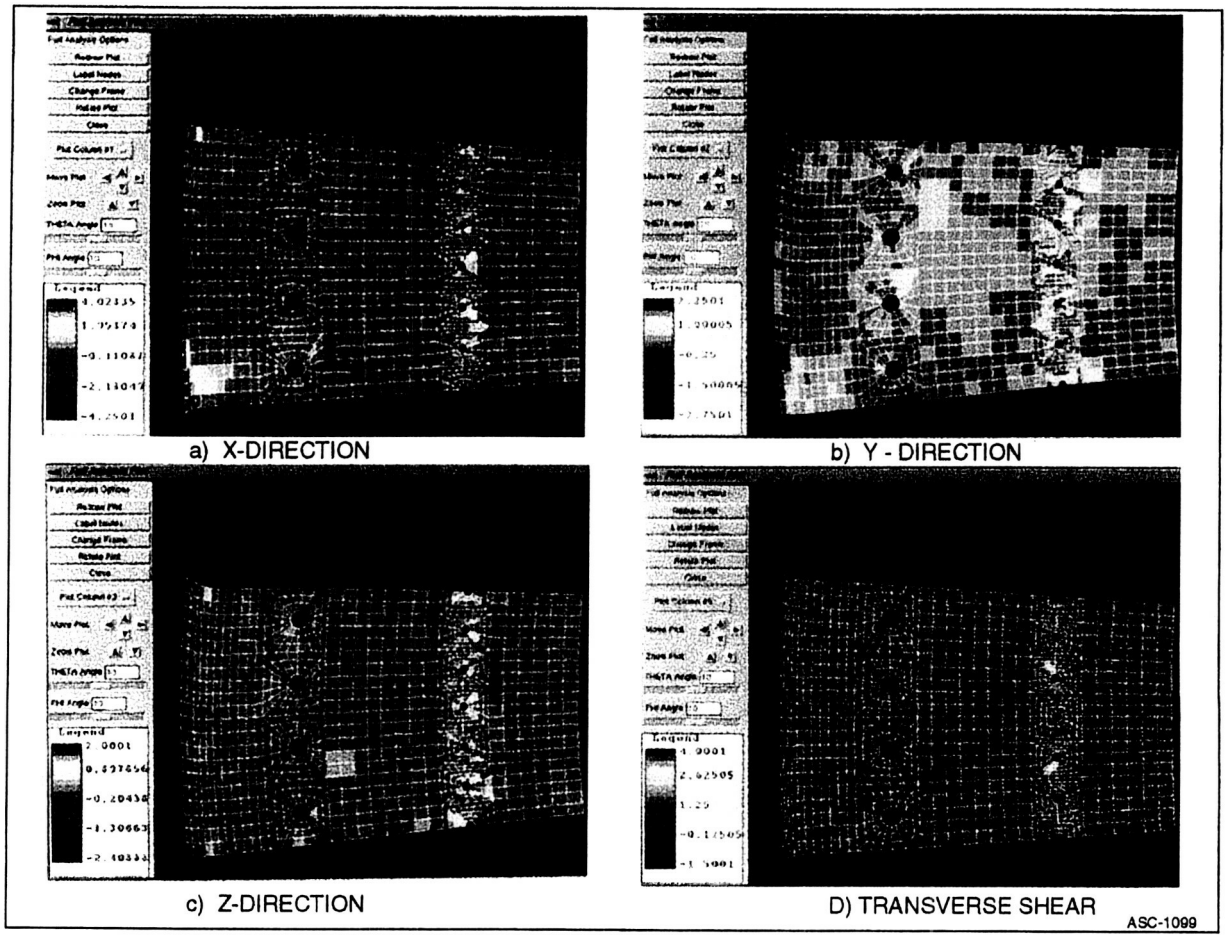

Figure 7-21. Stress Contour Plots for Combustor Without Sensors

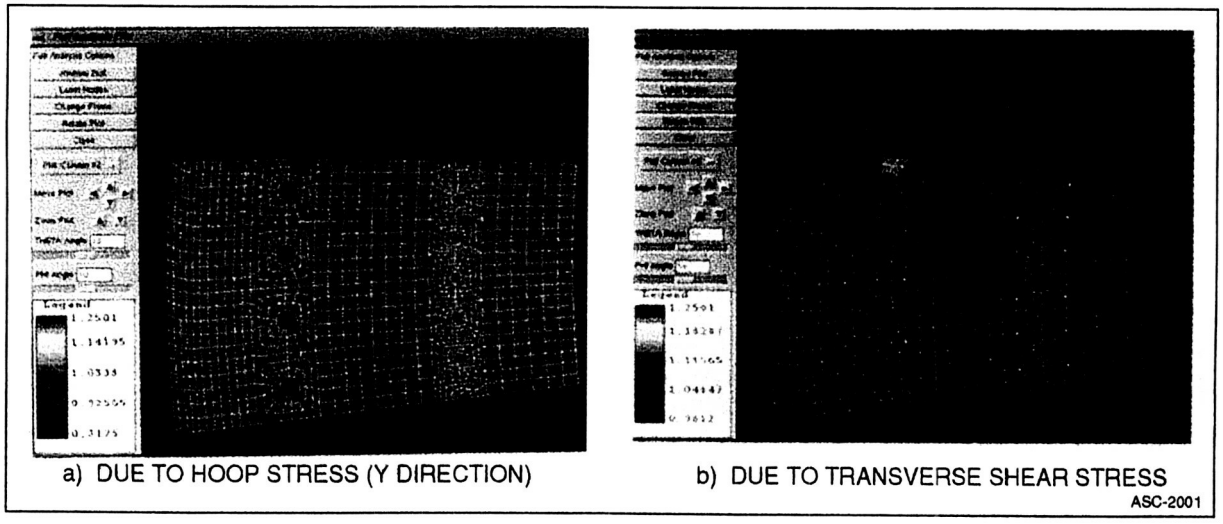

Figure 7-22. Reliability Contour Plot (at 0.99 Reliability) for Combustor Without Insertion of Sensors

7.3.2 CMC Combustor With Sensors

The performance of a CMC combustor with embedded sensors was simulated with eight sensors (Figure 7-17) inserted in critical regions near large holes. These sensors were 1/6 the thickness of the combustor wall. For simplicity, the finite element mesh used in the simulation was not regenerated (modified) to include fine mesh elements near points of application of the sensors. The results showed that stress and reliability at points not near the inserted sensors were not significantly changed from value obtained without insertion of sensors.

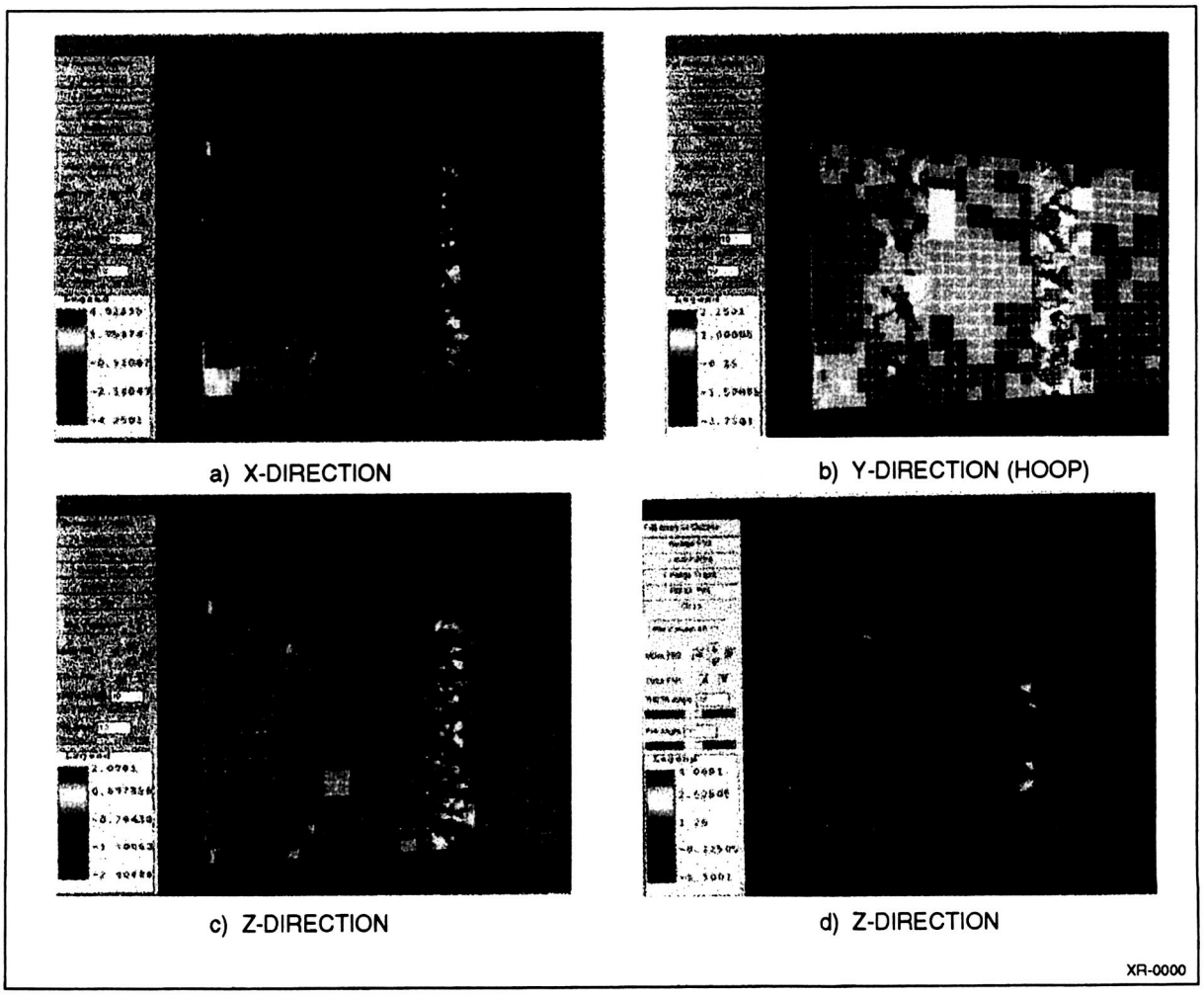

Figure 7-23. Stress Contour Plots for Combustor With Imbedded Sensors

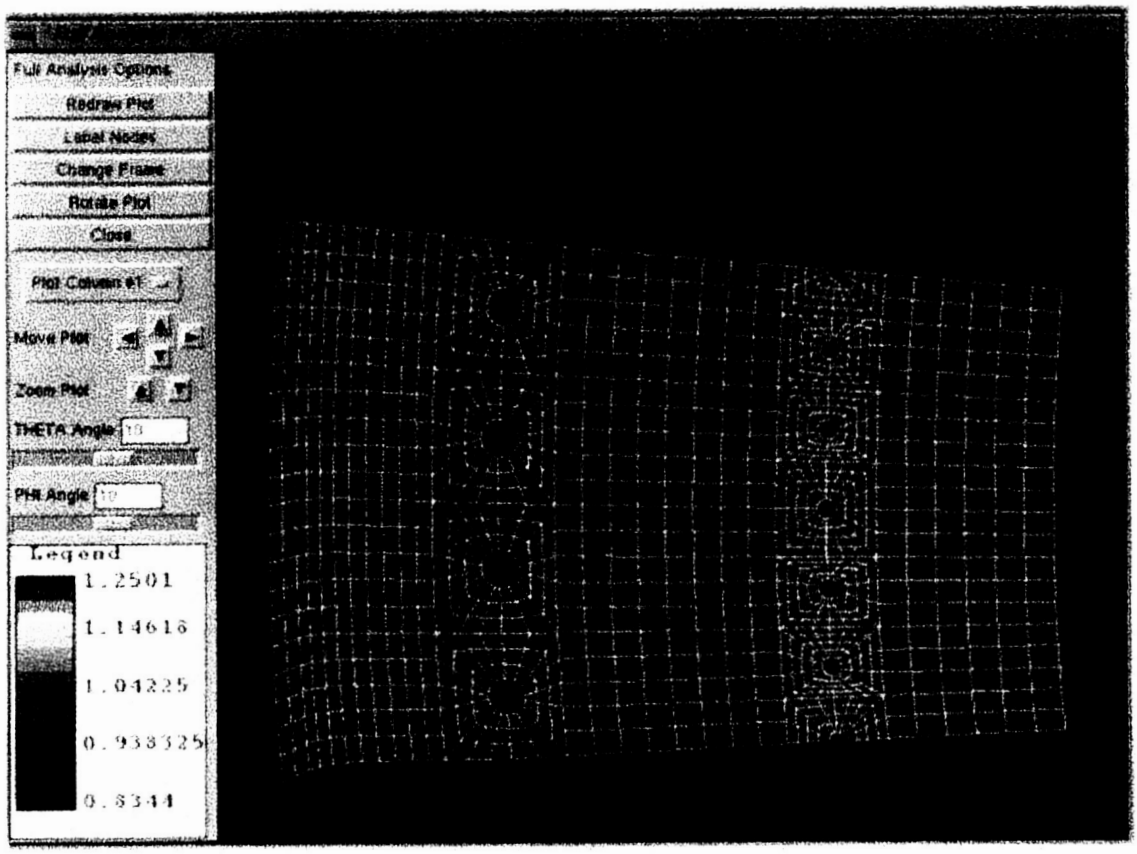

Figure 7-24. Reliability Contour Plot (at 0.99 Reliability for Top Layer of the Combustor With Inserted Sensors

8.0 Health Monitoring

The following steps are key to health monitoring of CMC combustors as shown in the flow diagram of Figure 8-1:

1. Obtain for monitoring in real time; temperature, pressure, and strain parameter data from sensors attached to an operating CMC combustor at experimentally established critical locations

2. Use mathematical techniques to obtain, for critical regions and in real time, distribution maps (temperature, temperature gradient, strain, and pressure maps) of monitored combustor parameters (in the hoop, axial and through the wall thickness directions) from sensor data in combination with experimentally verified and theoretical relationships. Compare these maps with engine operating parameter envelopes to ascertain needs for engine operating control adjustments.

3. Perform combustor health analysis using GENOA with FEM simulation based on a pre determined FEM and using fast parallel processing to obtain temperature stress/strain distribution maps and related structural responses (strain energy release rate, delamination and crack progression).

4. Use probabilistic simulation (equivalent to fuzzy logic) to provide instructions for controlling engine operation. (for example by controlling fuel injection, fuel to air ratio, and cooling air flow) to maintain the combustor within its operating temperature, and stress envelopes.

Successful CMC combustor health monitoring starts with the assumption that the development of sensors and sensor attachment progresses to provide long term (~3000 hours life) means of measuring temperature, strain and pressure in an operational of turbine engine. The necessary development capabilities are illustrated in Figure 8-1.

Real time mapping of temperature, temperature gradients and associated stresses and strains in a CMC combustor can be accomplished by inputting appropriate sensor data into integrated finite element, and composite mechanics (unit cell analysis: CEMCAN [21] and utilizing its existing capability to calculate associated stress/strain distributions using temperature, pressure, and temperature gradient inputs. The approach accounts for all types of composite behavior, structures, load conditions, and fracture process starting from damage initiation, to unstable propagation and to global structural collapse.

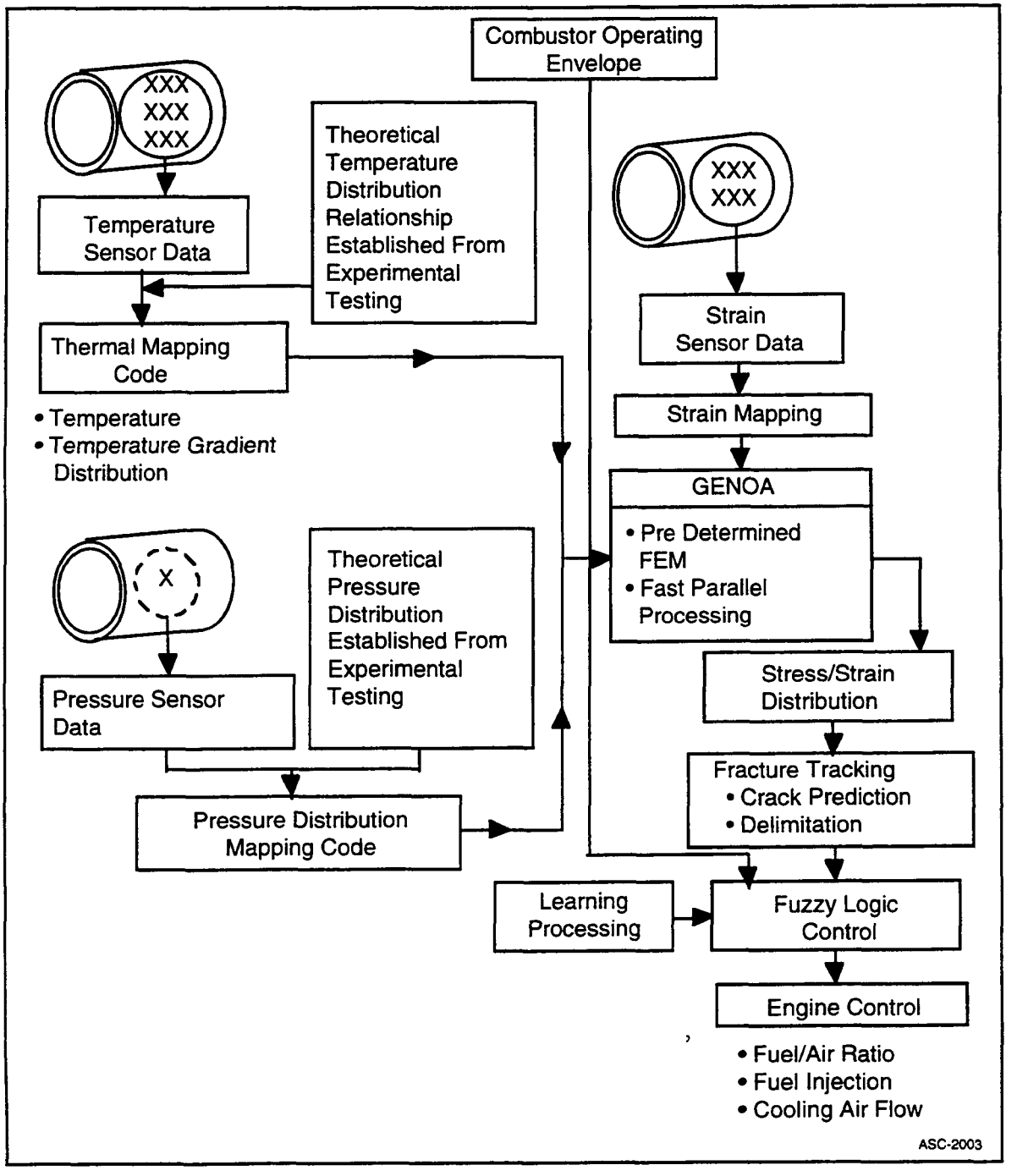

Figure 8-1. CMC Combustor Health Monitoring Control Flow Diagram

The crack progression approach is based on the following concepts [22]:

1. Any structure can sustain a certain amount of damage prior to structural fracture (collapse);

2. During damage propagation, the structure exhibits progressive degradation of structural integrity as measured by global structural behavior variables such as loss in frequency, loss in buckling resistance, or excessive displacements;

3. Critical damage can be characterized as the amount of damage beyond which a small additional damage or loading increase will cause rapid degradation in the structural integrity;

4. Structural damage is characterized by the following five sequential stages: (1) initiation, (2) growth, (3) accumulation, (4) stable or slow propagation (up to critical amount), and (5) unstable or very rapid propagation (beyond the critical amount) to collapse.

These concepts are fundamental to developing formal procedures to (1) identify the five different stages of damage, (2) quantify the amount of damage at each stage, and (3) relate the amount of damage at each stage of the degradation of global structural behavior.

Real time monitoring of progressive fracture in a CMC combustor can be performed by the existing real time simulation capability of GENOA/CEMCAN (by combination of composite mechanics with finite element method) to depict global structural behavior based on sensor data. Some guidance in incorporating structural behavior degradation capability in GENOA is available from the CODSTRAN code developed by NASA for use with polymer matrix composites. The CODSTRAN methodology depicts structural fracture toughness in terms of global Strain Energy Release Rate (SERR), a convenient parameter to identify the "critical damage amount."

9.0 References

1. P. A. Ehrenfeuchter and R. O. Claus, "Optical Fiber Wave Guide Methods for Advanced Materials," Virginia Tech, Blacksburg, VA, Sept 16, 1987.

2. NASA Tech Briefing Nov. 1994, Page 39.

3. F. Lord, "Infrared Temperature Measurement and Imaging Sensors," August 1994.

4. Przirembel, "Pyrometers from the Customer's Point of View", Pratt & Whitney FL, Remote Temperature Sensing Workshop, 1994, NASA LeRC.

5. R. C. Buchanan, ed. "Ceramic Materials for Electronics," Maracel Deker, Inc., New York, 1986.

6. A. Bumbalough, et. al., "Electronic Packaging and Interconnect Business Study," Remote Temperature Sensing Workshop, NASA Lewis Research Center, Oct 27, 1994.

7. K. G. Kreider, et. al., "Laser Transformed SiC Thin Films," accepted for publication in Diamond Silicon Carbide and Nitride Wide Badgap Semiconductors, Materials Research Society, 1994.

8. N. R. Quick, "Characterization of a Ceramic Sensor Synthesized by a Laser Conversion Process," AppliCote Associates, Randolph, NJ.

9. Communication From Allied Signal.

10. Lei, "High Temperature Thin Film Strain Gages", NYMA, Inc., Ohio, Proceedings of the 7th Annual HITEMP Review, Cleveland, Ohio 1994.

11. H. Grant, S. J. Przgbystewshi, et. al., "Thin Film Strain Gage Development Program-Strain Gages for Dynamic Measurement," NASA CR-174707, 1983.

12. K. Gamler, M. Headinger, and K. Hatton, "Advanced Fiber Reinforced CMC's Fabricated by CVI and DIMOX TM for Turbine Engine Applications," DuPont Lanxide Composites Inc., Newark, Delaware USA.

13. V. Chung, et. al. and C. Van Erp, "Ceramic Matrix Composite Materials in Advanced Gas Turbine Engine Combustors," U.S. Naval Air Warfare Center, Contract N00140-88-C-5875.

14. L. Boyce and T. B. Lovelace, "PROMISS User's Manual," Final Technical Report NAG 3-867, Appendix 1, 1990.

15. S. K. Mital, "Ceramic Matrix Composite Analyzer, "CEMCAN User's Guide," NASA Lewis Research Center, Cleveland, Ohio, 1994.

16. F. Abdi, "Concurrent Probabilistic Simulation of High Temperature Composite Response," Contract No. NAS3-26997, Oct. 1995.

17. L. Boyce, "Development of Advanced Methodologies for Probabilistic Constitutive Relationships of Material Strength Models," Phase 2," NASA NAG 3-867, 1989.

18. M. C. Shiao and C. C. Chamis, "A Methodology For Evaluating The Reliability and Risk of Structures Under Complex Service Environments," NASA TM-103244, 1990.

19. F. Abdi, "Development of COMET Nonlinear Design Optimization System" Fy 1995 Activity Summary Report, Nov. 24 1995.

20. D. A. Hopkins and P. L. N. Murthy, "METCAN - The Metal Matrix Composite Analyzer," Lewis Structure Technology," NASA CP-3003, Vol 2, pp. 141-156, 1988.

21. S. Mital, P. Murthy, and C. Chamis, "Simulation of Ceramic Matrix Composite Behavior Including Progressive Fracture and Load Redistribution," 36th AIAA/ASME/ASCE/AHS/ASC Structural Dynamics and Material Conference, Apr 10-13, 1995, New Orleans, LA.

22. 14th Annual Energy-Source Technology Conference and Exhibition Sponsored by the American Society of Mechanical Engineers, Houston, Texas, January 26-29, 1992.

REPORT DOCUMENTATION PAGE

Form Approved
OMB No. 0704-0188

Public reporting burden for this collection of information is estimated to average 1 hour per response, including the time for reviewing instructions, searching existing data sources, gathering and maintaining the data needed, and completing and reviewing the collection of information. Send comments regarding this burden estimate or any other aspect of this collection of information, including suggestions for reducing this burden, to Washington Headquarters Services, Directorate for Information Operations and Reports, 1215 Jefferson Davis Highway, Suite 1204, Arlington, VA 22202-4302, and to the Office of Management and Budget, Paperwork Reduction Project (0704-0188), Washington, DC 20503.

1. AGENCY USE ONLY (*Leave blank*)	2. REPORT DATE	3. REPORT TYPE AND DATES COVERED
	November 1996	Final Contractor Report

4. TITLE AND SUBTITLE

Multi-Disciplinary Development of a Smart CMC Combustor for an Intelligent Engine System

5. FUNDING NUMBERS

WU-505-63-5B
C-NAS3-27443

6. AUTHOR(S)

Frank Abdi, Roy Lorenz, Jeff Hadian, and Harvey Niska

7. PERFORMING ORGANIZATION NAME(S) AND ADDRESS(ES)

Alpha STAR Research Corporation
Los Angeles, California

8. PERFORMING ORGANIZATION REPORT NUMBER

E-10535

9. SPONSORING/MONITORING AGENCY NAME(S) AND ADDRESS(ES)

National Aeronautics and Space Administration
Lewis Research Center
Cleveland, Ohio 44135-3191

10. SPONSORING/MONITORING AGENCY REPORT NUMBER

NASA CR-198548
ASC-95-1002

11. SUPPLEMENTARY NOTES

Frank Abdi, Roy Lorenz, and Jeff Hadian, Alpha STAR Research Corporation, Los Angeles, California; Harvey Niska, Allied Signal Propulsion Engines, Phoenix, Arizona. Project Manager, Christos C. Chamis, Structures and Acoustics Division, NASA Lewis Research Center, organization code 5900, (216) 433-3252.

12a. DISTRIBUTION/AVAILABILITY STATEMENT

Unclassified - Unlimited
Subject Category 24

This publication is available from the NASA Center for AeroSpace Information, (301) 621-0390.

12b. DISTRIBUTION CODE

13. ABSTRACT ***(Maximum 200 words)***

The findings are described of an investigation to determine the feasibility of utilizing temperature and/or strain and stress sensor data in a computer program to monitor the health, in real time, of a ceramic gas turbine combustor operating at elevated temperatures (>2000°F). The ultimate purpose is to provide feedback to initiate corrective action should a threat to combustor health occur. This investigation entails evaluation of the feasibility of the following: (1) Selection of sensor technology and CMC material for potential use in developing a smart CMC combustor, (2) development of a finite element simulation model of a sensor equipped, smart, CMC combustor based on and verified with test data, (3) use of simulation model and GENOA, NESSUS and CEMCAN available computer codes, to calibrate, and perform: (a) finite element analysis to predict CMC combustor structural response under load, (b) probabilistic analysis of the CMC combustor operating with benefit of sensor input, and (c) probabilistic determination of sensor influence coefficients needed to enhance existing CEMCAN code capability for prediction of the structural response of a CMC combustor with embedded sensors, (4) modification of existing CMC data bank using CEMCAN to account for material property changes due to embedded sensors, (5) use of GENOA to assist in design of a ceramic combustor for a gas turbine engine. Results obtained establish the feasibility of every item enumerated above.

14. SUBJECT TERMS

Fiber composites; Composite mechanics; Finite element; Probability; Computer codes; Fracture; Stress analysis; Embedded sensors

15. NUMBER OF PAGES

91

16. PRICE CODE

A05

17. SECURITY CLASSIFICATION OF REPORT	18. SECURITY CLASSIFICATION OF THIS PAGE	19. SECURITY CLASSIFICATION OF ABSTRACT	20. LIMITATION OF ABSTRACT
Unclassified	Unclassified	Unclassified	